MULTISCALE APPROACH TO OPTIMAL CONTROL OF IN-SITU BIOREMEDIATION OF GROUNDWATER

BY

YONG LIU

B. Engr., Tsinghua University, 1994
M. Engr., Tsinghua University, 1997
M.C.S., University of Illinois at Urbana-Champaign, 2001

THESIS

Submitted in partial fulfillment of the requirements
for the degree of Doctor of Philosophy in Environmental Engineering
in the Graduate College of the
University of Illinois at Urbana-Champaign, 2001

Urbana, Illinois

Abstract

A previously-developed SALQR optimal control model holds great promise for improving in-situ bioremediation design, but field-scale design is not currently possible even with the most advanced supercomputing power available today. Our analysis identified that the computational bottleneck of the model is the two-step method for calculating analytical derivatives of the transition equation, which requires over 90% of the total computing time. Since the computational effort involved in calculating the derivatives is highly dependent on the spatial discretization used to solve the transition equation, the primary focus of this research is on spatial multiscale methods to reduce computational effort.

A framework for a full multiscale approach is developed that integrates a one-way spatial multiscale method, a V-cycle multiscale derivatives method and an efficient numerical derivatives method. The methodology for each individual component is given and various performance enhancement strategies and modeling issues such as dispersivity values and penalty weight are also discussed. Case studies showed significant computational savings achieved by individual methods and the combinations of all three components always outperform methods with only one individual component. The full multiscale approach enables solution of a case with about 6,500 state variables within 8.8

to 11.9 days, compared to one year needed by the previous single-grid model with analytical derivatives.

This study has also identified the importance of the interaction of PDE discretization and optimization. The bioremediation optimal control model is governed by a set of nonlinear PDEs (the transition equation), which describe the system response under given pumping rates. Since solving the PDEs is only a subproblem within PDE-constrained optimization, it is critical that refining optimization solutions be performed simultaneously with refining the mesh for the PDE. The full multiscale approach developed in this work achieves this goal by using approximate solutions early in the run when a broad search of the decision space is being performed. As the solution becomes more refined later in the run, more accurate estimates are needed to finetune the solution and finer spatial discretizations are used.

TO MY WIFE YUANCHENG

Acknowledgements

This material is based upon work supported by a Computational Science and Engineering (CSE) fellowship and teaching assistantship awarded to me at the University of Illinois at Urbana-Champaign and a National Science Foundation (NSF) Career Award under Grant No. BES 97-34076 CAR and a National Computational Science Alliance (NCSA) Grant under contract number BCS980001N to my advisor Professor Barbara Minsker. Any opinions, findings and conclusions or recommendations expressed in this material are those of mine and do not necessarily reflect the views of NSF, NCSA or CSE program.

I would like to thank my thesis advisor, Professor Barbara Minsker, for her invaluable directions and support throughout my graduate life at UIUC. Her persistence in facing of research uncertainties and challenges inspires me. Her guidance on academic thinking and writing is very helpful for my future career.

I would also like to thank the members of my thesis committee, Professor Albert Valocchi, Dr. Faisal Saied, and Professor Robert Skeel, for their valuable technical assistance and helpful discussions. I am also grateful to Professor Achi Brandt from Weizmann Institute of Science, for the invaluable discussions.

It was an enjoyable experience during the past four years working with my fellow graduate students and officemates, especially, Patrick Reed, Gayathri Gopalakrishnan, Beth Padera, J. Bryan Smalley, and William J. Michael.

Last but not least, my family deserves particular recognition for their unconditional support during past years. I am grateful to my parents, my sisters and my elder brother for their encouragements and sacrifices. And most of all I thank my wife Yuancheng, for her love, encouragement, optimism and sacrifices, without which all that I have achieved was not possible.

Table of Contents

CHAPTER

List of Tables

List of Figures

Chapter 1

Introduction

Solving large-scale optimal in-situ bioremediation design problems is expected to have huge economic benefits, yet it is constrained by the computational bottleneck in previous existing methods. In this chapter, we introduce the background of the research area, discuss our research goals and motivations, present major contributions of our work and outline the rest of the dissertation.

1.1 Groundwater Contamination and Remediation Design

A range of human practices in industrial, commercial, agricultural and military fields have contributed to groundwater contamination problems. As a result, about 300,000 to 400,000 sites have contaminated groundwater problems in the United States (National Research Council, 1994). Typical contaminants found in the groundwater include phenol, BTEX (Benzene, Toluene, Ethlybenzene, and Xylene) due to leaking underground gas storage tanks and DNAPL (dense nonaqueous-phase liquids) such as TCE (Trichloroethylene) due to the prevalent usage of industrial degreasing solvents.

Subsurface remediation is associated with tremendous cost. A recent report from the US Environmental Protection Agency states that the remaining remediation costs for contaminated soil and groundwater sites in the Superfund National Priorities List are

estimated at $187 billion in 1996 dollars (EPA, 1997). Russell et al. (1991) estimates that about $500 billion to $1 trillion are needed in the next 30 years to cleanup the contaminated sites in both private and public sectors to the stringent standard. Although conventional pump-and-treat cleanup systems have been extensively used, it was found inefficient in many scenarios due to the long remediation period and high cost. As an alternative, in-situ bioremediation has been found to be cost-effective for cleaning up petroleum hydrocarbon contaminants (National Research Council, 1994). This remediation technology uses indigenous microorganisms to degrade the contaminants in-place. A typical engineered aerobic in-situ bioremediation system is shown in Figure 1.1, where the design parameters are defined as locations and pumping rates for injection and extraction wells. The injection wells are used to deliver oxygen and nutrients, stimulating the growth of microorganisms and thereby accelerating degradation of pollutants. The extraction wells are used to increase the hydraulic gradient and enhance the transport of the injected substances.

In order to find an optimal design for in-situ bioremediation systems to achieve a specified water quality standard at minimum cost, an optimal control method called successive approximation linear quadratic regulator (SALQR) has been used in a coupled simulation and optimization model (Minsker and Shoemaker, 1998b). This optimal control model defines control variables as pumping rates and state variables as hydraulic heads and concentrations of substrate, oxygen and biomass. The model can identify optimal well locations and pumping rates to minimize pumping costs. However, previous work has shown that the model is computationally intensive (Minsker and Shoemaker,

1998a), which prevents its application at large-scale, complex field sites. Ignoring sparsity considerations, the computational work for solving the SALQR model is proportional to $O(N^3)$(Liao and Shoemaker, 1991), where N is the total number of state variables. The state variables are defined at the nodes of the finite element mesh within the simulation model, so significant increases in computational effort can be expected when using a fine mesh rather than a coarse mesh. As presented by Minsker and Shoemaker (1998a), a substantially finer mesh is required for designing in-situ bioremediation than for pump-and-treat design, due to the nonlinearity and dynamic properties of this remediation strategy. Thus, overcoming this computational bottleneck while still preserving the accuracy of the modeling is a key issue for applying this model to large-scale field sites where optimization is most needed.

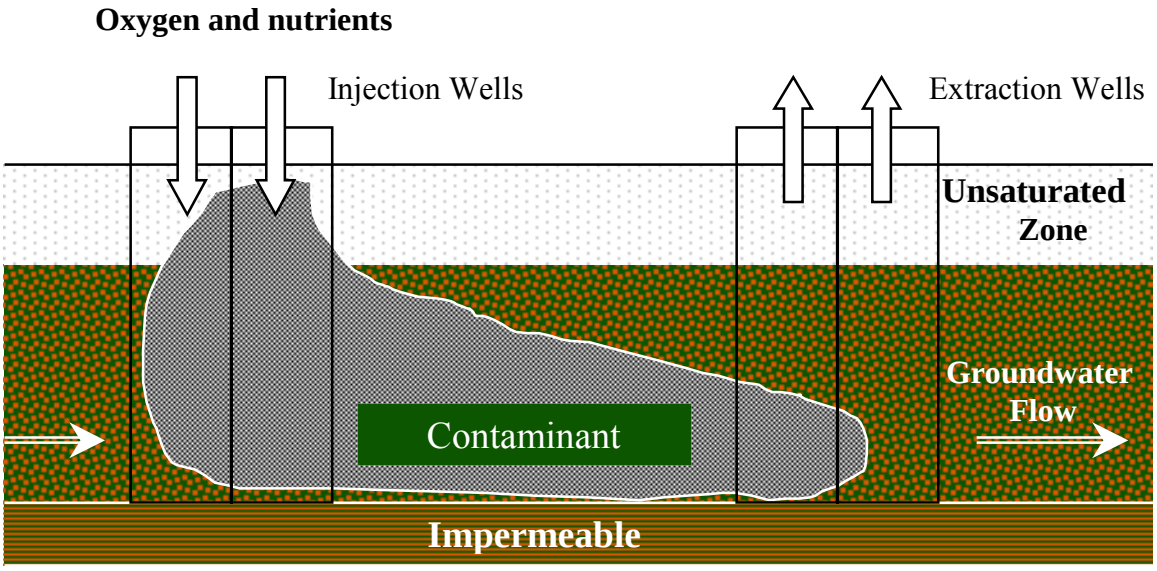

Figure 1.1: Schematic view of an engineered aerobic groundwater in-situ bioremediation system

1.2 Optimal Control Model Description

The discrete-time optimal control model of in-situ bioremediation can be formulated as follows (Minsker and Shoemaker, 1998b):

$$\underset{U_1 \ldots U_2}{Min}\ J(U) = \sum_{k=1}^{K} G(X_k, U_k, k) \tag{1.1}$$

subject to

$$X_{k+1} = Y(X_k, U_k, k), k = 1,\ldots, K \tag{1.2}$$

$$L(X_k, U_k, k) \le 0, k = 1,\ldots, K \tag{1.3}$$

where *J(U)* = the objective function, which is the sum of cost functions *G* in each management period k; *K* = the total number of management periods; *U* = the control vector, i.e. the pumping rate; and *X* = the state vector, which includes hydraulic heads and concentrations of the contaminant, oxygen and biomass. Equation (1.2) is a transition equation, which describes the change in state vector *X* from one management period (*k*) to the next (*k+1*) under the current control policy U. A management period is a user-defined time interval that can contain multiple simulation time steps. The control policy can only change once at the beginning of each management period. The transition equation is a two-dimensional finite-element contaminant fate and transport simulation model called Bio2D. Equation (1.3) is a set of constraints that stipulate the water quality standard to be met at the end of the clean-up, the upper and lower bound of the hydraulic heads at each well location, and any other possible conditions required for either state or

control variables. Detailed formulations for the Bio2D and constraint equations can be found in Appendix A and B, respectively.

When the model is solved using SALQR, the constraints are incorporated into the objective function using the following penalty function:

$$y = \sum_{k=1}^{K} \sum_{q=1}^{n_q} r[\max(0, f_{kq})]^{2.001} \tag{1.4}$$

where y = the penalty that is added to the objective function in equation (1); f_{kq} = violation of the constraint q in period k, where q is any of the constraints given in equations (1.3); n_q = the number of constraints in equations (1.3); and r = a scalar penalty weight greater than zero. The penalty weight r is initially set to a small value and the optimal solution is found. Then the weight is increased successively by a factor of 10 and the problem is re-solved until the constraint violations are sufficiently small.

SALQR is a variant of differential dynamic programming (DDP) in which the second derivative of the transition equation is assumed to be zero. SALQR consists of two iterative steps: a forward sweep and a backward sweep. An initial guess of the control policy is needed to start the algorithm. The forward sweep runs the simulation model to evaluate the effects of the current pumping rates, and the backward sweep computes derivatives of the objective function and transition equation to find an improved strategy. The algorithm stops when it converges to the optimal pumping policy. A detailed description of the SALQR method is given in Appendix D.

1.3 Research Goals

The objective of this research is to develop innovative multiscale methods for optimal in-situ bioremediation design that will enable medium- and large-scale design. This objective will be achieved through the following goals.

Our first goal is to identify the computational bottleneck of the existing algorithm and model. This entails computational complexity analysis both theoretically and experimentally. Although previous works (Liao and Shoemaker, 1991; Minsker and Shoemaker, 1998a) have done some analysis on SALQR model, the unique features of bioremediation design have not been fully exploited. The results of this goal will provide new insights on how we can enhance the SALQR model in general and specifically what we should do to improve computational efficiency for optimal bioremediation design.

Our second goal is to develop innovative multiscale methods for optimal in-situ bioremediation design and investigate the performance of each method. The motivation for using multiscale methods in the SALQR model is to apply the general principle of multiscale computation advocated by Brandt (1997, 2001) to overcome the computational bottleneck posed by the current optimal in-situ bioremediation design model. These new methods require theoretical analysis, design, implementation, and testing. Reducing the computational effort associated with the number of nodes in space is the major target. While these methods are developed for optimal bioremediation design, their applicability is much broader.

Our third goal is to solve a large-scale in-situ bioremediation design with thousands of state variables, which was not practically feasible with the previous model.

A case study will be solved using several multiscale methods developed in this research and model performance will be investigated.

1.4 Contributions of this Thesis

The main contributions of this thesis are as follows:

- A detailed analysis of the SALQR model reveals the true bottleneck for optimal in-situ bioremediation design and similar PDE-constrained optimal control models with management period formulation to be the transition equation derivatives calculations.
- Design and implementation of efficient numerical derivatives calculation. We exploited the calculation procedure of the one-sided divided difference derivatives approximation of the first derivatives of transition equation with respect to the state variables, which leads to an order of magnitude reduction in computing time for the derivatives calculation (Liu and Minsker 2001, in press).
- Design and testing of various multiscale methods (Liu et al. 2001; Liu and Minsker 2001, in press).
- Address various modeling issues associated with optimal design of groundwater remediation using multiscale methods, including impact of penalty terms, dispersivity value, Peclet number, etc.
- Successful solution of large-scale case study with thousand of nodes. Our application showed that with the full multiscale approach, a case that would have required nearly one year to solve now only needs 9 days to converge to the optimal solution.

1.5 Structure of this Thesis

This thesis is organized as follows. In Chapter 2, we survey previous work on multiscale methods in optimization, derivative-based optimization applications for groundwater remediation design and PDE-constrained optimization problems in general. In Chapter 3, we present detailed analysis of the SALQR model and identify the true bottleneck of the computational performance. In Chapter 4, we develop a one-way spatial multiscale method and apply it to different case studies. In Chapter 5, we develop an efficient numerical derivatives approach and analyze its computational performance both theoretically and experimentally. In Chapter 6, we present the multiscale V-cycle derivatives method with results and analysis. In Chapter 7, we present the full multiscale approach for optimal in-situ bioremediation design and investigate various strategies to enhance its performance. Note that Chapters 4-6 describes the individual components of the full multiscale method, and Chapter 7 presents the configurations and combinations of different components of the full multiscale method. Finally, in Chapter 8, we summarize the major findings and point out future research directions to extend and enhance this research.

Some auxiliary materials are presented in the Appendices. In Appendix A, we present the detail formulation of the simulation model BIO2D. In Appendix B, we present the detailed formulation of the optimal control model for in-situ bioremediation design. In Appendix C, we describe the first derivatives of the transition equation with respect to the state and control variables in mathematic format. In Appendix D, we

present the flow chart and algorithmic description of the SALQR method with management periods.

Chapter 2

Literature Review

This chapter describes previous work relevant to this research. Since the groundwater bioremediation optimal control model falls into the general category of PDE-constrained optimization, section 2.1 gives a review of approaches taken to solving such problems. Section 2.2 overviews previous work on multiscale methods for solving PDEs and optimization problems. A brief summary of previous optimal groundwater remediation design studies is given in Section 2.3. Finally, a summary of the literature review is given in Section 2.4.

2.1 PDE-constrained Optimization Problems

The optimal groundwater bioremediation design problem considered in this work (see Equations (1.1) to (1.4) in Chapter 1) is an example of PDE-constrained optimization. Solving an optimization problem governed by PDEs is generally much harder than solving PDEs alone, since solving PDEs is only a subproblem associated with optimization. In the optimization problem, the governing PDEs are called state or transition equations. As methods for solving large-scale PDE simulation models with millions of unknowns have matured, interest in solving large-scale PDE-constrained

problems arising in many areas of science and engineering has increased. Such optimization problems usually have two forms: inverse modeling and optimal design or control modeling. Inverse problems involve calibrating parameters in the simulation model using the observed known data. For example, a typical inverse problem in groundwater modeling may require estimation of hydraulic conductivity and storativity. Recent development and methods reviews for the groundwater inverse problem can be found in the literature (see, e.g., Woodbury and Ulrych 2000; Schulz et al. 1999; Zio 1997; Ferraresi et al. 1996; McLaughlin and Townley 1996).

In optimal design or optimal control modeling, literature is sparse for tackling large-scale problems. Most papers found in the literature are on optimal shape design or optimal flow boundary control where the PDE constraints are usually the Navier-Stokes or Euler flow equations and the objective function is an integral equation. A nonlinear programming method called Sequential Quadratic Programming (SQP) (Boggs and Tolle 2000; Arnold and Puta 1994) is typically used to solve the optimization problem where the PDEs are treated as equality constraints and incorporated into the objective function using Lagrange multipliers. Biros and Ghattas (1999, 2000) proposed a parallel version of Newton-Krylov solver to solve the resulting large-scale Karush-Kuhn-Tucker (KKT) system after applying the first-order optimality condition to an optimal flow control problem. A variant of SQP method was used to solve this problem with good scalability. However, no inequality constraints for state variables or control variables are present in their optimization problems. In addition, the control variables are located in the boundary whose dimension can be changed with different discretizations (hence the name optimal

boundary control or optimal shape design) and an adjoint state equation was used to calculate the gradient. These characteristics are quite different from the optimal control model of groundwater bioremediation used in this research.

Another active theoretical research area is applying automatic differentiation techniques for solving optimal control problems. Hovland et al. (2000) used automatic differentiation to generate the Hessian matrix for an SQP-like nonlinear optimization algorithm to solve an optimal boundary control problem similar to Biros and Ghattas (1999, 2000). Bartholomew-Biggs et al. (2000) and Christianson and Bartholomew-Biggs (2000) used automatic differentiation to evaluate the Newton direction for a discrete-time optimal control algorithm called Pantoja's algorithm (Pantoja 1988). Only a theoretical analysis was performed for using automatic differentiation with Pantoja's algorithm, without any real-world application.

2.2 Multiscale Methods in Simulation and Optimization

To enable large-scale solution of PDEs and PDE-constrained optimal design or control problems, multiscale methods have attracted considerable research interest in the past years. The term "multiscale method" has been used extensively in the literature within different contexts. The standard multigrid method is probably the most well-known multiscale method. The scope of applicability of multiscale methods is impressive, as indicated by Brandt (1997, 2001) in his survey paper. The most extensively researched application of multiscale methods is as fast partial differential equation (PDE) solvers known as multigrid solvers. As shown by many researchers (see,

e.g., Brandt 1977; Hackbusch 1979; Douglas 1984; Mavriplis and Jameson 1990), multigrid solvers exhibit a convergence rate for solving PDEs that is independent of the number of unknowns in the discretized system. In the following, we first sketch the basic idea of multigrid solvers and their applications in groundwater simulation modeling. We then review the multiscale methods applied in solving various optimization problems.

2.2.1 Multigrid Solvers for Groundwater Simulation Modeling

To understand how multigrid solvers work, it is necessary to understand the concept of error first. Expressed in terms of a discrete Fourier series, the error (the difference between the true solution and an approximated iterative solution) can be represented by various Fourier components of different wave numbers. Oscillatory error components refer to those with small wavelength, while smooth error components refer to those with large wavelength. There are two key components in multigrid solvers: smoothers and coarse grid correction. The smoothers are usually relaxation methods, such as Gauss-Seidel, which can damp out the high frequency (i.e., oscillatory) error components quite quickly but cannot effectively reduce the low frequency (i.e., smooth) error components. However, the high or low frequency components of the error are relative to the grid on which the solution is defined. Smooth components on a fine grid appear oscillatory when sampled on a coarse grid. The idea of coarse grid correction takes advantage of the grid-dependent feature of the error component. By restricting the residual on the fine grid to the coarse grid via a restriction operator, the error equation on the coarse grid is solved to get an error correction for the fine grid solution. After interpolating the coarse grid correction back to the fine grid via an interpolation operator

and adding the correction to the approximated solution, the low frequency error components on the fine grid now should also be reduced significantly, which is why multigrid solvers are so effective. This process can be repeated until some convergence criterion is met. An important aspect of the multigrid solvers is that the coarse grid solution can be approximated by recursively using the two-grid (coarse and fine) iteration idea. That is, on the coarse grid, relaxation is performed to reduce high frequency components of the errors followed by the restriction of the correction equation to yet an even coarser grid, and so on. Depending on how the algorithm moves up and down the grids, there are many variants of multigrid solvers, such as V-cycle, W-cycle and full multigrid. Detailed theoretical and numerical discussions of multigrid solvers can be found in Stüben and Trottenberg (1982), Hackbusch (1985) and Briggs(1987). The book by Joppich and Mijalković (1993) is especially helpful for engineers modeling process simulation.

Several applications of multigrid solvers in groundwater flow and solute fate and transport simulation can be found in the literature. Mckeon and Chu (1987) used a full approximation scheme (FAS) of multigrid methods to solve a nonlinear two-dimensional flow equation discretized by the finite difference method. Beckie et al. (1993) found that mixed finite element methods combined with domain decomposition and a multigrid solver can be effectively used to solve systems with over 4 million unknowns and strongly heterogeneous conductivity for their two-dimensional saturated groundwater flow simulation. Saied and Mahinthakumar (1998) presented parallel multigrid solvers for large-scale linear systems arising from the finite-element discretization of a three-

dimensional steady-state groundwater flow problem. Cheng et al. (1998) used multigrid methods to solve two existing three-dimensional finite-element subsurface flow and transport models. Li et al. (2000) combined multigrid methods and adaptive local grid refinement to solve a three-dimensional density-dependent groundwater flow and substrate transport model. Jones and Woodward (2001) used multigrid methods as preconditioners and Newton-Krylov solvers to solve a nonlinear, variably saturated groundwater flow problem. Note that all of these papers dealt with only a simulation model, but not a coupled simulation and optimization model, so standard multigrid solvers could be used.

2.2.2 Multiscale Methods for Optimization Problems

Solving optimal control or optimization problems using multiscale methods, however, is much more difficult than solving PDEs alone. One of the multiscale optimal control methods, called "one-shot" full multigrid minimization method, can be found in the field of optimal shape design (OSD) of aerodynamic systems, such as designing wing shapes (Ta'asan 1991; Arian and Ta'asan 1994a). This optimal control problem is governed by a set of elliptic equations and is solved by using an adjoint method based on a Lagrange multiplier method. The control variables are located on the boundary. Again, the state equation is treated as an equality constraint and the resulting KKT linear system was solved using multigrid solvers. Their "one-shot" method was applied to a two-dimensional OSD problem with a finite element discretization and showed efficient convergence behavior that was independent of mesh sizes (Arian and Ta'asan 1994b). Schulz and co-workers (Dreyer et al. 2000; Maar and Schulz 2000) developed similar

multigrid approaches as Ta'asan (1991) to solve the resulting KKT linear system. Both the SQP-like optimization algorithm and interior point optimization algorithm were used in their papers. The applications presented in their papers are again optimal shape design problems arising in structural truss topology design and turbine blade design.

Nash and his co-workers (Nash 2000; Lewis and Nash 2000) proposed a multigrid approach for discretized optimization problems constrained by PDEs. Their method focuses on applying the multigrid method to the whole optimization problem. However, there are no inequality constraints present in their example problems and the governing equation is a single PDE, not coupled systems of PDEs with nonlinearity. The objective function in their examples is explicitly related to the discretization of the state variables, so that at different level of discretization, a different value of objective function can be obtained. This type of objective function is not applicable to the groundwater bioremediation optimal control problem considered in this work.

Within the context of stochastic control, several papers have used multigrid methods. Akian et al. (1988) developed a full multigrid Howard (FMGH) algorithm for solving a continuous-time stochastic control problem using dynamic programming. Hoppe (1986) applied a multigrid method for solving Hamilton-Jacobi-Bellman equations arising in a continuous-time optimally controlled stochastic process. Both Akian and Hoppe used multigrid methods as a PDE solver to solve the elliptic PDE (the objective function) in their problems. Chow and Tsitsiklis(1991) presented an optimal one-way multigrid version of a successive approximation algorithm for solving a discrete-time continuous-state discounted-cost Markov decision problem, in which the

objective function is an integral equation. The problem is solved on a coarse grid initially and then the coarse grid solution is used as a starting point for the solution on a finer grid. Their method goes from the coarsest grid to the finest grid with most of the work taking place on coarse grids.

For these stochastic control problems, the multigrid methods are used in the objective function space, where the objective function (elliptic PDE or integral equations) is the computational bottleneck. However, in our problem, the computational burden is associated with calculating derivatives in the state variable space (see Chapter 3 for details). The number of control variables (pumping rates) is far less than that of state variables (hydraulic heads and concentrations at each node of the numerical mesh). Unlike previous multiscale studies, the objective function in our problem is quite easy to compute and requires no discretization. Hence, our method focuses on reducing the computational effort associated with state-space computations.

Another example of multiscale optimization is in neural networks optimization (Mjolsness et al., 1991). A general neural network objective function for continuous neural variables is composed of a sum of linear, quadratic, and cubic terms. An ordinary network can be transformed into a multiscale network by the addition of smaller and cheaper approximating networks at successive scales, with associated objective functions. Mjolsness and co-workers achieved a speedup of a constant factor (between 2 and 5), which is independent of the problem size, compared with the original single-scale computational work. Again note that this type of multiscale optimization also deals with only the objective function space.

There exists another well-known research field called multilevel optimization (Migdalas et al.1998) that is sometimes confused with multiscale methods. A typical multilevel optimization problem has a hierarchy of decision-makers and decisions are made at different levels in this hierarchy. Thus, this approach is entirely different from the above-mentioned multiscale methods.

2.3 Applications for Groundwater Remediation Design

This section briefly reviews the optimization methods that have been used for pump-and-treat and in-situ bioremediation design. The focus of this review is on applications of derivative-based optimization techniques, since that is the approach for which the multiscale methods developed in this work are most applicable.

Optimization techniques have been applied primarily to traditional pump-and-treat remediation design. Derivative-based nonlinear programming methods include the work by Ahlfeld et al. (1988), Merckx (1991), Bear and Sun (1998) and many others. SALQR (Chang et al. 1992; Mansfield and Shoemaker 1999) and SALQR with management periods or quasi-Newton methods (Culver and Shoemaker 1992, 1993) have also been used to find time-varying optimal pumping policies. Other applications of SALQR and DDP in the water resources field include multireservoir control (Murray and Yakowitz, 1979), groundwater quantity management (Jones et al., 1987), estuarine management (Li and Mays, 1995) and sedimentation control in reservoir-river systems (Carriaga and Mays, 1995).

In dealing with the calculation of the derivatives, analytical derivatives (Chang et al. 1992; Culver and Shoemaker 1992; Mansfield and Shoemaker 1999), discrete adjoint method (Merckx, 1991; Ahlfeld, 1988), discrete sensitivity equations method (Merckx 1991) and finite-difference approximations (Ahlfeld et al.1986; Gorelick et al.1984) have been used. The derivative calculations required a substantial amount of computing time in all of these applications. For example, Ahlfeld et al. (1988) showed that for a test case in his paper, about 11 hours were devoted to the calculation of the derivatives using the adjoint sensitivity method and 15.9 hours for running the simulation model. Only a fraction of 1 hour was used for the remaining operations of the optimization algorithm. Whiffen (1995) showed that one-sided finite difference approximations to the derivatives needed in SALQR took about 29 times the computing time required to compute the same derivatives analytically, and that derivatives computed using automatic differentiation took about 3 times the CPU of analytical derivatives.

Due to the nonlinearities related to biomass growth, a substantially finer mesh is required for in-situ bioremediation than for pump-and-treat design. This causes the computational challenges mentioned in Chapter 1. Minsker and Shoemaker's SALQR model (1996) was the first application of formal optimization methods to in-situ bioremediation design. Yoon and Shoemaker (1999) compared the computational performance of eight different optimization methods, including SALQR, for groundwater bioremediation design, and claimed that SALQR was consistently faster on all of the example problems, but is not necessarily the most accurate method. However, note that the size of the two examples presented in Yoon and Shoemaker's paper is rather small

(case 1 only has 90 grid points and case 2 only has 162 grid points). As mentioned in Chapter 1, the poor scalability of the SALQR algorithm prevents application to large-scale problems, but has less effect when the problem size is small. Investigation of multiscale technique to allow application SALQR to middle- and large-scale problems is the focus of this research work.

2.4 Summary

In this chapter, we have surveyed existing work on PDE-constrained optimization problems, multiscale methods in simulation and optimization, and derivative-based optimal design for groundwater pump-and-treat and in-situ bioremediation. As a frontier problem in computational science and engineering, PDE-constrained optimization poses a computational challenge even for the most advanced supercomputing power available today. Multiscale methods have been found very efficient for handling very large-scale simulation modeling, but very few examples were found in PDE-constrained optimization. In subsequent chapters, we develop innovative multiscale methods for optimal design of groundwater in-situ bioremediation. Solving large-scale optimal bioremediation design problems is expected to be highly rewarding, since substantial cost savings could be achieved at large complex field sites if optimal designs can be used. The methods developed in this work are also expected to be applicable for other PDE-constrained optimization problems.

Chapter 3

Analysis of Computational Effort of Optimal In-Situ Bioremediation Design

This chapter will analyze the computational effort associated with both the forward sweep and backward sweep in the SALQR method, which will reveal the exact computational bottleneck of the existing model.

3.1 Previous Work

Earlier work on the computational complexity analysis of SALQR and DDP has mainly focused on demonstrating the linear growth rate of the algorithm with respect to the time steps, although the cubic growth rate of the computational complexity with respect to the number of state variables and control variables has also been shown in the theoretical analysis (Yakowitz and Rutherford 1984; Liao and Shoemaker 1991). However, their analysis has mainly focused on the steps that involve updating the search directions, but not the derivative calculations (see Appendix D for more details on these steps). Analytical derivatives have been used in both pump-and-treat and bioremediation design in previously published SALQR models for groundwater remediation. For the pump-and-treat remediation design, Mansfield et al. (1998) and Mansfield and

Shoemaker (1999) reduced the computational complexity of calculating the first derivatives of the transition equation with respect to the state variables by utilizing the sparsity of the matrices. However, no complexity analysis for the management period derivative calculations was presented in their papers. Culver and Shoemaker (1992) presented derivative calculations for both simulation period derivatives and management period derivatives in pump-and-treat design. They found that in their application the calculation of the derivatives over management period requires less work than in the general case. No complexity analysis in terms of growth rate was given for the management period derivatives, although the overall cost for calculating derivatives was described as $O(N^3)$, where N is the number of state variables. Minsker and Shoemaker (1996) presented detailed derivation of the analytical derivatives of the bioremediation transition equation used in this work with respect to the state and control variables, but no computational complexity analysis was presented. Minsker and Shoemaker (1998a) performed experimental analysis to show that up to 98% of the computing time was used in the backward sweep. However, no detailed analysis was presented to discover the exact computational bottleneck.

SALQR is a derivative-based optimization technique that requires the first and second derivatives of the objective function, penalty function, and constraints and the first derivatives of the transition equation. Derivatives of the objective function, penalty function and constraints are usually easy to calculate and thus analytical derivatives are used. Since the transition equation is often a numerical model such as a finite-element or finite-difference simulation model for groundwater remediation design, it is a challenging

and computationally expensive task to calculate the analytical derivatives of the simulation model. The following sections present analysis that reveals the exact computational bottleneck of the bioremediation optimal control model studied in this work.

3.2 Theoretical Analysis of the Computational Effort

As discussed in Chapter 1 (and detailed in Appendix D), SALQR is an iterative method that consists of two steps: forward sweep and backward sweep. The forward sweep simply involves running the simulation model under the current pumping policy. To approximate the original continuous partial difference equations given in Appendix A, the simulation model uses a linear basis function in space with an approximation accuracy order of $O(h)$), where h is the spatial grid size. A fully-implicit backward-Euler differencing method is used in the time stepping scheme (except for the reaction terms, which are explicit) with an approximation accuracy order of $O(t)$, where t is the simulation time step. The current model uses a banded Gaussian elimination direct solver in LAPACK (subroutines `DGBSV` or `DGBTRF` and `DGBTRS`) to solve the discretized system of equations. The complexity associated with these direct solvers is $O((s+1)^2N)$, where s is the bandwidth (e.g. for a tri-diagonal matrix, s=1; see the definition in Iserles's book (Iserles 1996)) and N is the total number of state variables. For this application, the forward sweep consumes less than 5% of the total CPU time for solving the SALQR model.

In the backward sweep, a quadratic approximation of the "cost to go" function, which is the total cost from the current management period to the end, is made at each management period running backwards from K to 1, where K is the number of the last management period. Several matrices, such as A_k, B_k, C_k, D_k, E_k…., (see Appendix D for the definition of these matrices), must be calculated in each management period during one iteration of the optimization procedure. However, these matrices themselves require the first and second derivatives of the transition equation (i.e. ∂Y/ ∂X and ∂Y/∂U in Appendix C), the objective function, and the constraints to be evaluated. The derivatives of the objective function and constraints are easy to calculate analytically, but the derivatives of the transition equation are quite complex. Hence, the transition equation (i.e., simulation model) is linearized when calculating the derivatives so that at each management period a linear quadratic regulator (LQR) is solved using the first-order necessary condition of optimality. With this approximation, the backward sweep is equivalent to the stagewise Newton's method (Murray and Yakowitz 1984; Dunn and Bertsekas 1989; Pantoja 1988). However, the linearization of the transition equation leads to a deterioration of the convergence rate of the DDP method, which has a quadratic convergence rate, because the Hessian matrix of the original optimal control problem (OCP) will not typically come close to that of the OCP with the linearized transition equation (Murray and Yakowitz, 1984).

Previous numerical experiments (Minsker and Shoemaker1998a) found that about 95~98% of the total computing time were spent on the backward sweep. Our further analysis of the CPU time distribution found that more than 90% of the total time on the

backward sweep was actually used on the calculation of the first derivatives of the transition equation with respect to the state variables and control variables over each simulation period and management period. This is the bottleneck of this model.

This computational bottleneck is caused by the current two-step method used to calculate the first derivatives of the transition equation. The first step of the method is to calculate the derivatives within each simulation time period, which involves a matrix inversion and multiplication of a dense and a banded matrix. These operations involve $O(N^3)$ computational complexity (see equations (21), (26)-(28), (32), (35)-(37), (41), (44)-(46) and (50) in Minsker and Shoemaker 1996), where N is the total number of non-Dirichlet state variables. The second step of the method is to use the product rule for differentiation to obtain derivatives across each management time period, since each management period consists of several simulation time steps (the number of simulation time steps within one management period can be denoted as d). This involves multiplication of matrices of dimension N by N, with $O(N^3)$ computational complexity (see equations (13) and (14) in Culver and Shoemaker 1992). The sparsity pattern was lost in these approaches because of the matrix inversion and multiplications. See Appendix C for the details of the first derivative calculation at each simulation period and management period.

To find the updated control policy in each management period, matrices A_k, B_k, C_k, D_k, E_k , P_k, Q_k (see Appendix D for the definition of these matrices) must be calculated. However, only matrix A_k has a computational effort of $O(N^3)$; others are only on the order of $O(N^2m)$, or $O(Nm^2)$ or $O(m^3)$, where m is the number of control variables.

Since the number of state variables (N) is usually much larger than that of control variables (m) for this application, we know that $N^3>>mN^2>>Nm^2>>m^3$. Although the calculation of matrix A_k has a computational complexity of $O(N^3)$, it is only calculated once in each management period. Thus, its contribution to the total computing time is less important than the calculation of the first derivatives of the transition equation. This can be further demonstrated by the subsequent experimental analysis.

3.3 Experimental Analysis of the Computational Efforts

To illustrate the bottleneck of the computing time, the CPU time distribution is derived for an example with 6 management periods. Each management period consists of 30 simulation time steps. The number of non-Dirichlet state variables N is 335 and the dimension of the control variables m is 5.

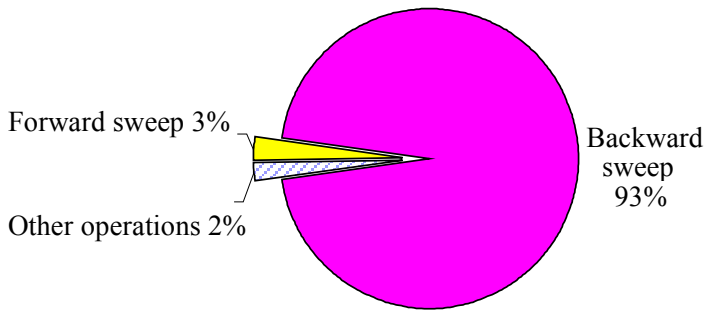

Figure 3.1: CPU time distribution of SALQR model with 6 management periods

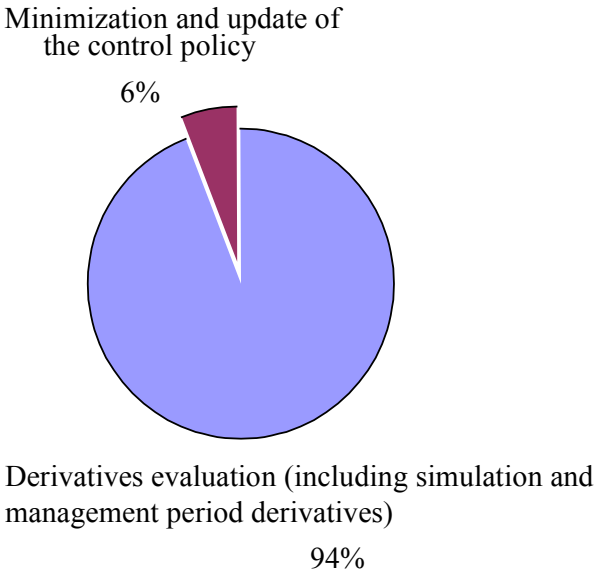

Figure 3.2: CPU time distribution in one management period of the backward sweep

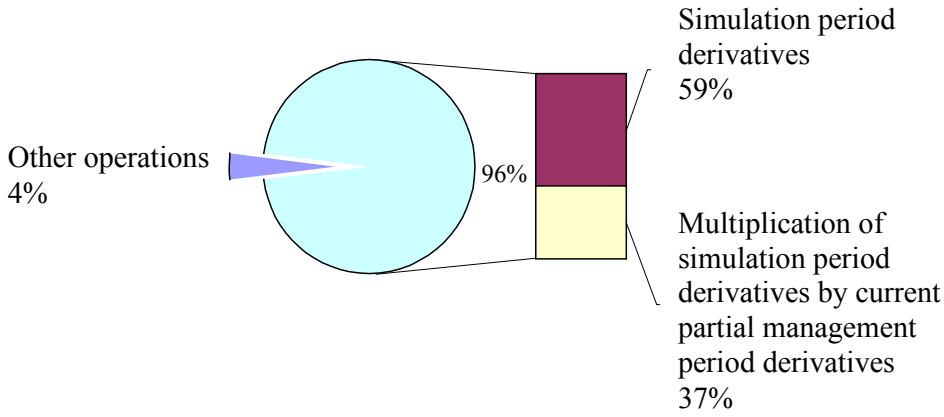

Figure 3.3: CPU time distribution in one simulation period derivative evaluation (within one management period of the backward sweep)

As can be seen in Figure 3.1, about 93% of the total computing time was spent on the backward sweep, while only 3% of the total time was used in the forward sweep. Figure 3.2 shows that within each management period of the backward sweep, about 94% of the computing time was used to calculate the first derivatives of the transition equation with respect to the control variables and state variables, which includes the calculation of both the simulation and management period derivatives. Figure 3.3 shows that in one simulation period, about 59% of the computing time was used to calculate the current simulation period derivative, which is the first step in the current two-step method described above, while 37% of the time was used to obtain the partial management period derivatives, which is the second step in the two-step method.

3.4 Summary

A detailed analysis presented in this chapter reveals the exact bottleneck of the SALQR model, which is the two-step analytical derivatives calculation. The management period formulation is essential for in-situ bioremediation, because the short simulation periods (such as a half day) required to accurately model in-situ bioremediation would be impractical for changing the pumping rates. However, the two-step analytical management period derivatives approach developed in previous work exhibits a computational complexity of $O(N^3)$, where N is the number of state variables. Our experimental results further showed that more than 90% of the CPU time was spent on the derivatives calculation. The multiscale methods presented in subsequent chapters are

developed to alleviate this computational bottleneck and enable large-scale solution of bioremediation design problems.

Chapter 4

One-way Spatial Multiscale Method

This chapter describes the one-way spatial multiscale method for optimal in-situ bioremediation design. As shown in the previous chapters, the fundamental barrier of applying the current optimal control model to large-scale groundwater remediation is the cubic growth rate of the computing time with respect to the number of state variables. In order to overcome this barrier, several spatial multiscale methods are developed and tested in Chapters 4-7. This chapter presents the first method, which solves the optimization problem by using a coarse grid optimal solution as a starting point for finer grid optimization. Since this method is designed to treat the optimization problem as a whole, it is applicable to any PDE-constrained optimization problem as long as the governing PDEs can be spatially discretized into different scales.

4.1 Description of the Methodology

4.1.1 Basic Idea

As indicated by Minsker and Shoemaker (1998a), the single-grid version of their model is computationally intensive and field scale modeling is not possible at present. Table 4.1 lists the estimated computing time for one iteration of the single-grid model

with different numbers of nodes. The estimated CPU time is based on an NCSA SGI/Cray Origin2000 supercomputer using serial code. It's clear that the computing time increases dramatically when the total number of nodes in the finite element mesh increases. This means that even with cutting edge computing power, a relatively large-scale domain cannot be modeled in a reasonable time period. However, Table 4.1 also tells us that if initially we do some iterations on the coarse mesh and then use the result of control policy obtained on the coarse mesh as an initial guess on the finer mesh, we could save some computing time in the fine mesh. In principle, this idea is called nested iteration. As stated by Joppich and Mijalković (1993), nested iteration involves finding a reasonable initial guess for a finer grid iteration by computing approximations on coarser grids that are successively interpolated to finer grids. This idea has been used successfully to solve PDEs within the full multigrid (FMG) method in the literature (Joppich and Mijalković 1993). A variant of FMG, one-way multigrid, proceeds "one-way" from a coarse level to a fine level by interpolating the results at the coarser level to a finer one without coarse grid correction. As pointed out by Douglas (1996), one-way multigrid algorithm has been the standard method for combustion problems for at least 25 years and is very effective for hard engineering problems. The nested iteration principle was also applied together with successive over relaxation (SOR) method for solving a two-dimensional Laplace equation (Kronsjö and Dahlquist 1971). We developed a one-way spatial multiscale method that combines the nested iteration principle with the SALQR method. Details on the method are given in the following sections.

Table 4.1: Estimated CPU time per iteration for different number of nodes

Number of Nodes (1)	CPU time per iteration (2)
6321	885 days
1625	15 days
429	6.6 hours
119	8.5 minutes
36	17 seconds

4.1.2 Discretization Procedure

To construct multiple scales of the optimal control model (see Equations (1.1) to (1.4) in Chapter 1), we need to describe how to do the discretization procedure. Since the simulation model Bio2D (see Appendix A) is a two-dimensional finite element model, the multiple scales can be built by discretizing both the simulation model in the forward sweep and its derivatives, which are calculated in the backward sweep, using different uniform mesh sizes. Initially, the simulation model can be discretized using grid size h to construct the coarsest level mesh. Then, for all finer levels, we can successively refine the mesh uniformly by rescaling the grid size ($h \rightarrow h/2$). Let L be the level of the mesh, where smaller L stands for a coarser mesh. The mesh size on level L is $h*2^{-L}$, $L = 0$ being the coarsest level. Then the total number of elements at level $L+1$ is the quadruple of that at level L. A graphical representation of this refinement process can be seen in Figure 4.1, where one element at level L is equally divided to four elements at level $L+1$.

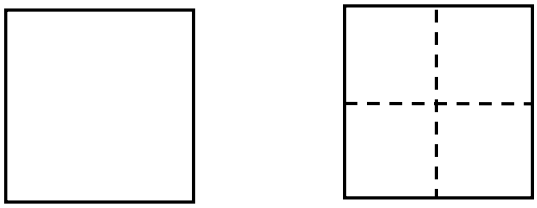

Level *L* **Level *L+1***

Figure 4.1: Mesh refinement

4.1.3 Interpolation Procedure

As can be seen from the problem formulation presented in Chapter 1, there are two kinds of variables that are defined on the single-grid model: control variables and state variables. To utilize the nested iteration principle, we need an interpolator to translate the results from coarse grids to finer grids. Let P_1 be the interpolator for the state variables and P_2 be the interpolator for the control variables. Following the notation in Stüben and Trottenberg (1982), for state variables, we use the standard bilinear interpolator, which can be represented by the stencil shown in Figure 4.2. This bilinear interpolator works in the fashion illustrated by Figure 4.3. In Figure 4.3, the "+" stands for the nodes shared by both the coarse mesh and the fine mesh and the "×" stands for new nodes on the fine mesh that need to be interpolated. In other words, there are 4 corner points, 4 edge points and 1 center point in the fine mesh and only the edge points and center point need to be interpolated. The number (1/2) above the arrow shows how much the weight of the value contributes to the interpolated value indicated by the arrow. Figure4.3 (a) shows the first step of the interpolation. The edge points at the top and bottom are interpolated first. Figure 4.3(b) shows the second step. The remaining edge points and the center point are interpolated at this step.

For control variables, we use identity operator, $P_2 = I$, which means that the dimension of the control variables do not change at different scales because we define the control variables on the coarsest grids. For applications where this is not possible, methods for interpolating well pumping rates must be used (see, e.g., Huang and Mayer 1997).

$$\frac{1}{4}\begin{bmatrix}1 & 2 & 1\\ 2 & 4 & 2\\ 1 & 2 & 1\end{bmatrix}_{h}^{h/2}$$

Figure 4.2: Stencil of bilinear interpolator

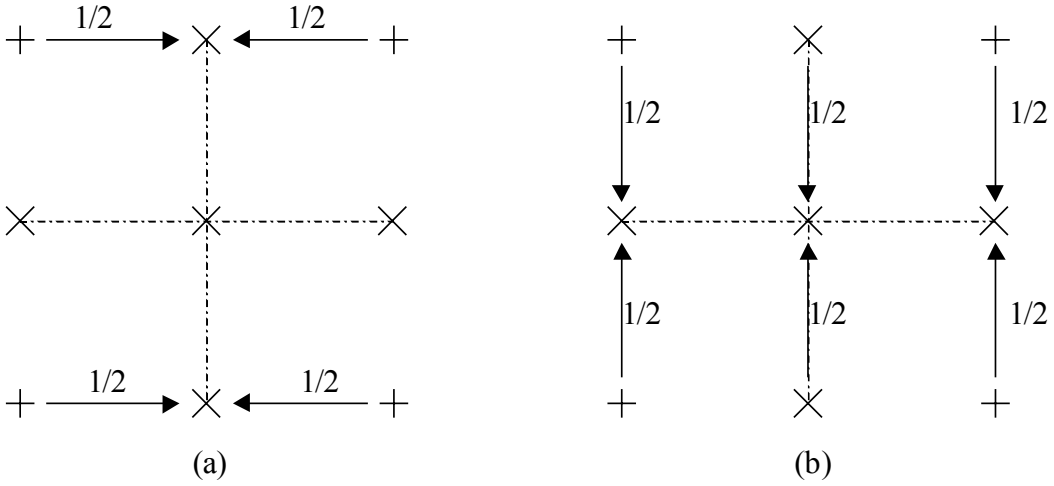

Figure 4.3: Two steps of standard bilinear interpolator

4.1.4 Algorithmic Description

To summarize the above description, the one-way spatial multiscale method can be described using a flow diagram shown in Figure 4.4. Starting from the coarsest level, where the whole problem is defined, the model is first solved to convergence using SALQR method. After that, a mesh refinement is performed to construct a finer mesh and the interpolation procedure is conducted to transfer the initial state variables and control variables to the finer level. SALQR is used again to solve the whole optimization problem on the finer level. Depending on how many levels we wish to solve, we can carry out the same procedure again until we reach the predefined finest level. The final optimal control policy is then found on the finest mesh. The goal of this multiscale approach is to preserve the solution accuracy while reducing the computing time significantly.

4.2 Application of One-way Spatial Multiscale Method

In the following, the one-way spatial multiscale method presented above will be applied to a test site. The application is intended to show the advantages of the methodology. The test site is adapted from the Borden aquifer, Ontario, Canada, which has been extensively studied in the literature (see, e.g., Mackay et al.1986; Graham and McLaughlin 1991).

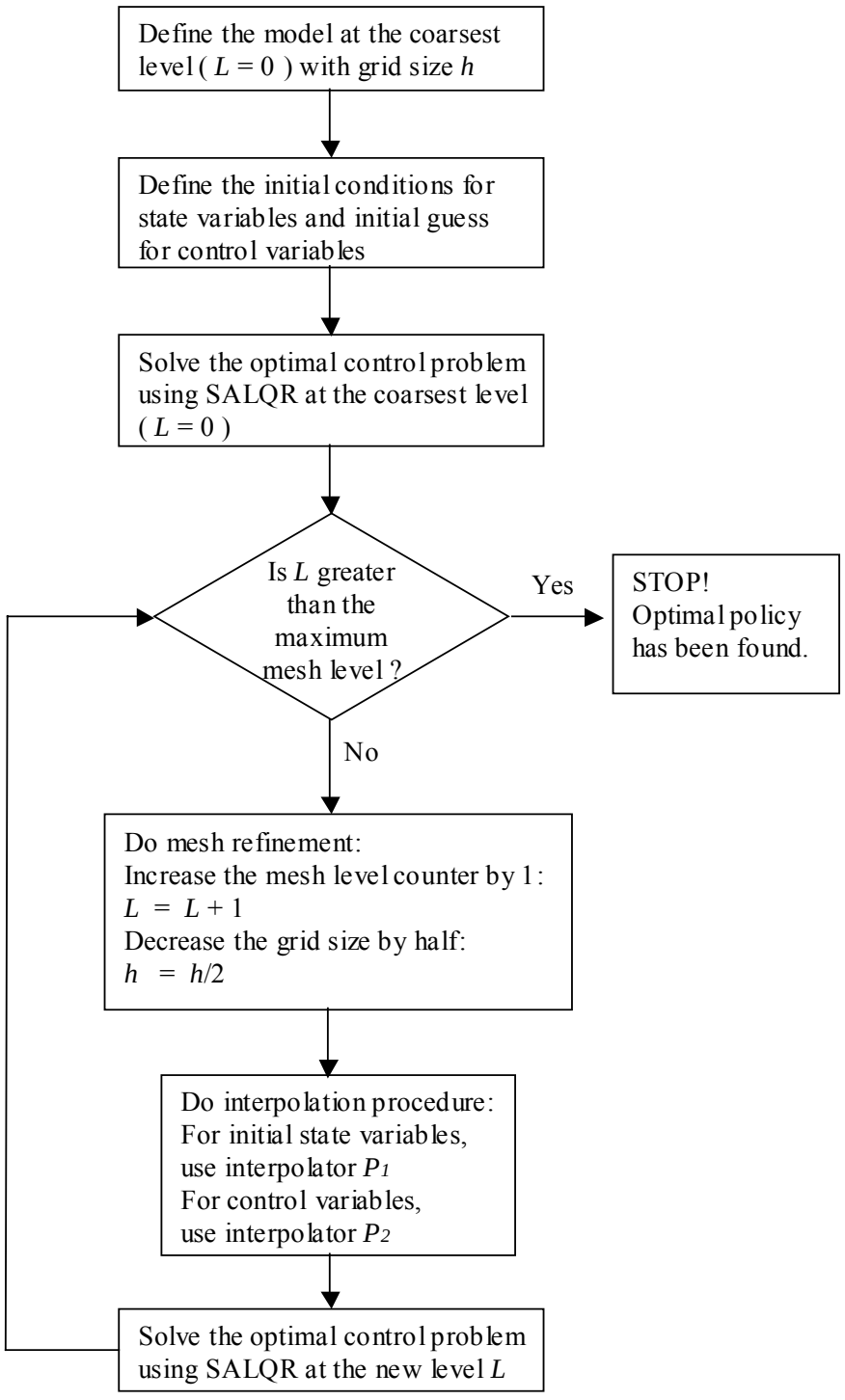

Figure 4.4: Flow diagram for one-way spatial multiscale method

4.2.1 Description of the Test Site

A plan-view schematic of the site with the coarsest mesh is shown in Figure 4.5. The domain size is 160 m in the x-direction and 120 m in the y-direction, resulting in a total area of 19,200 m^2 . The boundary conditions are also shown in Figure 4.5. The potential injection wells are well numbers 1-8 and the potential extraction wells are well numbers 0 and 9.

The physical parameter values for the aquifer and the site are given in Table 4.2 (hydraulic conductivity, porosity, aquifer thickness, and soil bulk density) and were taken from Graham and McLaughlin (1991). The values of longitudinal dispersivity (α_L) and transverse dispersivity (α_T) were chosen based on the recommendation by Gelhar et al. (1992). As indicated by Gelhar et al., the reliable ratio of α_L/α_T is about 3 to 10 for modeling field scale in the range of 100 m, the reliable value for α_L is about 10 m, and the reliable value for α_T is around 1 m. The lower dispersivity values (α_L = 9.8 m, α_T = 1.7 m) in Table 4.2 were what we intended to model. However, we encountered convergence difficulties with these values at the coarse levels, so we also considered relatively large dispersivity values (α_L = 15.55 m, α_T = 3.4 m). The biological parameters were selected for phenol and were taken from the literature (Minsker and Shoemaker 1998b). The operating parameter for oxygen concentration in the injection water is assumed to be 8 mg/L, which is consistent with the normal dissolved oxygen concentration in water (Minsker and Shoemaker 1998b). The time step used in the simulation model was chosen to ensure that the Courant number is no more than one for the range of pumping rates tested in the simulation model during the optimization run,

thus minimizing the numerical errors caused by the time stepping scheme. The Peclet number is only required to be within two at the finest level since multiple spatial meshes will be used and only the finest level is guaranteed to meet the spatial accuracy requirement.

The initial phenol concentration profile is depicted in Figure 4.6 on the finest mesh and shows an initial peak concentration of 40 mg/L. Initial oxygen and biomass concentrations were assumed to be 3 mg/L and 0.0026 mg/L, respectively, at all nodes. Concentrations of phenol, oxygen, and biomass were assumed to be evenly distributed in the vertical direction, so that the use of the two-dimensional depth-averaged simulation model Bio2D was justified.

This site is assumed to be cleaned up in 6 months and is operated in 6 management periods, which means that the pumping rates can be changed every month. The relatively short duration and small domain were selected for this test case so that the multiscale results could be compared with results solved fully on the finest scale without excessive computational effort. The water quality standard is chosen to be no more than 1 mg/L phenol. The contaminant concentration located at the free flow boundary (on the right in Figure 4.5) must be maintained to be less than 1 mg/L in all of the management periods. At the end of the cleanup, contaminant concentration at all the nodes on this site must meet the water quality standard.

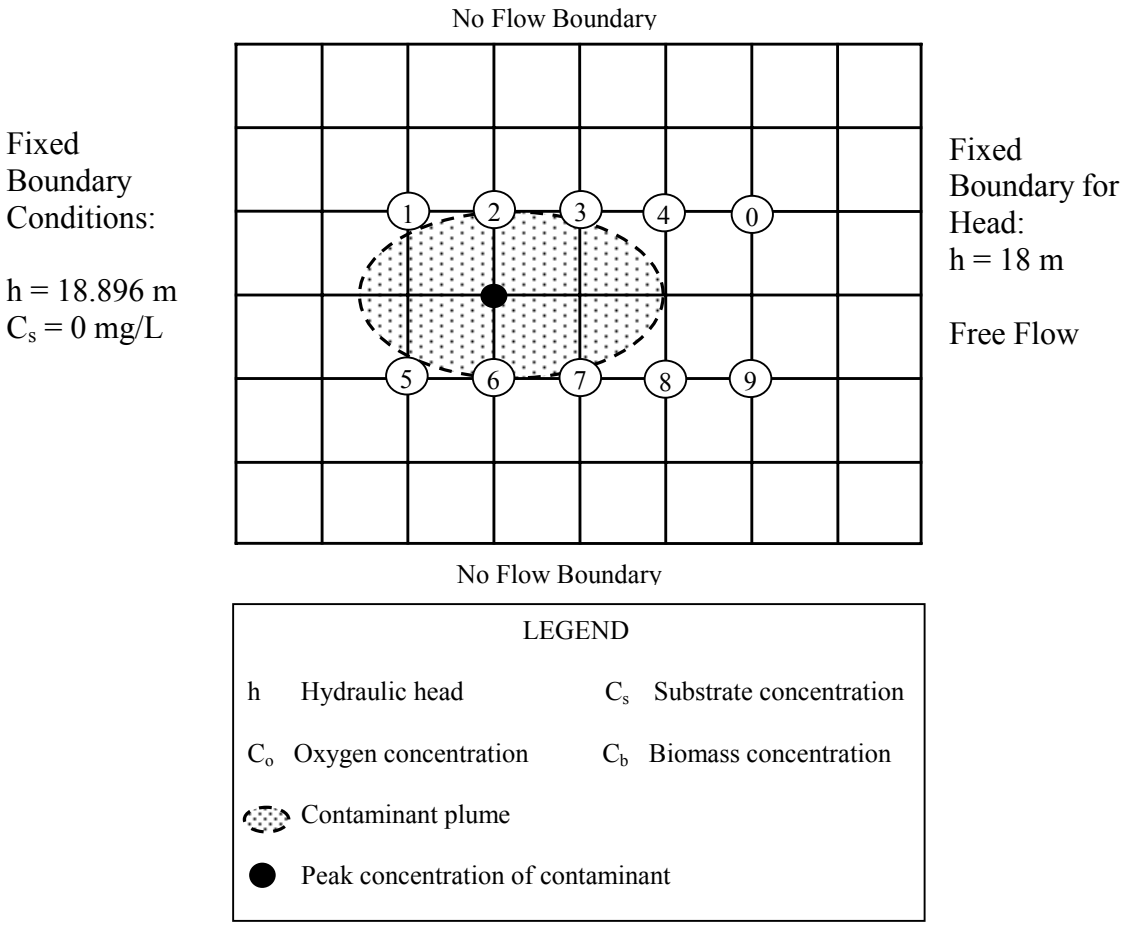

Figure 4.5: Plan view schematic of the test site

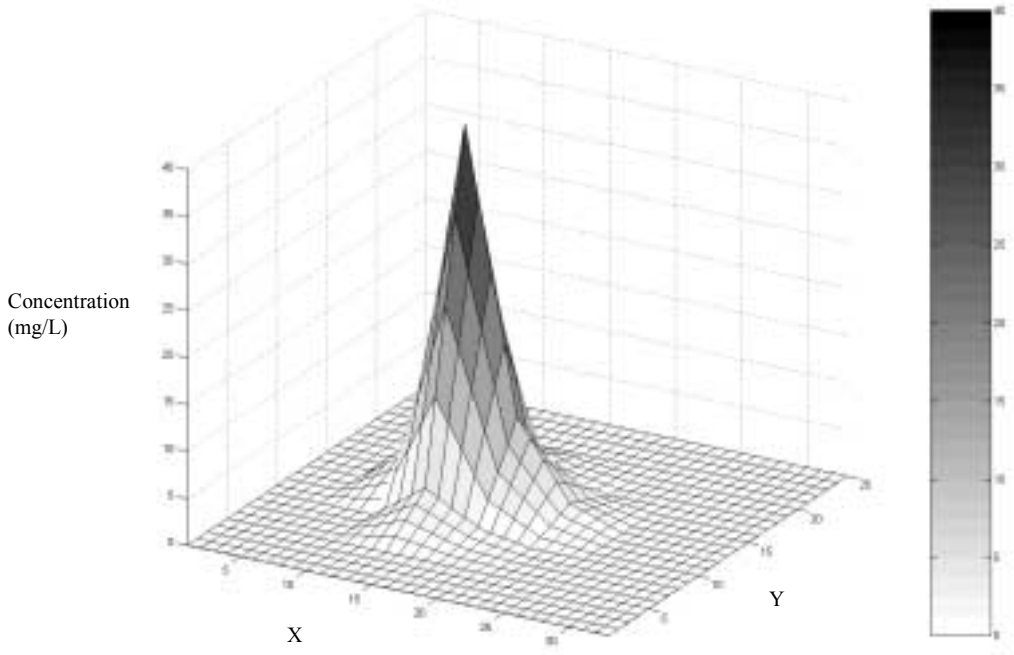

Figure 4.6: Initial contaminant plume at the test site

Table 4.2: Aquifer, operating, and biodegradation parameters for the test site

Parameter (1)	Value (2)
Contaminant	Phenol
Hydraulic conductivity K_h	6.18 m/day
Hydraulic gradient J	0.0056
Porosity θ	0.33
Aquifer thickness b	9 m
Longitudinal dispersivity α_L	9.8 m **(**15.55 m**)**
Transverse dispersivity α_T	1.7 m (3.4 m)
Time step Δt	12 hours
Oxygen concentration in injection water C_o'	8 mg/L
Substrate Retardation factor Rs	1.04
Soil bulk density ρ_b	2.00 g/cm^3
Biomass partition coefficient K_b	2.93 cm^3/g
Maximum specific growth rate for biomass μ_{max}	0.27 /hr
Substrate half-saturation coefficient K_s	49.6 mg/L
Substrate inhibition coefficient K_i	10^{20} mg/L
Oxygen half-saturation coefficient K_o	1 mg/L
Ratio of oxygen to substrate used F_{os}	3.0
Yield coefficient Y_c	0.7031 mg/mg
Endogenous respiration rate for bacteria r_b	2.083×10^{-3} /hr
Background organic carbon concentration c_c	715 mg/L
Background organic carbon utilization rate k_c	4.17×10^{-7} /hr

4.2.2 Three-level Case Study

To test the performance of our one-way multiscale method, a three-level case study was created based on the test site presented above. Note that this problem was actually solved for half of the domain shown in Figure 4.5 because the aquifer properties, concentrations, and well sites are symmetric. The number of elements and nodes in Table 4.3 is only counted for the half-domain.

As can be seen from Table 4.3, Level 1 is the coarsest level and Level 3 is the finest level. The number of elements at Level 2 is quadruple that at Level 1, while the number of elements at Level 3 is quadruple that at Level 2. Within each level, the penalty weight (r in Equation (B.10) at Appendix B) started from the same initial penalty weight and was successively increased to a terminal penalty weight that allowed violations of the substrate concentration constraints (Equations (B.3) and (B.4) at Appendix B) less than 1% of the water quality standard.

Table 4.3: Three-level case study

	Element Size (1)	Number of Elements (2)	Number of Nodes (3)
Level 1	20 m × 20 m	24	36
Level 2	10 m ×10 m	96	119
Level 3	5 m × 5 m	384	429

4.3 Results and Discussions

All of the runs for the case study were conducted on an SGI Origin 2000 supercomputer using only serial code. Numerical results are discussed in the following sections. We first discuss the results for the case with larger dispersivity values (α_L = 15.55 m, α_T = 3.4 m) in the first three sections and then compare them to the case with smaller dispersivities (α_L = 9.8 m, α_T = 1.7 m) in the section that follows.

4.3.1 Objective Function Value vs. Iterations

The objective function value consists of the sum of the pumping costs in equation (B.1) and the penalty value in equation (B.10) (See Appendix B). Pumping strategies that allow water quality violations will result in adding a penalty into the objective function. As can be seen from Figure 4.7, separate runs using the Level 1 mesh and Level 3 mesh starting from same initial random guess result in very similar convergence behavior (in terms of iterations). However, if we use our one-way multiscale approach to solve this problem (i.e., the optimal pumping strategy from Level 1 mesh is used as the initial condition on Level 2 mesh, and then the converged result on Level 2 is again used as the initial condition on Level 3 mesh), the number of iterations needed on Level 3 is much less than that for the standalone run on Level 3, where Level 3 is the most computationally intensive level. A complete run of our one-way spatial multiscale method includes 3 components, i.e., Level 1 , Level 1 to Level 2 and Level 2 to Level 3, as plotted in all the following figures.

Note that the objective function value does not change significantly when interpolating the converged result on Level 2 to Level 3 mesh, which indicates that the optimal solution on the Level 2 mesh is a very good starting solution for the Level 3 mesh. Our later discussion explains why extra iterations were needed after the interpolation. Also note that the significant increase in the objective function value when interpolating the converged result on Level 1 to Level 2 results from penalties associated with the optimal solution on the coarse mesh. After interpolation to the finer mesh, the improvement in numerical errors results in violations of the concentration constraints.

4.3.2 Objective Function Value vs. CPU time

Figure 4.8 shows the computational savings (in terms of CPU time) associated with solving fewer iterations on the fine mesh. It is evident from this figure that the computing effort associated with Level 1 and Level 2 mesh solutions is much less than that of the Level 3 mesh solution. A single run on the Level 3 mesh starting from random initial guess needs about 117 hours, while a single run on the Level 1 mesh with the same initial guess only needs 4.3 minutes. Using our one-way multiscale approach, however, only about 54.5 hours are needed for the same terminal penalty weight (r = 500) to get satisfactory results at Level 3. A terminal penalty weight refers to the last and largest penalty weight r used in equation (B.10) (recall that r in equation (B.10) in Appendix B is successively increased during the model solution). About 53% of the CPU time was saved by using our one-way multiscale approach. Also note that the most CPU time (about 98% of the total) was spent on the finest level (Level 3) for the multiscale approach.

4.3.3 Maximum Violation vs. Iterations

Since we use a penalty function to convert the constrained optimization problem to an unconstrained optimization problem, a penalty value is added to the objective function for constraint violations. Although the objective function values change little from Level 2 to Level 3, Figure 4.9 shows that unacceptable violations of the concentration standards would occur if the coarser mesh solutions were used. Figure 4.9 shows the maximum (i.e., largest) violation occurring in each iteration vs. the iteration number for the different meshes. Note that when the optimal pumping policy obtained on the Level 1 mesh is used as an initial guess on the Level 2 mesh, a significant increase in the maximum violation occurred. The same phenomenon was observed when interpolating from Level 2 to Level 3, although it is not severe as from Level 1 to Level 2. This indicates that numerical errors on the Level 1 and Level 2 mesh did affect the accuracy of the optimal solution. This also explains why 7 iterations are needed on the finest mesh (Level 3) after interpolation to reduce the maximum violations and adjust the optimal solution on the finest mesh to reflect the increased numerical accuracy.

4.3.4 The Impact of Low Dispersivities

In this section, we discuss the results for the case with lower dispersivity values (α_L = 9.8 m, α_T = 1.7 m). We found that at Level 1 and Level 2, starting from various random initial guesses, the case with lower dispersivity values did not converge at all. The significant numerical errors caused by high Peclet numbers at Level 1 and Level 2 led the SALQR algorithm to choose extremely large pumping rates and diverge. To overcome this difficulty, we modeled this case at Level 1 using artificially high

dispersivity values (α_L = 15.55 m, α_T = 3.4 m), then used the optimal results obtained at Level 1 to interpolate to Level 2 and Level 3 using the actual lower dispersivity values. This approach overcame the numerical difficulties caused by low dispersivity values or high Peclet numbers. Although the converged result at Level 1 was obtained using different and large dispersivity values, it still gave a good starting point for Level 2. Due to the overestimation of the dispersivity values at Level 1, however, the maximum violation after the interpolation from Level 1 to Level 2 (about 234%, see Figure 4.10) is significantly larger than that in the previous case using the same dispersivity values at all levels (only 49%, see Figure 4.9).

When we examine the computational savings from using our one-way spatial multiscale approach, about 50.4% reduction in computing time at the finest level was still achieved, as shown in Figure 4.11. Note that because of the higher dispersivity values used at Level 1, the objective function value increased dramatically after interpolation from Level 1 to Level 2. This is consistent with the large violations observed in Figure 4.10.

4.3.5 The Impact of Penalty Weight

During our numerical experiments, we found that, for different terminal penalty weights used in the optimization model (r in equation (B.10) in Appendix B), the result of interpolation was different. If a higher terminal penalty weight is used in the coarse mesh and the converged result from the coarse mesh is used as the initial condition for the finer mesh with the same terminal penalty weight, the number of iterations and CPU time spent on the finer mesh will be about the same as if the model started from an initial

guess on the finer mesh, and the advantage of the initial solution at the coarse scale is lost. Therefore, choosing an appropriate terminal penalty weight is a key consideration in applying this spatial multiscale technique. Our choice of terminal penalty weight is based on observing the maximum violations of substrate concentrations over all the monitoring wells. If the maximum violation of substrate concentration is less than 1% of the standard at the current penalty weight on the coarse mesh, then the penalty weight does not increase any further. When interpolating to a finer mesh, the penalty weight is first decreased to the same initial one used on the coarse mesh, then successively increased to the terminal penalty weight.

To further save computing time on the finest level, which is our target solution, we can halt the run on the finest level early before it converges with the terminal penalty weight. Our halting criteria is that as soon as the maximum violation of substrate concentration is less than 1% of the standard with the terminal penalty weight, we can stop the run and accept that solution. The data presented in the above sections adopted this halting criteria on the Level 3 mesh for both the standalone Level 3 run and the interpolated Level 3 run.

4.4 Summary

We developed a one-way spatial multiscale method for solving an optimal control model of in situ bioremediation of groundwater. The optimization problem is solved with a coarse mesh initially and then the optimal strategy found with the coarse mesh is successively interpolated to finer meshes. Initial state variables in the coarse mesh are

interpolated to finer meshes using a bilinear interpolation operator. Applying this approach to a case study provided computational savings of over 50% compared with the standalone finest mesh solution. This approach also shows advantages for modeling sites with low dispersivities. By using relatively large dispersivities at the coarse levels and then reducing the dispersivities at finer levels, we still achieved computational savings of about 50%. The choice of terminal penalty weight was also shown to be critical to the success of the spatial multiscale method. Good results were obtained when the penalty weight was decreased after interpolation to a finer mesh and when a terminal penalty weight was used that gave a maximum violation of the substrate concentration constraints of less than 1% of the standard.

Our one-way spatial multiscale method shows promise for modeling larger, more complex sites to assist in optimal in situ bioremediation design. The method is also applicable to any other coupled simulation and optimization model in which the simulation model can be discretized to multiple spatial scales.

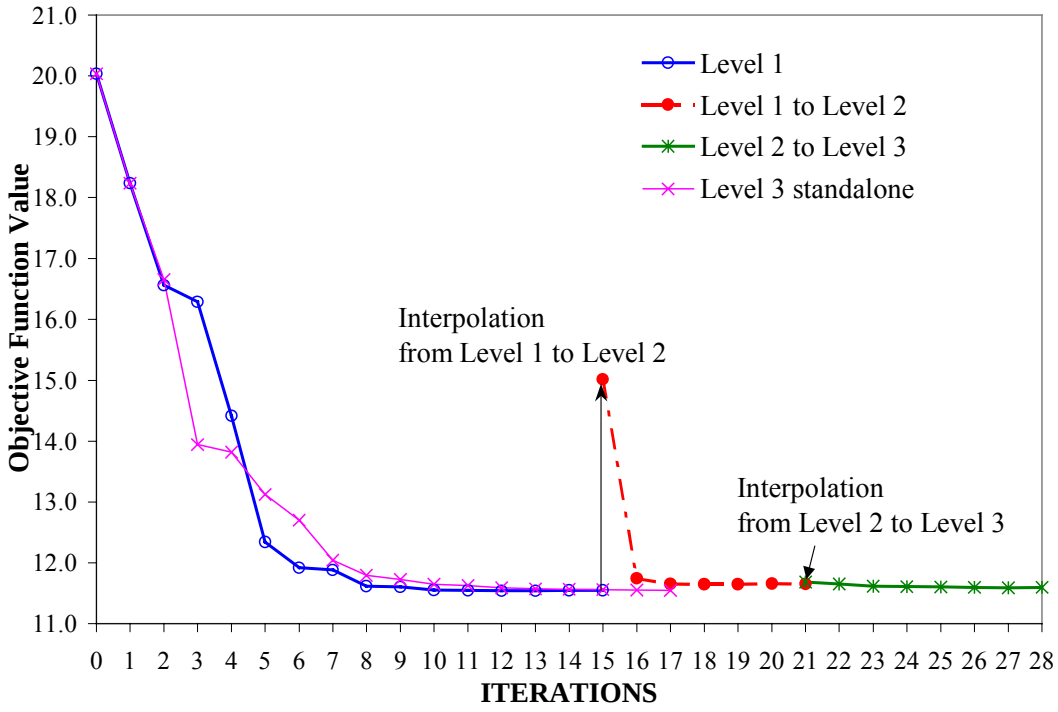

Figure 4.7: Objective function value vs. iterations for the higher dispersivity case

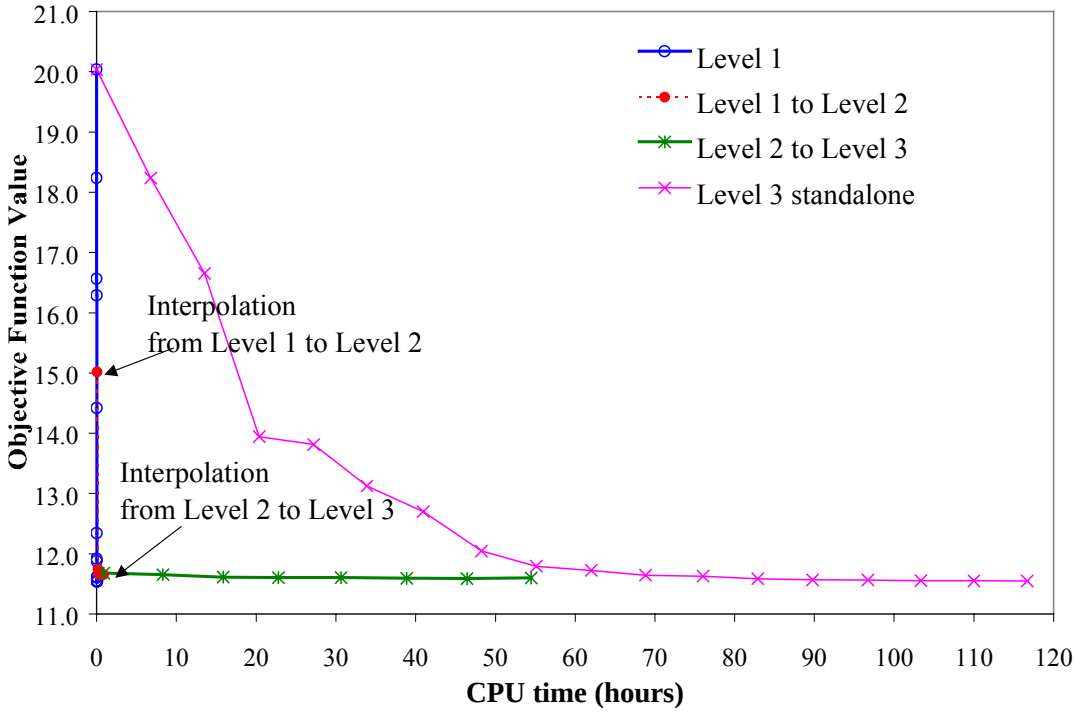

Figure 4.8: Objective function value vs. CPU time for the higher dispersivity case

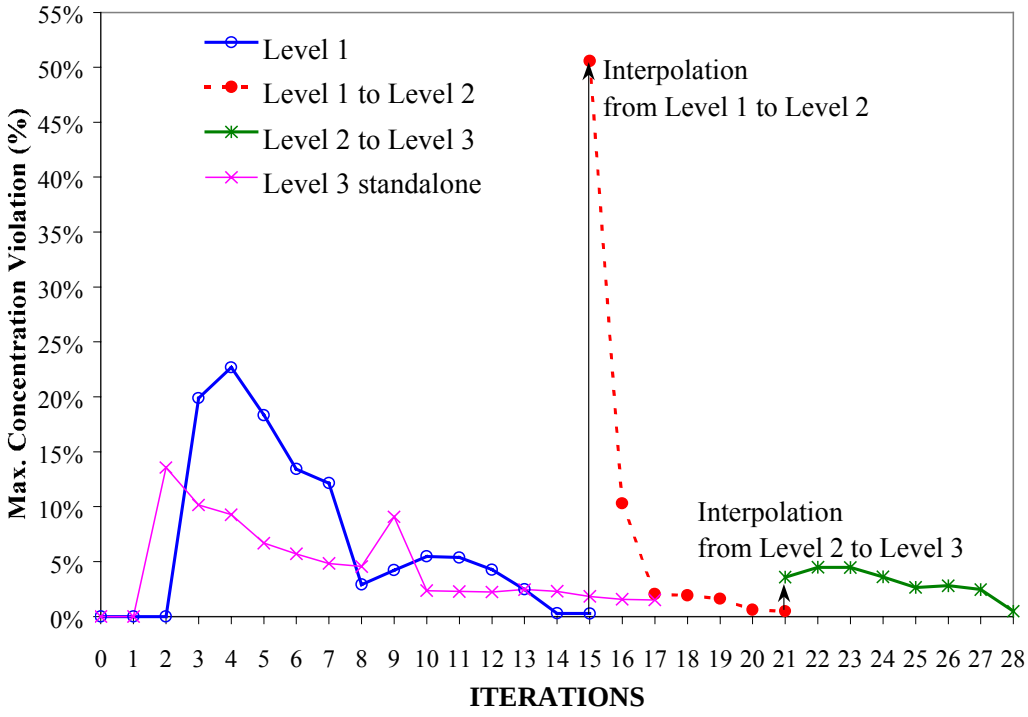

Figure 4.9: Maximum concentration violation vs. iterations for the higher dispersivity case

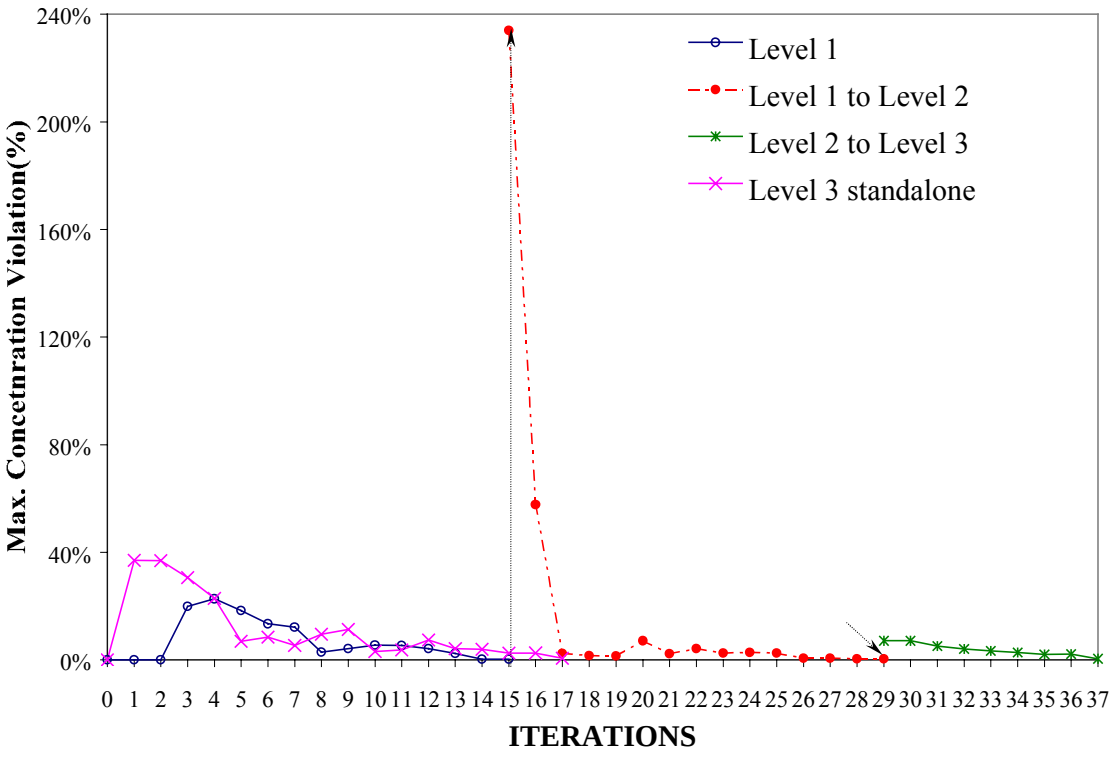

Figure 4.10: Maximum concentration violation vs. iterations for the lower dispersivity case

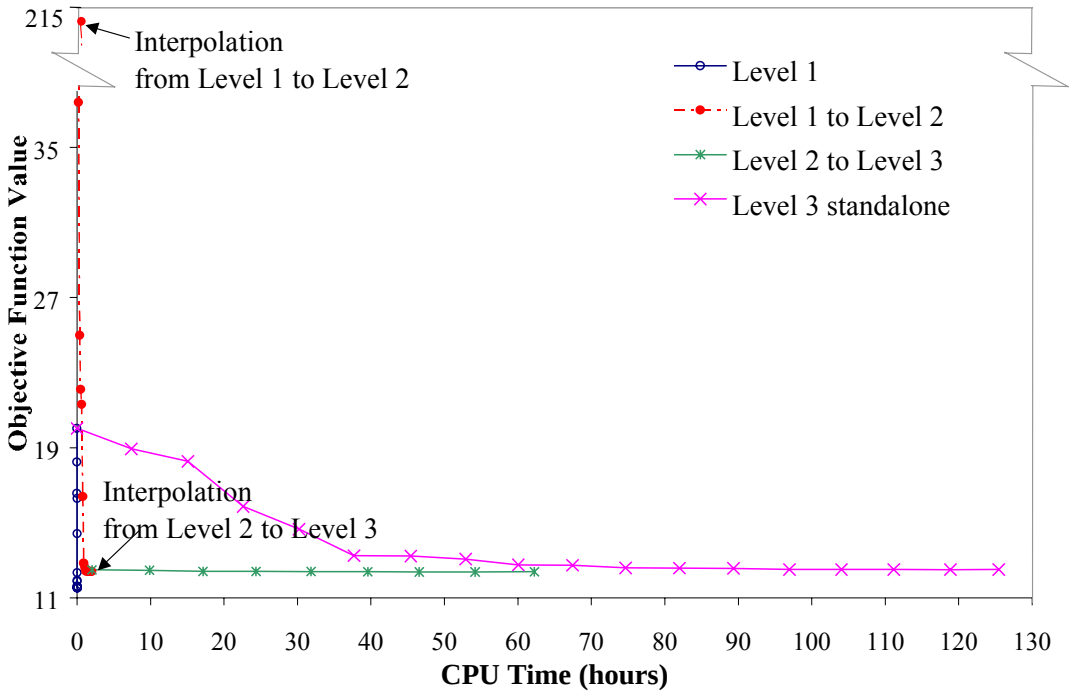

Figure 4.11: Objective function value vs. CPU time for the lower dispersivity case

Chapter 5

Efficient Numerical Derivatives Method

This chapter develops an efficient numerical derivatives method. Developing a numerical derivatives method is necessary to implement the second spatial multiscale method, multiscale derivatives, in the next chapter. We develop a highly efficient implementation of one-sided forward divided difference numerical derivatives that exploits the solution procedure for performing numerical perturbations. Both theoretical analysis and numerical experiments are performed. Note that the one-way spatial multiscale method developed in the last chapter is still applicable when the model uses the efficient numerical derivatives method.

5.1 Description of the Methodology

The major concerns for implementing derivatives in an optimization model are speed, accuracy and ease of implementation, which will be analyzed in the following sections. Our analyses show that our numerical derivatives implementation outperforms the previous analytical derivatives in terms of both speed and ease of implementation, without loss of accuracy.

To understand the advantages of our numerical derivatives method, a brief review of the previous analytical derivatives method is needed. As presented in Chapter 3, more

than 90% of the total CPU time for the backward sweep was used on derivative evaluations. Moreover, the cubic growth rate of the derivatives calculation prohibits solution of any medium- to large-scale problems with several hundred to thousands of nodes within a reasonable time period. Furthermore, the analytical derivatives have to be re-derived each time the simulation model changes, limiting flexibility of the management model. Thus, this approach is human-labor intensive and impractical for complex two- or three-dimensional simulation models.

Despite the above limitations, it is commonly held that analytical derivatives usually provide better accuracy and faster computing times once coded. Whiffen (1995) showed that one-sided divided difference approximations of the derivatives took 29 times the CPU time required to compute analytical derivatives in his SALQR model. Although the implementation details of Whiffen's numerical derivatives were not given, the general belief that numerical derivatives are slower than analytical derivatives is not necessarily true, as will be demonstrated below.

A one-sided divided difference approximation of the derivatives ∂Y/ ∂X and ∂Y/∂U at each management period can be formulated as follows:

$$\left(\frac{\partial Y}{\partial X}\right)_k = \left[\frac{\partial Y}{\partial X_1}\frac{\partial Y}{\partial X_2}\cdots\frac{\partial Y}{\partial X_i}\cdots\frac{\partial Y}{\partial X_{N-1}}\frac{\partial Y}{\partial X_N}\right]_k \tag{5.1}$$

$$\left(\frac{\partial Y}{\partial U}\right)_k = \left[\frac{\partial Y}{\partial U_1}\frac{\partial Y}{\partial U_2}\cdots\frac{\partial Y}{\partial U_j}\cdots\frac{\partial Y}{\partial U_{m-1}}\frac{\partial Y}{\partial X_m}\right]_k \tag{5.2}$$

$$\frac{\partial Y}{\partial X_i} = \frac{Xnew - Xold}{\Delta X_i} \quad , i = 1,\ldots N \tag{5.3}$$

$$\frac{\partial Y}{\partial U_j} = \frac{Xnew - Xold}{\Delta U_j} \quad , j = 1,\ldots m \tag{5.4}$$

where *Xnew* and *Xold* are the state vectors before and after the perturbation respectively, which both have a dimension of N, where N is the total number of non-Dirichlet state variables; subscript i and j are the ith state variable or jth control variable in the state vector or control vector; and the subscript k stands for the management period counter. The dimension of $\partial Y/\partial X_i$ is a column vector of length N. The dimension of $\partial Y/\partial U_j$ is a column vector of length m, where m is the total number of control variables. Each of the k matrices $\partial Y/\partial X$ has dimension N by N and is composed of N vectors of $\partial Y/\partial X_i$ for the kth management period. Correspondingly, each matrix $\partial Y/\partial U$ has dimension N by m and is composed of m vectors of $\partial Y/\partial U_j$ for the kth management period. Since the pumping rates (control vector U) change only at each management period, $\partial Y/\partial X$ and $\partial Y/\partial U$ are only calculated once at each management period k by direct perturbation in one step. This is in contrast to the previous analytical derivatives method, where management period derivatives can only be obtained at the second step after the simulation time step derivatives have been calculated. In the numerical derivatives method, each perturbation requires one run of the simulation model from the beginning of one management period to the end of that management period.

Efficiency of the implementation described previously depends on how the simulation model is run under the perturbation. The most obvious implementation would require re-solving the simulation model without using any information available in the forward sweep of the algorithm, which would certainly be inferior to the analytical derivatives method. The efficient implementation of numerical derivatives presented

herein is based on the observation that, when calculating the first derivatives of the transition equation with respect to the state variables, small perturbations of a single state variable only affect the right-hand-side of the resulting linear system of equations describing the transition equation (after all, running any numerical groundwater fate and transport model can eventually be reduced to solving a linear system of equations). Thus, saving the results of the previous forward sweep and the LU factorization results of the left-hand-side matrix, where the simulation model is run normally, benefits the perturbation run of the simulation model since only the right-hand-side of the system equation need be reformulated and backward substitution applied to obtain the simulation results under the perturbation. This method is general in that it is independent of the simulation model (i.e., remediation technology) used and is much easier to implement than the previous analytical derivatives method. Detailed implementation of this method for the optimal control model of groundwater bioremediation is presented subsequently. Note that only the implementation for the state vector derivatives $(\partial Y/\partial X)$ is presented. The control vector derivatives $(\partial Y/\partial U)$ must be calculated using the standard method of solving the entire simulation model for each perturbation since each perturbation affects the left-hand-side of the transition equation. However, given that the dimension of the control vector is usually much smaller than the state vector, computational effort is most often driven by the state vector derivatives calculation.

5.2 Design of Efficient Numerical State Vector Derivatives

To facilitate the detailed presentation of how the numerical derivatives method is implemented efficiently, it is useful to examine the actual representation of the state variable derivatives in matrix format:

$$\left(\frac{\partial Y}{\partial X}\right)_k = \left[\frac{\partial x_{k+1}}{\partial x_k}\right] = \begin{bmatrix} \frac{\partial h_{k+1}}{\partial h_k} & \frac{\partial h_{k+1}}{\partial c_{s,k}} & \frac{\partial h_{k+1}}{\partial c_{o,k}} & \frac{\partial h_{k+1}}{\partial c_{b,k}} \\ \frac{\partial c_{s,k+1}}{\partial h_k} & \frac{\partial c_{s,k+1}}{\partial c_{s,k}} & \frac{\partial c_{s,k+1}}{\partial c_{o,k}} & \frac{\partial c_{s,k+1}}{\partial c_{b,k}} \\ \frac{\partial c_{o,k+1}}{\partial h_k} & \frac{\partial c_{o,k+1}}{\partial c_{s,k}} & \frac{\partial c_{o,k+1}}{\partial c_{o,k}} & \frac{\partial c_{o,k+1}}{\partial c_{b,k}} \\ \frac{\partial c_{b,k+1}}{\partial h_k} & \frac{\partial c_{b,k+1}}{\partial c_{s,k}} & \frac{\partial c_{b,k+1}}{\partial c_{o,k}} & \frac{\partial c_{b,k+1}}{\partial c_{b,k}} \end{bmatrix} = \begin{bmatrix} 0 & 0 & 0 & 0 \\ 0 & \frac{\partial c_{s,k+1}}{\partial c_{s,k}} & \frac{\partial c_{s,k+1}}{\partial c_{o,k}} & \frac{\partial c_{s,k+1}}{\partial c_{b,k}} \\ 0 & \frac{\partial c_{o,k+1}}{\partial c_{s,k}} & \frac{\partial c_{o,k+1}}{\partial c_{o,k}} & \frac{\partial c_{o,k+1}}{\partial c_{b,k}} \\ 0 & \frac{\partial c_{b,k+1}}{\partial c_{s,k}} & \frac{\partial c_{b,k+1}}{\partial c_{o,k}} & \frac{\partial c_{b,k+1}}{\partial c_{b,k}} \end{bmatrix} \quad (5.5)$$

where x_k and x_{k+1} are the state vectors at the beginning and end of the current management period k, respectively; each state vector includes four different state variables: hydraulic head h_k, concentrations of substrate $c_{s,k}$, oxygen $c_{o,k}$, and biomass $c_{b,k}$; and the other terms are defined as above. In the simulation model used in this work, a head-independence assumption assumes that the hydraulic head in one management period is independent of the head in the previous period; that is, the aquifer storativity is assumed to be sufficiently small that it can be neglected without significant error. This assumption leads to the zero entries in the derivative matrix in equation (5.5)(see more details on this assumption in Minsker and Shoemaker 1996 and Mansfield and Shoemaker 1999). Note that this assumption is not necessary for the method that follows, however. The N by N dimension of the matrix is composed of the number of non-Dirichlet nodes of hydraulic head, concentrations of substrate, oxygen and biomass (i.e.,

$N = n_h + n_s + n_o + n_b$, where n_h, n_s, n_o and n_b are the number of non-Dirichlet nodes of hydraulic head and concentrations of substrate, oxygen and biomass, respectively). For simplicity, $n=n_h=n_s=n_o=n_b$ is assumed here. This is a requirement of neither the method nor the model, but it simplifies the notation and analysis. Each entry (both zero and non-zero ones) in equation (5.5) is a block matrix of size n by n. Note that the general formulation of equation (5.1) is equivalent to equation (5.5). In equation (5.5), each column represents n columns of equation (5.1). For each perturbation in equation (5.5), the simulation model produces new values of the state vector and one column vector in the derivative matrix can be calculated using equation (5.3). To elucidate the perturbation method further, the exact formulation of the simulation model equations for concentrations is subsequently given in terms of the finite element coefficient matrices. The equation for hydraulic head is not presented because, for our simulation model, the state derivatives of the head equation are zero, as shown in equation (5.5). For models with transient hydraulic head equations, a similar approach to that given below for the concentration equations could be followed.

For substrate, oxygen and biomass concentrations, the system of equations is as follows:

$$\left([N]+\frac{[M_s]}{\Delta t}+\sum_{i=1}^{m}u_{t,i}[P_c]^i\right)\{c_{s,t+1}\}=\frac{[M_s]}{\Delta t}\{c_{s,t}\}+\sum_{i=1}^{m}u_{t,i}[P_c]^iC_s^{'}+\{F_s\} \tag{5.6}$$

$$\left([N]+\frac{[M_o]}{\Delta t}+\sum_{i=1}^{m}u_{t,i}[P_c]^i\right)\{c_{o,t+1}\}=\frac{[M_o]}{\Delta t}\{c_{o,t}\}+\sum_{i=1}^{m}u_{t,i}[P_c]^iC_o^{'}+\{F_o\} \tag{5.7}$$

$$\left([N]+\frac{[M_b]}{\Delta t}+\sum_{i=1}^{m}u_{t,i}[P_c]^i\right)\{c_{b,t+1}\}=\frac{[M_b]}{\Delta t}\{c_{b,t}\}+\sum_{i=1}^{m}u_{t,i}[P_c]^iC_b^{'}+\{F_b\} \tag{5.8}$$

where, $c_{s,t}$, $c_{o,t}$, and $c_{b,t}$ are substrate, oxygen and biomass concentration vectors at the beginning of the current simulation time step (t), respectively; $c_{s,t+1}$, $c_{o,t+1}$, and $c_{b,t+1}$ are substrate, oxygen and biomass concentration vectors at the end of the current simulation time step ($t+1$), respectively; and Δt is the simulation time step. The coefficient matrices and vectors in the above equations are the standard form that results when linear quadrilateral elements are used. For more details, see equations (9)-(12), (14)-(15) and (17)-(18) of Minsker and Shoemaker (1996). One perturbation of any one of the elements in the concentration vectors ($c_{s,t}$, $c_{o,t}$, and $c_{b,t}$) at the beginning of the current management period k results in solving equation (5.6)-(5.8) d times from the first simulation time step to the last simulation time step within that management period, where d is the number of simulation time steps within one management period. The new values of the concentration vectors can then be used to calculate the one-sided forward divided difference derivatives $\partial Y/\partial X$ using equation (5.3) and to generate one column entry in equation (5.5). The perturbations of $c_{s,t}$, $c_{o,t}$, and $c_{b,t}$ for $\partial Y/\partial X$ only change the right-hand-side vectors in equations (5.6)-(5.7). Specifically, only the $\{F_s\}$, $\{F_o\}$ and $\{F_b\}$ vectors need to be reformulated, which contain the biological kinetics for biodegradation (rate of substrate degradation, denoted by r_s). For example, the $\{F_s\}$ vector contains the following term:

$$r_s = \frac{\mu_{\max}}{Y_c}\left(\frac{c_{s,t}}{K_s + c_{s,t} + \frac{(c_{s,t})^2}{K_i}}\right)\left(\frac{c_{o,t}}{K_o + c_{o,t}}\right) \tag{5.9}$$

where μ_{max} is the maximum specific growth rate for biomass; Y_c is the biomass yield coefficient; K_s is the substrate half-saturation coefficient; K_i is the substrate inhibition coefficient; and K_o is the oxygen half-saturation coefficient. See equations (11), (15) and (18) in Minsker and Shoemaker (1996) for further details on the $\{F_s\}$, $\{F_o\}$ and $\{F_b\}$ vectors. In their derivation of the analytical derivatives, Minsker and Shoemaker (1996) assumed that the simulation time step is sufficiently small that the concentrations of substrate and oxygen in equation (5.9) can use the previous time step values ($c_{s,t}$ and $c_{o,t}$) without introducing significant errors, which avoids iterative solution of the simulation model. However, in the current method, this assumption is no longer required. If an iterative solution is used in the simulation model, the perturbed simulation model can also be iteratively solved without changing the left-hand-side of the system equations. Iteratively solving the simulation model equations increases the computing cost per run, but will not affect the applicability of our method.

For the other terms in the right-hand-side vectors in equations (5.6)-(5.8), the matrices $[M_s]/\Delta t$, $[M_o]/\Delta t$ and $[M_b]/\Delta t$ are not affected by the concentration perturbations and the matrix-vector multiplications between these matrices and their corresponding concentration vectors $c_{s,t}$, $c_{o,t}$, and $c_{b,t}$ need not be recalculated fully because there is always only one entry in the concentration vectors changing (the perturbation). Instead of doing the matrix-vector multiplication between a matrix $[M_s]/\Delta t$, $[M_o]/\Delta t$ or $[M_b]/\Delta t$ and a full vector $c_{s,t}$, $c_{o,t}$, or $c_{b,t}$, then the perturbation vector with only one nonzero entry (the perturbation) can be used and the result added to the original normal matrix-vector multiplication result in the forward sweep to form the

first terms in equations (5.6)-(5.8). The computational effort for obtaining this term thus reduces to O(N) from O(N^2). The pumping source term $\sum_{i=1}^{m} u_{t,i}[P_c]^i C^{'}$ is constant with respect to concentrations ($C^{'}$ represents the injection concentration, which is assumed to be constant).

In summary, calculating the derivative matrices of equation (5.5) by perturbing concentrations in (5.6)-(5.8) only changes the right-hand-side of each equation relative to the runs in the forward sweep. This result occurs because only the right-hand-side vector is affected by perturbations in the initial state variables at the beginning of the management period, the importance of which is explained subsequently. Note that in performing the perturbations, perturbation increments of 0.01% for substrate and oxygen and 0.0001% for biomass concentrations were found to produce sufficiently accurate numerical derivatives. Of course, the appropriate perturbation increment may vary for different applications.

5.3 Theoretical Analysis of the Computational Effort Associated with the Numerical Derivatives Method

Given that each perturbation to obtain equation (5.5) can be obtained by reformulating the right-hand-side vectors and performing back substitution, the theoretical computing effort for running the perturbed simulation model is on the order of O(N), where N is the number of non-Dirichlet state variables. Thus, calculating derivative

$\partial Y/\partial X$ using the one-sided divided difference method with N perturbations is only $O(N^2)$. This is an order of magnitude reduction in the computing time compared to the previous analytical derivatives method, which is $O(N^3)$, as we analyzed at the beginning of this section. Calculating the first derivatives of the transition equation with respect to the control variables ($\partial Y/\partial U$), which, as mentioned earlier, requires re-solving the whole simulation model, entails $O(m(s+1)^2N)$ work, where s is the bandwidth (e.g., for a tri-diagonal matrix, s=1; see the definition in Iserles, 1996) and m is the total number of control variables. Since the number of control variables (i.e. pumping wells) is usually far less than the number of nodes in the finite element mesh, the number of runs of the full simulation model for $\partial Y/\partial U$ contributes less to the total computing time. In the actual implementation of this method, the growth rate will be slightly higher than quadratic due to the calculation of $\partial Y/\partial U$ and storage of the results of the forward sweep run.

5.4 Case Study

5.4.1 Description of the Test Case

To test the performance of our numerical derivatives method, a four-level case study was created based on the test site presented in Chapter 4. A scenario with dispersivity values of α_L = 15.55 m and α_T = 3.4 m was used in this analysis. Note that this problem was actually solved for half of the domain shown in Figure 4.5 because the aquifer properties, concentrations, and well sites are symmetric. The number of elements and nodes in Table 5.1 is only counted for the half-domain. Note that the number of non-Dirichlet state variables is four times the number of numerical nodes if the dimensions of

the hydraulic heads and concentrations of substrate, oxygen and biomass are assumed to be the same.

As can be seen from Table 5.1, Level 1 is the coarsest level and Level 4 is the finest level. The first three levels were used to test the performance of both the numerical and analytical derivatives but Level 4 was only used to test the numerical derivatives because Level 4 required excessive computing time (about 15 days per iteration) when using analytical derivatives.

Table 5.1: Four-level case study

	Element Size (1)	Number of Elements (2)	Number of Nodes (3)	Number of State Variables (4)
Level 1	20 m × 20 m	24	36	144
Level 2	10 m ×10 m	96	119	476
Level 3	5 m × 5 m	384	429	1716
Level 4	2.5 m × 2.5 m	1536	1625	6500

5.4.2 Results and Discussions

This section presents the numerical results for the case study, which were obtained on an SGI/Cray Origin 2000 supercomputer using only one 195MHz processor. To compare performance of the numerical and analytical derivatives, the model was initially run for one iteration at all four levels for the numerical derivatives method and at the first three levels for the analytical derivatives. The CPU time was recorded for each run and plotted in Figure 5.1, along with the theoretical predicated values of $O(N^3)$ and $O(N^2)$ growth rate. Note that the CPU time per iteration at Level 4 using numerical

derivatives is approximately 2.3 days and the estimated CPU time per iteration at Level 4 using analytical derivatives is about 15 days, which were off the scale and are hence not shown.

As can be seen from Figure 5.1, the CPU time per iteration using analytical derivatives grows dramatically with the increase in level number as the number of state variables increases (as predicted in Table 4.1). Based on the measured CPU times per iteration using analytical derivatives, the growth rate can be fit and the result is $O(N^{2.97})$, which is very close to the theoretical prediction $O(N^3)$ of the SALQR model (Liao and Shoemaker, 1991). In contrast, the CPU time per iteration using numerical derivatives implemented in this study has a much lower growth rate. Based on the measured CPU times per iteration using numerical derivatives, the growth rate can be calculated and denoted as $O(N^{2.18})$, which is close to the prediction calculated in the methodology section. This is a significant improvement over the previous analytical derivatives method. The lower order growth rate implies that as the number of state variables increases, more and more computational savings can be obtained using our numerical derivatives method over analytical derivatives. Although at Level 1 the analytical method was actually slightly faster than the numerical method presented herein, as the grid size increased the analytical method became much slower than the numerical method. For realistically sized optimal control problems, it is expected that the numerical method will be substantially faster than the analytical method.

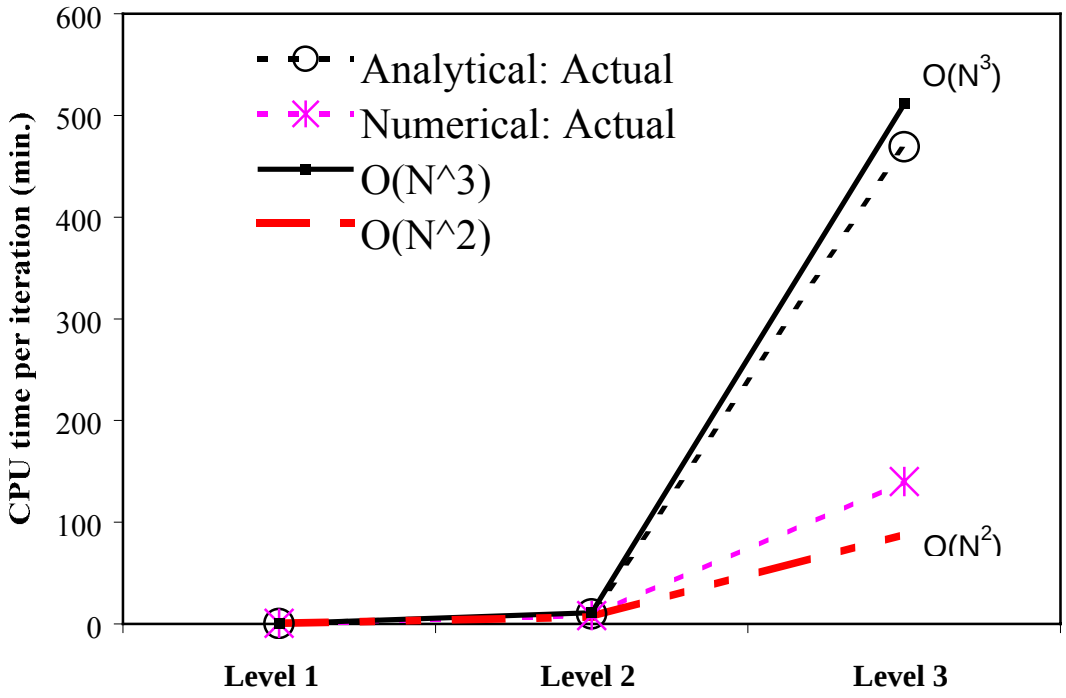

Figure 5.1: CPU time per iteration at different levels. The CPU times per iteration at Level 4 for both numerical derivatives and analytical derivatives are not shown because they are both off the scale of the plot.

Two complete runs of the model using both analytical and numerical derivatives at Level 3 were conducted to make a full comparison. Both runs started with the same initial guess of the pumping rates and had the same initial and terminal penalty weight for constraint violations. Figure 5.2 shows the change in objective function value versus CPU time for each run.

The results in Figure 5.2 demonstrate the potential computational savings associated with using our numerical derivatives method over analytical derivatives. In Figure 5.2, the computing time for the analytical derivatives method to converge was about 117 hours, while the numerical derivatives method required only 37.8 hours, which is over a two-thirds reduction in computing time. The accuracy of both methods can be quantified by comparing the value of the final objective function, the SALQR termination parameter (θ) and the number of iterations. The SALQR termination parameter θ is related to the expected decrease in the objective function due to the execution of one additional SALQR iteration (see details in Whiffen and Shoemaker, 1993). All runs were terminated at θ values of less than 0.01. The actual value of θ, number of iterations and objective function value for both methods can be found in Table 5.2.

Table 5.2: Comparison of numerical and analytical derivatives methods

	Numerical Derivatives Method (1)			Analytical Derivatives Method (2)		
	θ Value	Iterations	Objective	θ Value	Iterations	Objective
Results	3.56E-03	16	11.59	9.41E-03	17	11.55

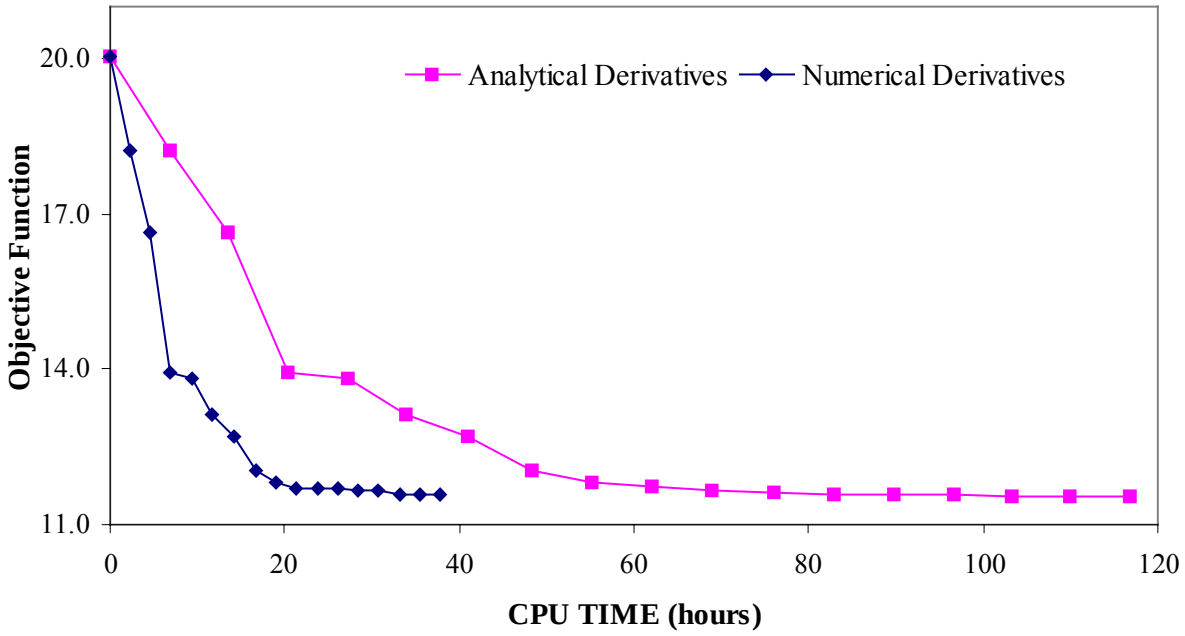

Figure 5.2: The change of objective function versus CPU time using different derivative methods

As shown in Table 5.2, values of θ for both the numerical and analytical derivatives methods were less than the required termination value of 0.01, which means that all runs successfully terminated. Moreover, there is no practical difference in the final objective function value. The number of iterations using the numerical derivatives method was less than that using the analytical derivatives method, indicating that accuracy does not deteriorate using the numerical derivatives method. In fact, the numerical derivatives may even be more accurate because the management period derivatives are directly calculated. In the analytical derivatives method, the management period derivatives are the product of 60 simulation period derivative matrices since each management period consists of 60 simulation time steps. When the matrices contain numerous small floating-point numbers of different scales, these multiplications can cause significant numerical rounding errors (Minsker and Shoemaker, 1998a).

Note that both derivatives methods identified solutions with nearly identical cost (In fact, the costs only differ by 0.4%) but the pumping rates were somewhat different. The optimal pumping rates obtained by both derivatives methods can be found in Figures 5.3 to 5.8. Since there are 6 management periods in this case study, for each well location, there is a change in pumping rates in each management period. It is very interesting that for the first 3 management periods, the pumping rates and patterns are almost the same for both methods. However, in the last three management periods, different pumping patterns are found to be optimal. The injection wells reach minimum pumping rates in management period 5 for the solution obtained from the numerical derivatives method, while the analytical derivatives method produces a solution whose

minimum pumping rates are in the last (6^{th}) management period. Within all of the management periods, the extraction wells are essentially not used in all of the solutions obtained from both methods. As indicated by Minsker and Shoemaker (1998a), optimal design of in-situ bioremediation design is a nonlinear optimization problem that has multiple optimal. However, from the cost perspective, there is no practical difference between these two solutions, yet we obtained the solution using the efficient numerical derivatives with almost an order of magnitude reduction of computing time than the previous analytical derivatives method.

5.5 Summary

We developed an efficient numerical derivatives method for the bioremediation optimal control model. The numerical derivatives implemented herein were carefully designed and generalized to be a significant improvement over previous analytical derivatives, achieving a reduction of almost one order of magnitude in computational effort. An efficient one-sided forward divided difference numerical derivatives calculation for state vector was implemented, which only requires assembling the right-hand-side vector of the linear systems of equations of the simulation model and performing backward substitution. The derivative calculation is reduced from $O(N^3)$ to nearly $O(N^2)$, where N is the number of non-Dirichlet state variables. Applying the numerical derivatives method in a case study with over 1,600 state variables reduces computing time by more than two-thirds over the previous analytical derivatives method without loss of accuracy. This reduction will be even greater for applications with more

state variables, enabling solution of much larger-scale problems than previously possible. Finally, the numerical derivative approach developed in this study for the SALQR model could likely be adapted to other derivative-based optimization models. The computational savings that could be achieved in those models would depend on the form of the derivatives; further study would be needed to determine whether the computational savings would be comparable.

Analytical Derivatives Method

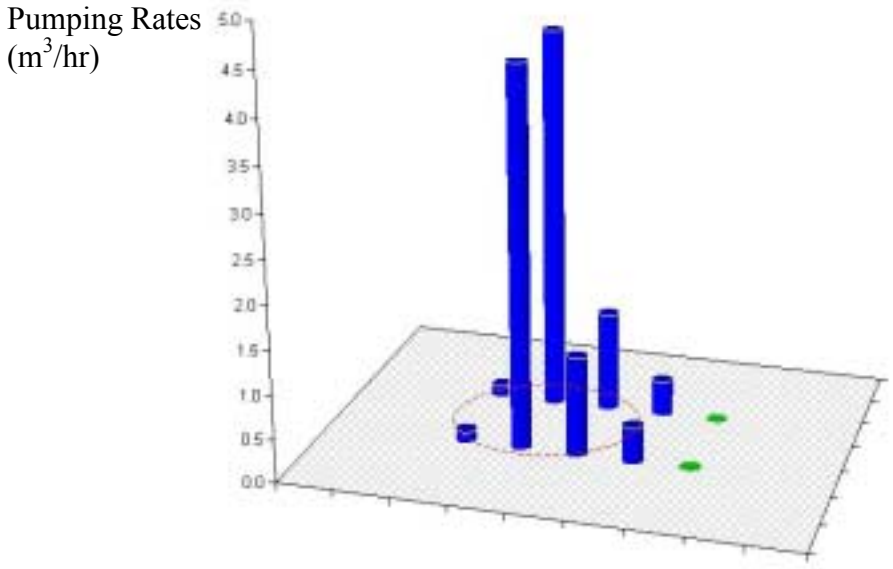

Efficient Numerical Derivatives Method

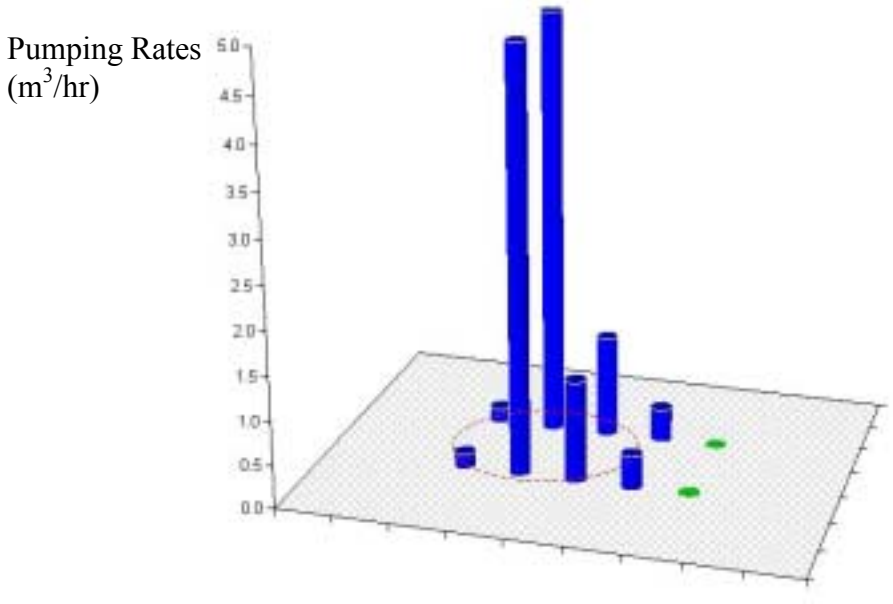

Figure 5.3: Pumping rates in management period 1 using different derivatives methods (dark black columns represent injection wells and gray ones represent extraction wells)

Analytical Derivatives Method

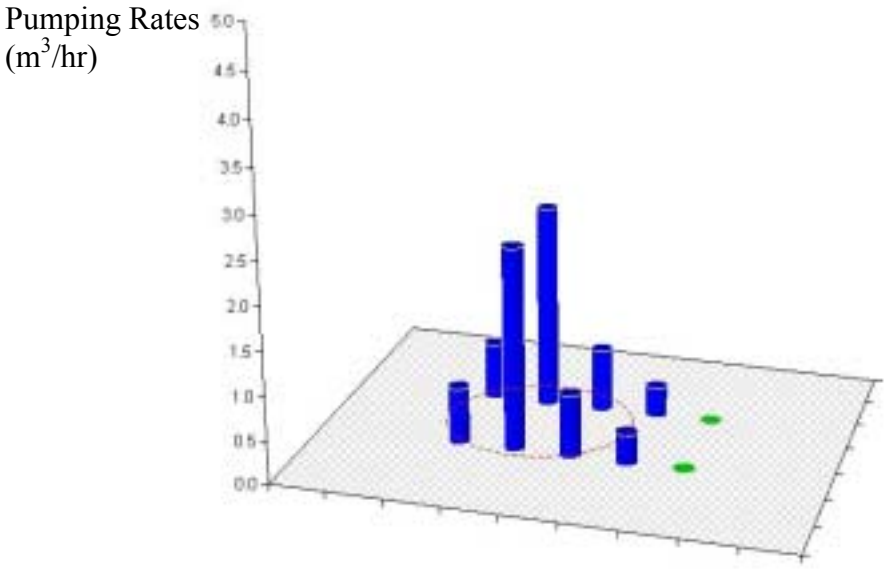

Efficient Numerical Derivatives Method

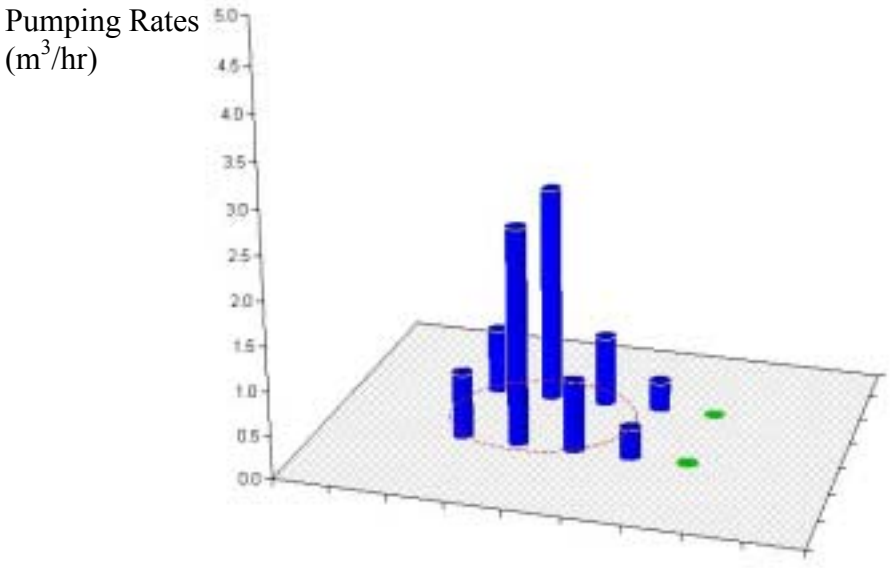

Figure 5.4: Pumping rates in management period 2 using different derivatives methods (dark black columns represent injection wells and gray ones represent extraction wells)

Analytical Derivatives Method

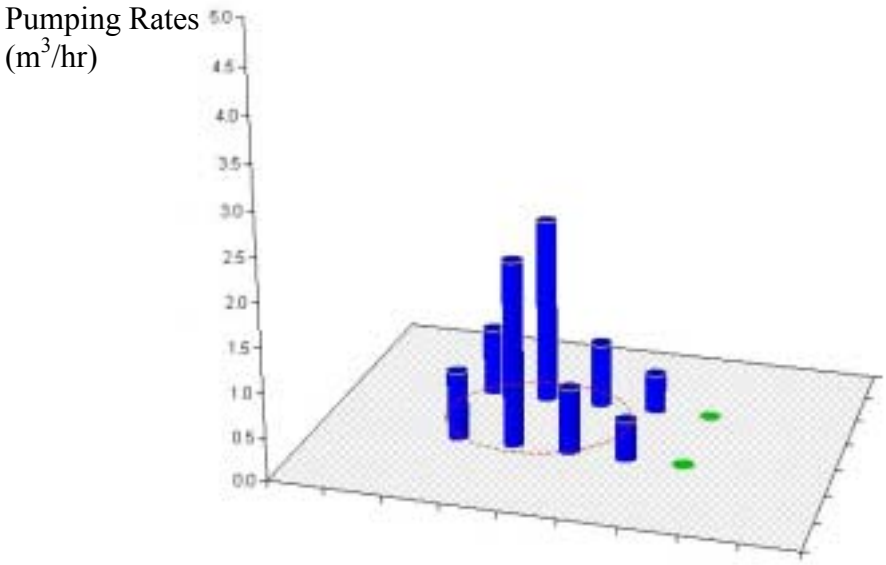

Efficient Numerical Derivatives Method

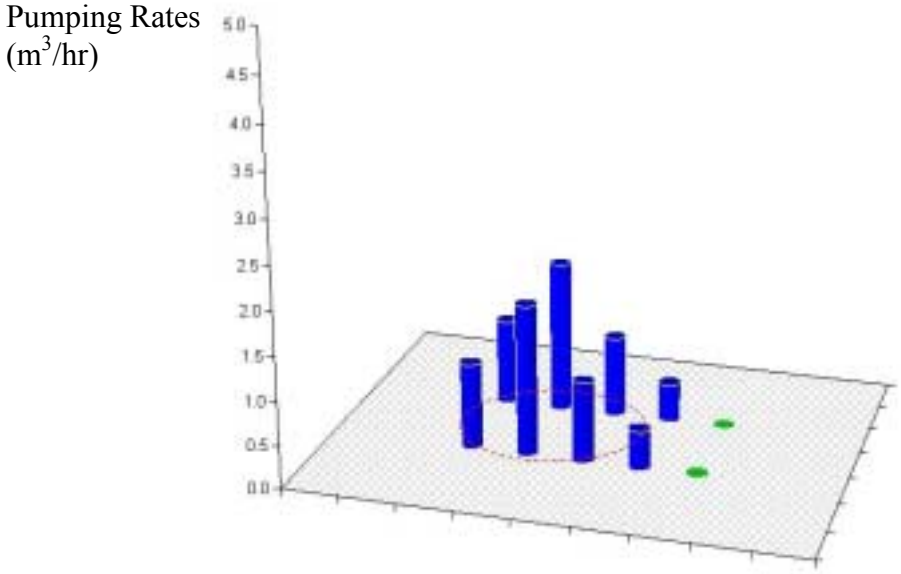

Figure 5.5: Pumping rates in management period 3 using different derivatives methods (dark black columns represent injection wells and gray ones represent extraction wells)

Analytical Derivatives Method

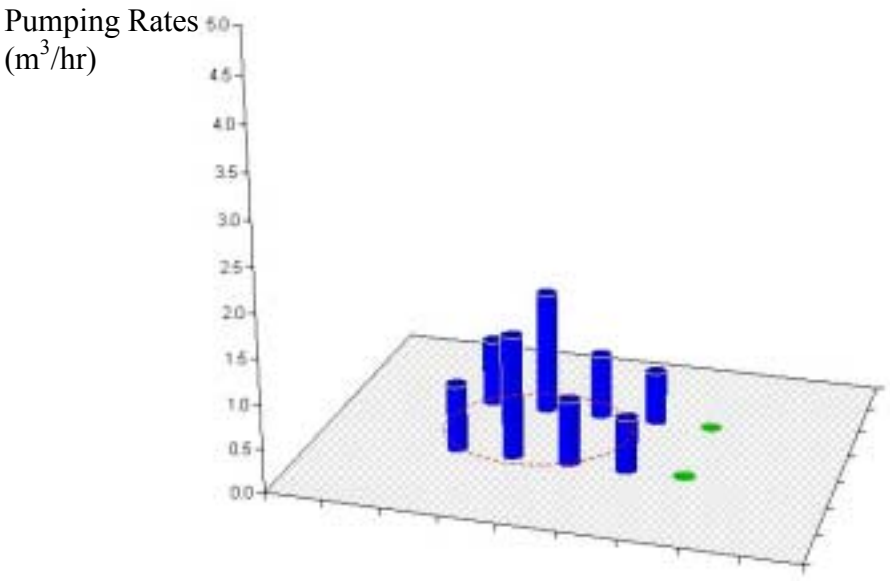

Efficient Numerical Derivatives Method

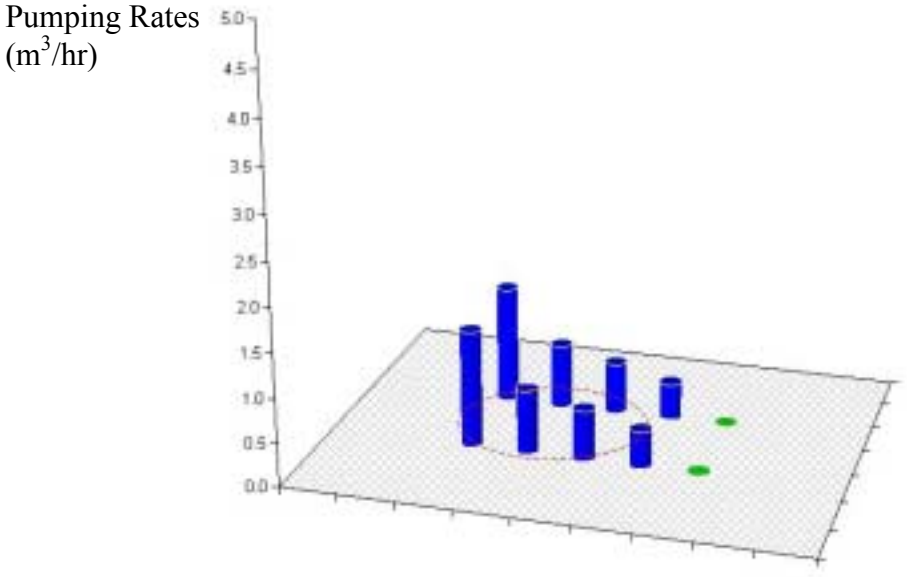

Figure 5.6: Pumping rates in management period 4 using different derivatives methods (dark black columns represent injection wells and gray ones represent extraction wells)

Analytical Derivatives Method

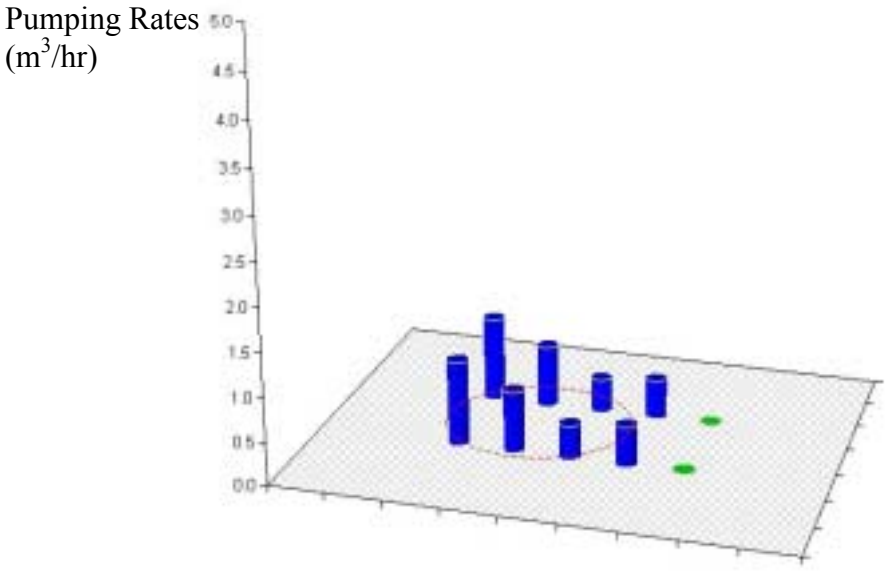

Efficient Numerical Derivatives Method

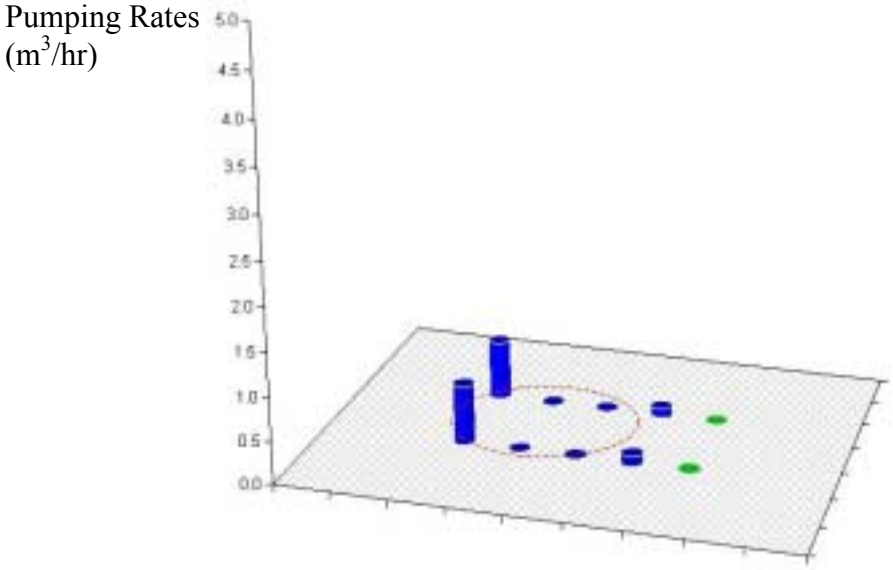

Figure 5.7: Pumping rates in management period 5 using different derivatives methods (dark black columns represent injection wells and gray ones represent extraction wells)

Analytical Derivatives Method

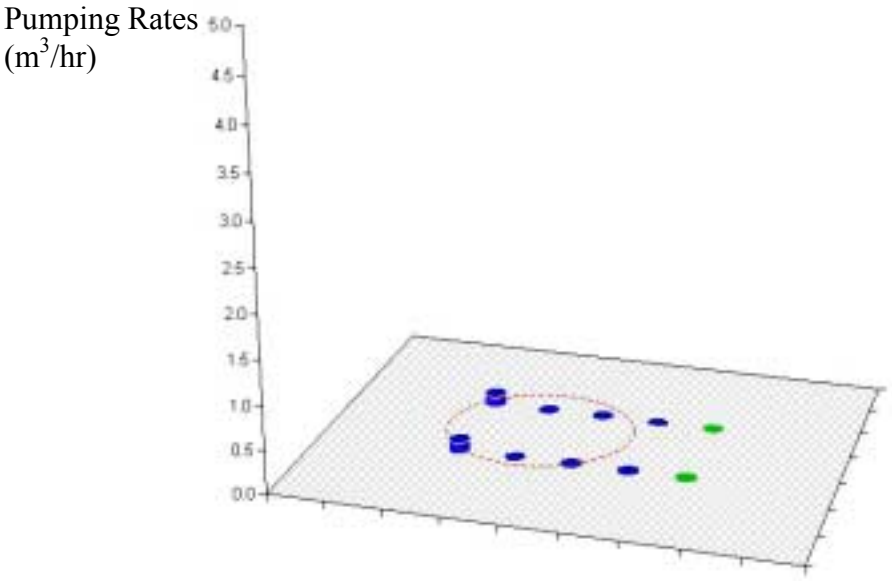

Efficient Numerical Derivatives Method

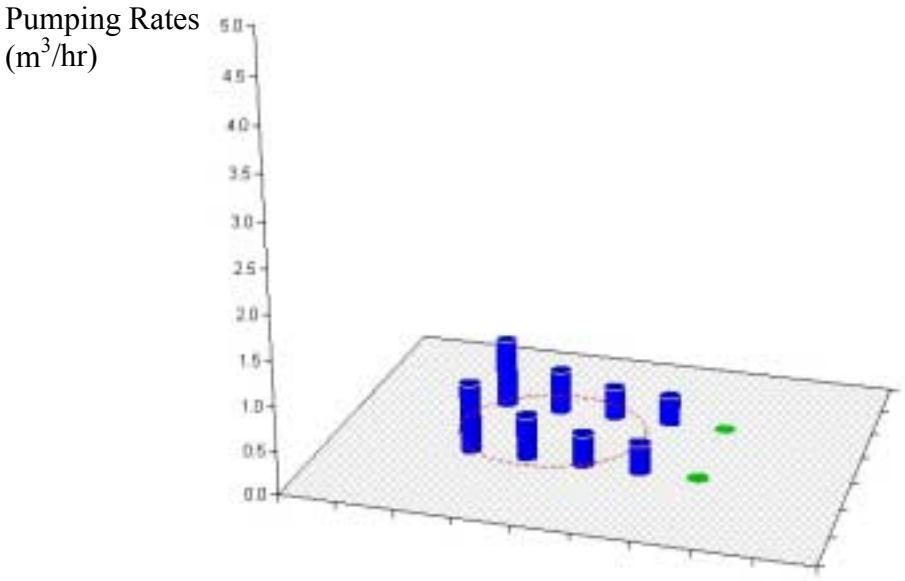

Figure 5.8: Pumping rates in management period 6 using different derivatives methods (dark black columns represent injection wells and gray ones represent extraction wells)

Chapter 6

Multiscale Derivatives Method

The efficient numerical derivatives method developed in the last chapter not only reduces computing time for the derivatives calculation, but also enables implementation of a V-cycle multiscale derivatives method, which will be described in this Chapter. Since the derivatives calculation is the most computationally demanding part of solving the optimal groundwater bioremediation design problem with management periods, as discussed in Chapter 3, further reduction of computing time using multiscale derivatives method is expected to be highly beneficial.

6.1 Description of the Methodology

When calculating the derivatives on a fine mesh, the multiscale derivatives method first switches to a coarser mesh to calculate the derivatives at that level, and then switches back to the fine level by interpolating the coarse grid derivatives to the fine grid using bilinear interpolation. This switching pattern is similar to the V-cycle iteration in multigrid solvers for partial differential equations (see Douglas 1996), although the operations and calculations at each level are completely different. This V-cycle switching pattern does not affect the forward sweep, which is always run at the finest level.

Notice that this method is independent of the simulation model used in the coupled simulation and optimization model, but does depend on decoupling the derivatives at different nodes, as the subsequent description of the implementation details will show. The efficient numerical derivatives method implemented in Chapter 5 decoupled the numerical derivatives at different nodes, which enables the multiscale derivatives method to be used in the bioremediation optimal control model. Also note that the multiscale derivatives method is applied only to the calculation of the first derivatives of the transition equation with respect to the state variables, since its calculation is the most computationally intensive portion of the model, as explained in Chapter 3 and 5.

6.2 Design of the Multiscale Derivatives

The multiscale derivatives method developed in this work consists of three steps: switching to a coarser level when at the fine level, calculating the derivatives at the coarser level, and interpolating the coarser derivatives back to the finer level. The first two steps are straightforward and the coarse grid derivatives calculation follows the methodology presented in Chapter 5. The interpolation step will be described as follows.

The interpolation process can be explained from Figure 6.1. As can be seen from the example two-level meshes in this figure, the dimension of the coarse mesh is 12 (3×4) and the dimension of the fine mesh is 35 (5×7). This means that the length of each column in derivative equation (5.1) in Chapter 5 is 48 (4×12) at the coarse mesh and 140 (4×35) at the fine mesh, assuming uniform mesh refinement and the numbers of non-Dirichlet nodes of hydraulic head and concentrations of substrate, oxygen and biomass

are the same. On the fine mesh, three types of derivative calculations are performed, which will be explained subsequently.

First, for those grid points that are shared by both the fine grid and coarse grid (denoted by black points in Figure 6.1), the derivative values at any black point with respect to perturbations at any black point can be obtained directly from the coarse mesh. For example, as shown in Figure 6.1, the value of $\partial C_{s,k+1}(af)/\partial C_{s,k}(af)$ is the same as that of $\partial C_{s,k+1}(ac)/\partial C_{s,k}(ac)$, where *s* stands for substrate and *k* stands for the *k*th management time period. Second, for those points that only exist on the fine mesh, such as the hollow circle point denoted as *bf*, the derivative values of any point on the fine mesh with respect to perturbations at these points must be calculated using the fine mesh because no corresponding coarse mesh perturbations are available. For example, the value of $\partial C_{s,k+1}(bf)/\partial C_{s,k}(bf)$ or $\partial C_{s,k+1}(af)/\partial C_{s,k}(bf)$ should be calculated using a perturbation of $C_{s,k}$ at the point *bf* on the fine mesh. Finally, the derivative values for those points that only exist on the fine mesh, such as point *bf*, with respect to the perturbation at those points shared by both the coarse and fine meshes, can be interpolated using the coarse grid derivatives. For example, the value of $\partial C_{s,k+1}(bf)/\partial C_{s,k}(af)$ can be obtained using a standard bilinear interpolator at the fine mesh. See Liu et al. (2001) and Chapter 3 for details on the bilinear interpolation method used in this work. Note that this approach cannot be used in the analytical derivatives method because all of the derivatives were obtained simultaneously by solving a linear system of equations with multiple right-hand-side vectors (see Minsker and Shoemaker 1996). Furthermore, this method is applicable to three-dimensional models, where similar derivatives must be calculated when using

derivatives-based method such as SALQR, although the interpolation method should be changed to trilinear interpolator other three-dimensional interpolators.

The multiscale derivatives method produces inexact gradient information for the optimization problem. However, the computational savings can be beneficial, as we will examine subsequently.

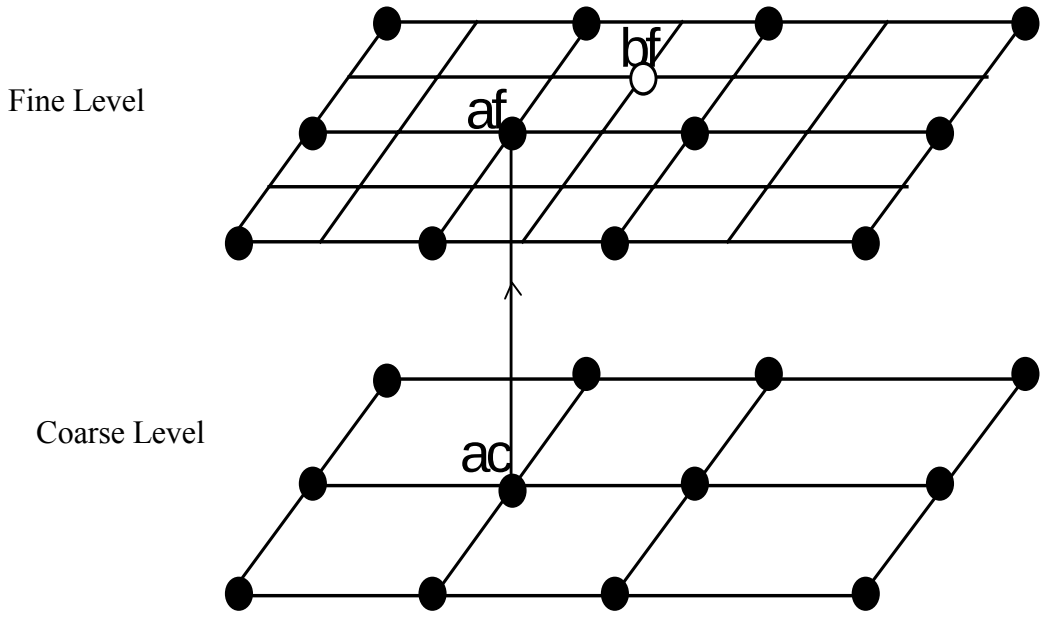

Figure 6.1: Derivatives in coarse and fine mesh

6.3 Theoretical Estimation of the Computational Savings

The computing savings can be estimated by looking at how many derivatives values were not calculated through the one-sided divided difference method on the finest mesh. The current method uses a uniform two-dimensional mesh refinement for simplicity. In this case, the ratio of the number of nodes in the coarse mesh to that in the fine mesh can be calculated as follows

$$\frac{cnx * cny}{fnx * fny} = \frac{cnx * cny}{(2 * cnx - 1) * (2 * cny - 1)} \approx \frac{cnx * cny}{(2 * cnx) * (2 * cny)} = \frac{1}{4} \tag{6.1}$$

where *cnx* and *cny* are the number of nodes in the *x* and *y* directions at the coarse mesh, respectively, and *fnx* and *fny* are the number of nodes in the *x* and *y* directions at the fine mesh, respectively. Hence, the computational saving is theoretically about 25%, not including the computational cost of interpolation and the coarse grid derivatives calculation, which are usually small compared to the one-sided divided difference calculation on the fine mesh.

6.4 Results of Numerical Experiments for the Multiscale Derivatives Method

To demonstrate the advantages of using V-cycle multiscale numerical derivatives, a bilevel run was performed at Level 3 and Level 2 using the V-cycle multiscale derivatives method, based on the test case used in Chapter 5. During our numerical experiment, we found that the V-cycle multiscale derivatives produce good convergence behavior during the initial iterations but cannot converge if such derivatives are used

during late iterations when the model required accurate predications of small perturbations near the optimal solution. This result is understandable because V-cycle multiscale derivatives are not the exact representations of the system response at the fine mesh level. To take advantage of the computational savings provided by the V-cycle multiscale derivatives and still obtain convergence, a simple switch mechanism was implemented to switch from V-cycle multiscale derivatives to normal fine-mesh numerical derivatives once the percentage change in the objective function value between two consecutive iterations becomes small, indicating that the current solution is likely within the neighborhood of the optimal solution and more accurate derivatives are required. The percentage change P_s is defined as follows

$$P_s = \frac{\left|(obj_{i+1} - obj_i)\right|}{obj_i} \times 100\% \tag{6.2}$$

where obj_{i+1} and obj_i are the objective function values at iteration $i+1$ and i, respectively. In this problem, P_s = 0.6% is chosen, which means that when the percentage change is less than or equal to 0.6%, the next iteration will switch to using normal one-sided forward divided difference numerical derivatives on the fine mesh. The result of this procedure is shown in Figure 6.2, along with the normal numerical derivative results at Level 3 for comparison.

As can be seen from Figure 6.2, the CPU time per iteration using normal numerical derivatives at Level 3 is about 2.3 hours, while the V-cycle multiscale derivatives is about 1.8 hours, which is about a 22% reduction. This is close to the theoretical prediction of 25%. The total computing time for using V-cycle multiscale

derivatives with the switching mechanism is about 27 hours and the total computing time for using numerical derivatives alone is about 37.8 hours, which is about a 29% reduction in computing time. The higher overall reduction results from the V-cycle multiscale derivatives method with switching mechanism requiring a fewer total number of iterations (14 iterations vs. 16 iterations for numerical derivatives alone). It is believed that the reduction in the number of iterations results from the model following a slightly different search path with the multiscale derivatives; hence, this reduction may not necessarily occur in other applications of this method. Note that the combined reduction of using multiscale derivatives with switching mechanism over the previous analytical derivatives method (117 hours, see Chapter 5) is about 77%, a significant improvement in computational performance.

6.5 Summary

A framework for multiscale derivative implementation in an SALQR model has been presented. Using the numerical derivatives implementation presented in Chapter 5, the V-cycle multiscale derivative method approximated the derivatives at the fine level by interpolating the derivatives from the coarser level, which provides a theoretical reduction of 25% and an actual reduction of 22% per iteration in our case study. The total computing time for using V-cycle multiscale derivatives for the case study with more than 1,600 state variables represented approximately a 29% reduction in computing time compared to the numerical derivatives method alone, or a 77% reduction compared to the previous analytical derivatives method. These methods clearly provide a substantial

reduction in computing time relative to previous methods even for a relatively small test case. When these methods are combined with the one-way spatial multiscale method (Liu et al. 2001, also see Chapter 4), even greater savings should be possible. A comprehensive study of all of the multiscale methods developed in this work will be presented in the next chapter.

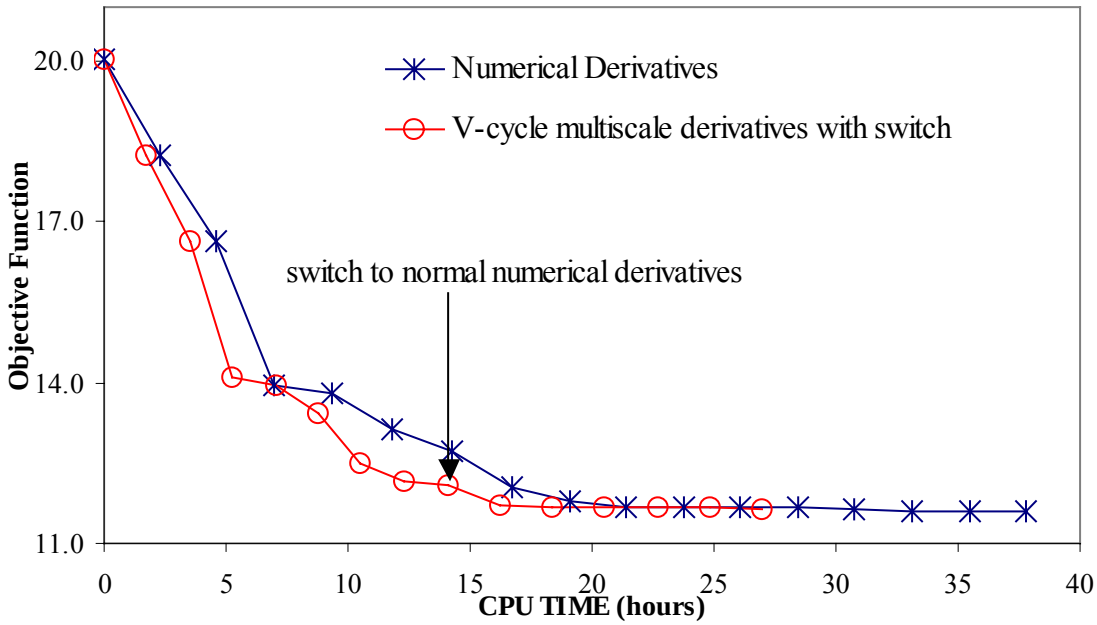

Figure 6.2: The change of objective function value versus CPU time using numerical derivatives and V-cycle multiscale derivatives with switch

Chapter 7

Full Multiscale Approach for SALQR Model

As previous chapters have shown, individual methods, including one-way spatial multiscale method (Chapter 4), efficient numerical derivatives method (Chapter 5), and multiscale derivatives method (Chapter 6), can significantly reduce the computational time associated with solving bioremediation optimal control model. To further reduce the computing time, a full multiscale approach is developed in this Chapter, which combines the methods developed in the previous chapters. Several strategies are also investigated to improve the computational performance of the approach further. Case studies show the computational savings with different configurations of different components of the full multiscale approach.

7.1 Description of the Methodology

The full multiscale computational approach is a combination of the one-way spatial multiscale method, efficient numerical derivatives method, and multiscale V-cycle derivatives method. As can be seen from Figure 7.1, this method starts from the coarsest mesh (Level 1) and solves the model to convergence. Then the converged results are interpolated to the finer mesh (Level 2) and the model runs using the converged results

from Level 1 as the starting point. At Level 2, when the derivatives are needed in the backward sweep, the V-cycle multiscale derivatives method developed in Chapter 6 is used. The model switches back to the coarser level (Level 1), obtains the coarse grid derivatives, and then interpolates back to the current level using a standard bilinear interpolator. The efficient one-sided divided difference method presented in Chapter 5 (also see Liu and Minsker, 2001, in press) is used to calculate the numerical derivatives so that those derivatives that cannot be interpolated can be calculated separately on Level 2. Once the model converges at Level 2, the solution is interpolated to the finer mesh and a similar procedure is performed at Level 3. This process continues until the model reaches the finest level (in Figure 7.1, the finest level is Level 3) and converges.

A more general description of the methodology is given as follows.

(1) For a given problem, set up a hierarchy of meshes where the mesh sizes $h_1 > h_2 > \ldots > h_{L-1} > h_L$, L being the finest level with the desired level of accuracy and 1 being the coarsest level.

(2) Starting from the coarsest level (Level 1), solve the model (both forward and backward sweep) to convergence.

(3) For *Level* = 2 to *L*

a. Interpolate the results from *Level*–1 to *Level* using a bilinear interpolator.

b. Start with this value to perform a two-level cycle of the V-cycle multiscale derivatives calculation.

i. Calculate derivatives at *Level-1*.

ii. Interpolate derivatives to *Level* using standard bilinear interpolation.

iii. Calculate remaining derivatives at *Level*.

c. Continue until convergence at *Level*.

(4) Stop after convergence at the finest level.

Notice that in Figure 7.1, the single-line arrow stands for the interpolation of the solution between coarse level and fine level as discussed in Chapter 4, and the double-line arrow stands for the switch and interpolation of the derivatives between coarse level and fine level as discussed in Chapter 6. Since the operation targets are different in these two cases, different representations are used in Figure 7.1.

The finest level is determined by the spatial accuracy requirement of the simulation model. As a rule of thumb, the finite element method requires a Peclet number less than 2 for modeling accuracy in space. Since the full multiscale approach focuses on computational time reduction in space, it is not necessary to require the Peclet number to be less than 2 at all levels except the finest level.

7.2 Strategies for Performance Enhancement

Several possible strategies have been investigated to enhance the performance of the full multiscale approach presented in Section 7.1. These strategies are discussed below.

7.2.1 Local Effect of the Derivatives

When examining the spatial structure of the first derivatives of the transition equation with respect to the state variables, we found two distinct regions: a peak region and a smooth region. Figure 7.2 shows an example of the spatial structure of the first derivative of oxygen concentration at the beginning of management period 2 with respect to the biomass concentration at the beginning of management period 1($\frac{\partial c_{o,t+1}}{\partial c_{b,t}}$ in Appendix C, where t =1). We call this the "local-effect" of the derivatives, which means that a small perturbation of the value of one state variable can only have significant effect in the next time step in its surrounding area but will have little effect in remote areas.

To solve the derivatives at the fine level only at the peak area, the boundary conditions must be obtained from the coarser grid derivatives calculation. This was done by performing a coarse grid perturbed simulation run and then using the interpolated state variables at the finer grid as the boundary conditions for the peak area's simulation. One-sided forward difference was then used to calculate the derivatives at the peak area.

Exploiting this type of local structure has been quite successful for solution of PDEs (Brandt 2001) and it initially appeared quite promising for derivative calculations as well. However, this "local-effect" strategy was not sufficiently accurate for calculating derivatives. The errors come from two factors: the approximated boundary conditions derived from the coarse grid simulation and the error propagation due to the transition in time during one management period. The derivatives can be off by several orders of magnitude even though satisfactory state values can be obtained.

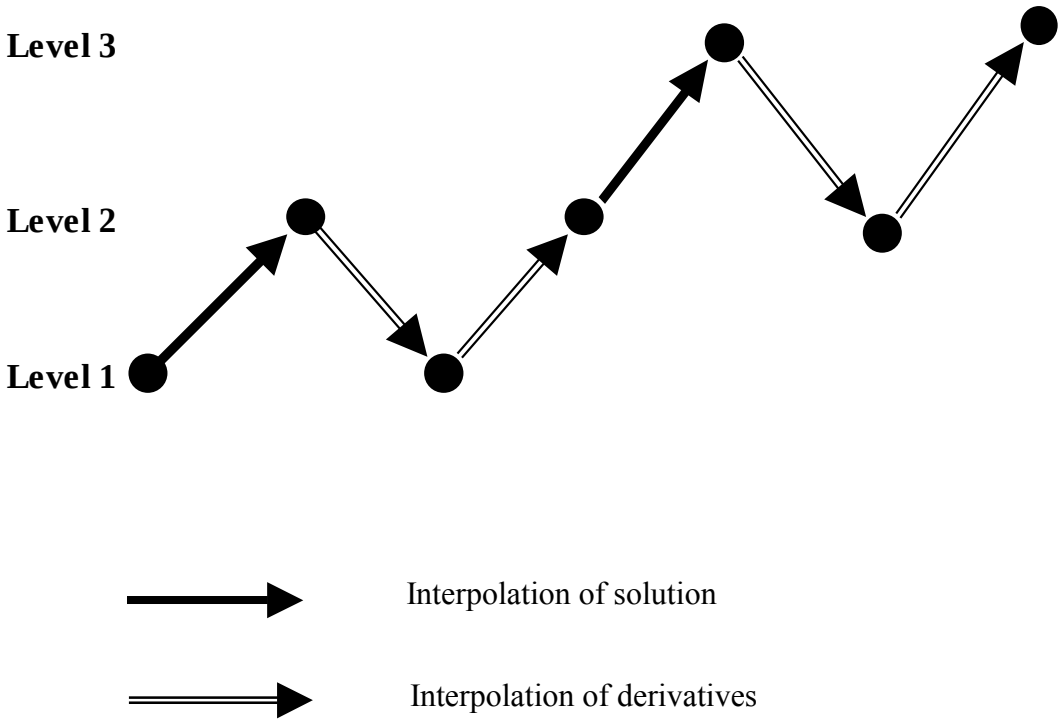

Figure 7.1: The structure of the full multiscale computational approach for SALQR model

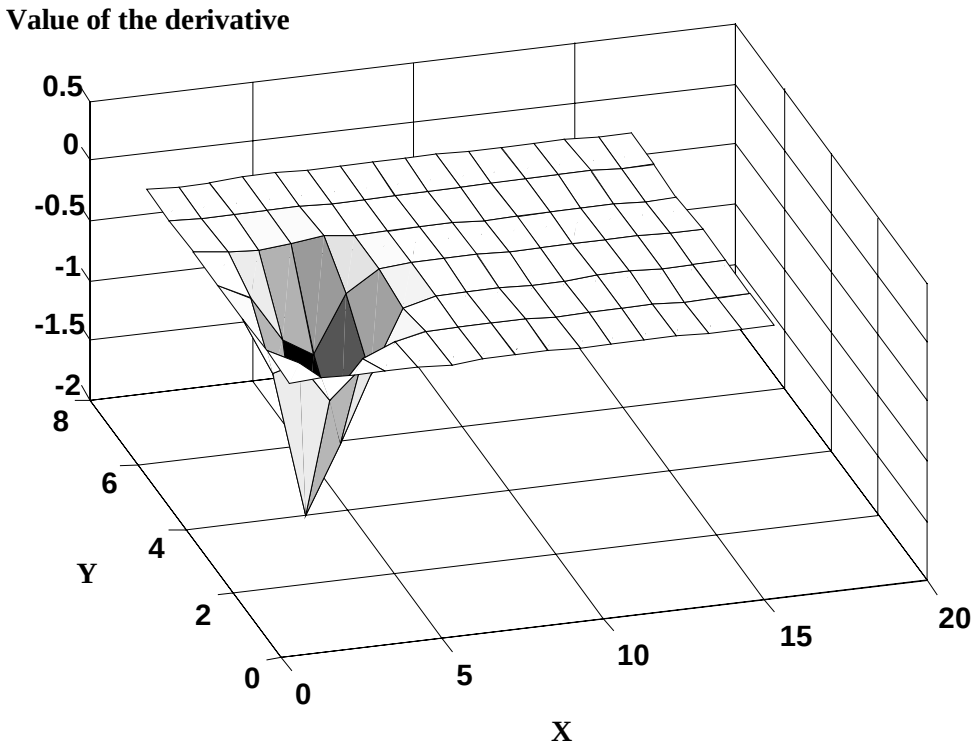

Figure 7.2: Local spatial structure of an example derivative, showing the first derivative of oxygen concentration at the beginning of management period 2 relative to the biomass concentration at the beginning of management period 1.

An example of the errors from using a "local-effect" approach to calculate the derivatives is given in Table 7.1 for the case presented in Chapter 5. A sub-domain was chosen around the peak area for the first derivative of substrate concentration at the beginning of management period 2 relative to the substrate concentration at the beginning of management period 1 ($\frac{\partial c_{s,t+1}}{\partial c_{s,t}}$ in Appendix C, where t=1), which has matrix structure similar to the derivative shown in Figure 7.2. One derivative value was calculated using both the local-effect approach (i.e., calculating with fine mesh only in the sub-domain) and the standard full domain calculation. Although the predicted concentration values at the end of the first management period from each method are very close (see column 3 in Table 7.1), the derivative values are different by 3 orders of magnitude.

Table 7.1: Comparison of local-effect and full domain calculation of derivatives

	Concentration at the Beginning of the First Management Period (Before Perturbation) (1)	Amount of Perturbation (2)	Concentration at the End of the First Management Period (3)	Derivative (4)
Local-effect	0.0182218026849478	0.00005891460520268	0.0182924123982399	1.198509487574120
Full Domain	0.0182218026849478	0.00005891460520268	0.0182222599965325	0.007762278693509

Increasing the area of the sub-domain can improve the accuracy of the derivatives calculation slightly, but results in significant loss of computational performance. In fact, some larger sub-domains can require even more CPU time than the full domain because,

when solving the perturbed linear system for the sub-domain, an LU factorization has to be done for the sub-domain since it cannot be obtained from the forward sweep. This is different from the full domain approach described in Chapter 5, where the left-hand-side matrix can be obtained from the forward sweep. Actual computational savings decrease dramatically when the area of the sub-domain increases, as can be seen from Table 7.2. When the sub-domain is about one-third of the full domain area, the computational savings is only 3% compared to the full domain approach. Moreover, the accuracy is still not sufficient (the data for Table 7.1 were obtained using one-third of the full domain). For these reasons, this approach was not investigated further.

Table 7.2: Computational savings of local-effect sub-domain method

Percentage of the sub-domain area over the full domain (1)	Computational Savings in terms of CPU time (2)
18%	13%
21%	12%
24%	10%
33%	3%

7.2.2 Temporal Multiscale Approach

Due to the time-dependent nature of the bioremediation optimal control model, it is possible to use multiple scales in the management periods during the solution

procedure, hence the idea of a "temporal multiscale approach". The temporal multiscale method focuses on using multiple management periods to solve the whole optimization problem. Assuming that the optimal value of each control variable is a continuous function of the management period, as shown in Figure 7.3, when the intervals of the management period are refined, more and more accurate approximations to the underlying continuous form of the control variables can be obtained (see the continuous line in Figure 7.3). This approach can be described in the following steps:

(1) Solve the whole optimal control model initially with only one management period

(2) Interpolate the control policy to the model with two management periods and solve the whole optimization problem again

(3) Successively refine the management periods and repeat using a similar procedure

This process is halted when the management periods are as short as the user has specified, which is typically the shortest period for which it is reasonable for the pumping rates to be changed (e.g., weekly during site visits).

However, note that SALQR is only linear with time steps, so the computational savings will not be as significant as with the spatial multiscale methods. In addition, it is difficult to interpolate the control variables (i.e., the pumping rates) over different time scales, other than by simply using the pumping rates obtained in the coarser management period as initial values for the finer temporal scale. Using this approach, the model was solved for the case presented in Chapter 5, starting at one management period, refining to two management periods and then finally solving for six management periods. As can be seen from Table 7.3, the number of iterations required for two management periods is

only one iteration less than that for the coarse level with one management period, and the number of iterations for six management periods is even one more iteration than the coarser level with two management periods. The total CPU time for the temporal multiscale method is 62.1 hours, compared to 37.8 hours using the standard solution with six management periods. The reason for this degraded performance is that solutions with more management periods are sufficiently different that no advantage is gained from starting with the optimal solution at a coarser level. For example, Figure 7.4 shows the optimal pumping rates for well number 1 (see Figure 4.5 for the location of well number 1) when the number of management periods is two and six. The initial guess for the six management period level, which is obtained from the optimal results for the level with two management periods, is sufficiently different from the optima solution that many iterations are required. Given these results, this approach was not considered further.

Table 7.3: Computational performance of temporal multiscale method

	Number of Management Periods (1)	Number of Iterations (2)	CPU Time (hr) (3)
Temporal Multiscale Solution	1	11	22.1
	2	10	15.9
	6	11	24.1
	Total	32	62.1
Standard Solution	6	16	37.8

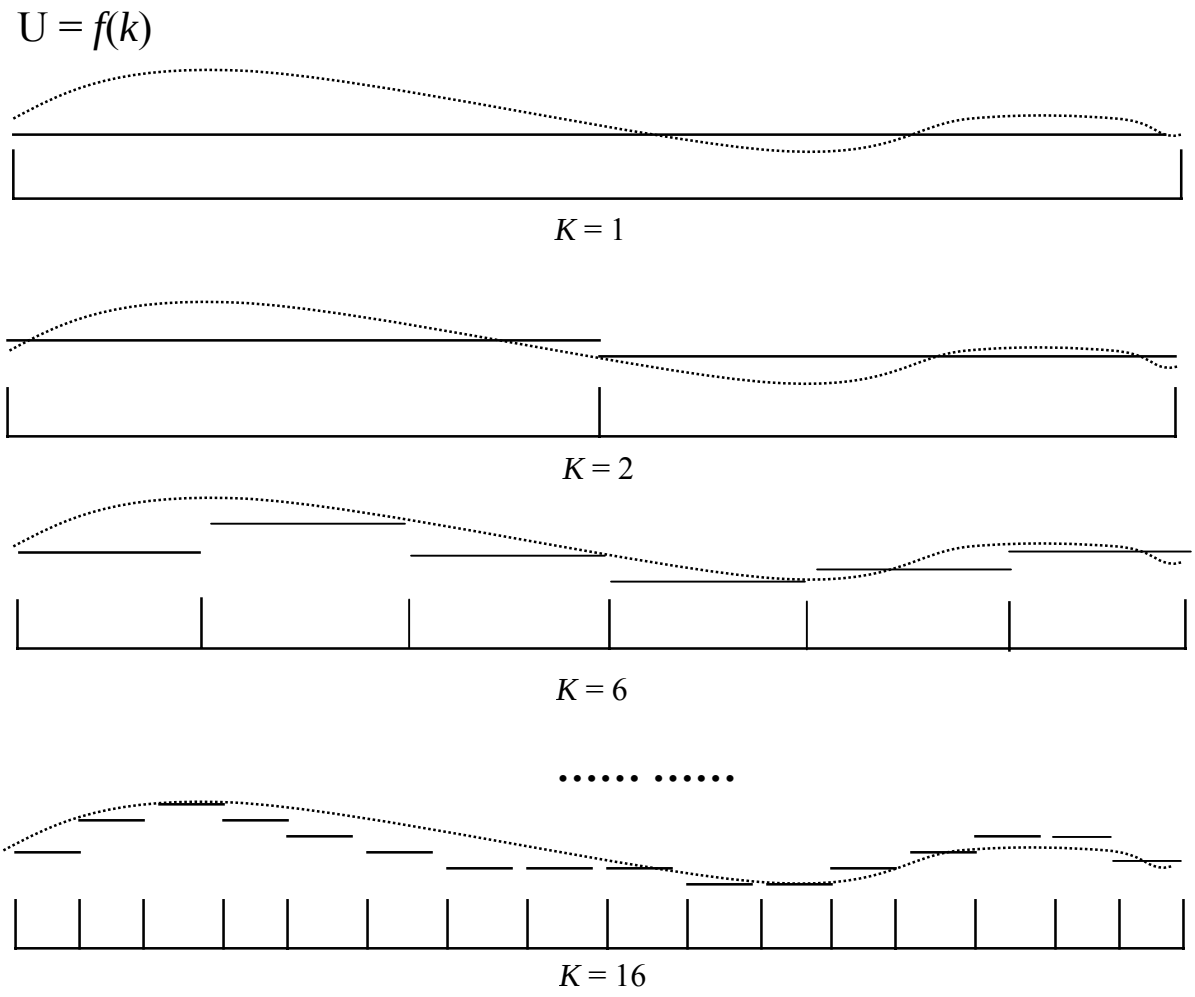

Figure 7.3: Optimal control variable estimates for different numbers of management periods (*K*)

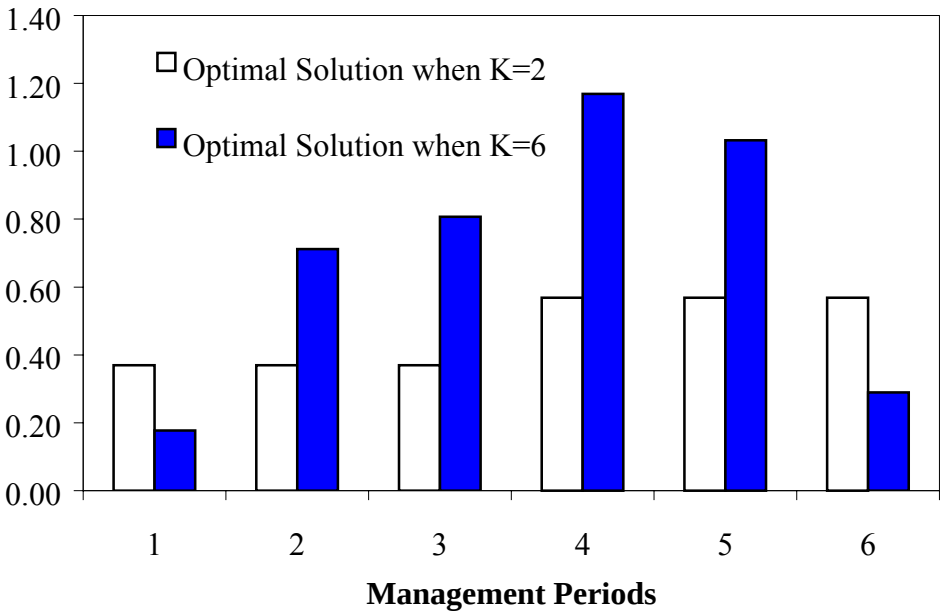

Figure 7.4: Optimal pumping rates at well location 2 using different number of management periods (*K*)

7.2.3 Configuration of the Full Multiscale Method

As described in the first section of this chapter, the full multiscale method consists of the following individual components: one-way spatial multiscale method, efficient numerical derivatives, and V-cycle multiscale derivatives method. In order to obtain the best possible computational performance of the full multiscale method, different configurations of the individual components have been investigated.

Figure 7.5 shows the five configurations, or schema, that were tested. Schemas 1 to 3 use both the V-cycle derivatives calculation and the one-way spatial multiscale method. For comparison, only the one-way spatial multiscale method is used in schema 4 and 5 with different starting levels. All five schemas use the numerical derivatives approach because, as shown in Chapter 5, it is substantially more efficient than the analytical derivatives approach. Moreover, the V-cycle multiscale derivatives method can only be used with the numerical derivatives approach because it is dependent on decoupling of the derivatives calculation.

Note that V-cycle multiscale derivatives can switch back and forth between more than two levels, for example by calculating derivatives at Level 3 starting at Level 1. However, since most of the computing time is still spent on the fine level (Level 3) and coarser levels (Level 1) are not likely to improve accuracy, only a bilevel V-cycle derivatives method is used in the configurations. A final note is that at the finest level, which is usually determined by the accuracy requirement of the simulation model, it is not advantageous to use the V-cycle derivatives method. At this stage, the SALQR algorithm is fine-tuning pumping rates and the V-cycle approximation slows down

convergence. Variations of Schemas 1 through 3 were run with the V-cycle derivatives approximation added at Level 4, but these runs did not converge within five iterations (the maximum convergence required for schemas 1 through 3) and were halted. For this reason, these schemas are not shown in Figure 7.4.

7.3 Results and Discussion for Full Multiscale Approach

To test the approaches developed in this chapter,, the case study presented in Chapter 4 was used (see Table 4.2 for site characteristics and model parameters and Figure 4.5 for the schematic view of the test site). The four-level mesh hierarchy developed in Chapter 5 was implemented to test the schemas shown in Figure 7.5.

The first test of the full multiscale approach is to compare its performance to the other methods, including solving the model at a single level with analytical derivatives from Minsker and Shoemaker (1998a). Given the substantial computational effort required for the analytical derivatives methods, this comparison was only performed at Level 3 (see Table 5.1 for the level information). This comparison, given in Figure 7.6, shows the advantage of using the full multiscale approach over other methods. In Figure 7.6, when using only a single grid (i.e., running the whole optimal control model at Level 3), the efficient numerical derivatives method outperforms the analytical derivatives with a 68% reduction in computing time using a single grid (38 vs. 117 hours). The one-way spatial multiscale method can be applied with either the numerical derivatives method or

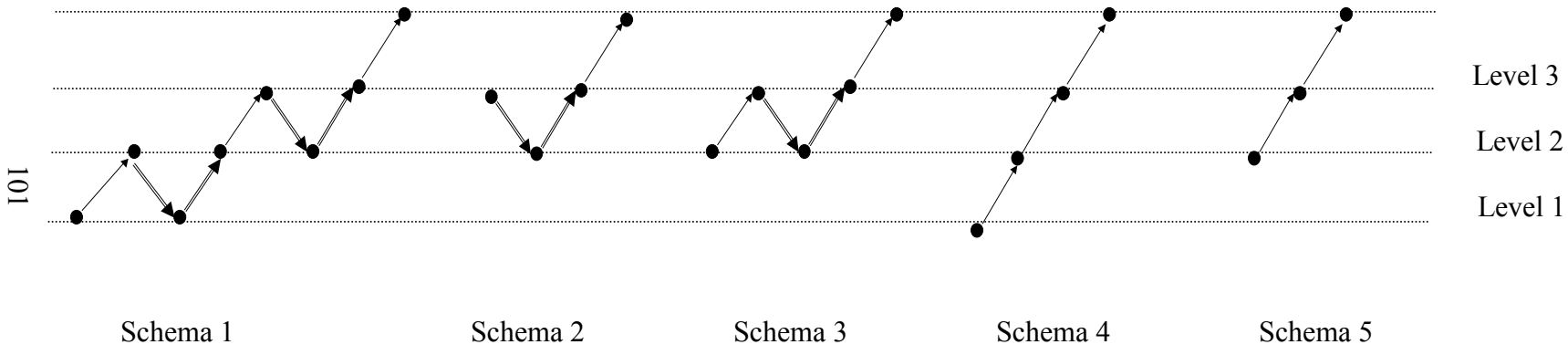

Figure 7.5: Configuration of full multiscale method

the analytical derivatives method. Combining the one-way spatial multiscale method with the efficient numerical derivatives method results in a 70% reduction in computing time over the analytical derivatives single-grid approach and a 36% reduction over the one-way spatial multiscale method with analytical derivatives. However, the one-way spatial multiscale method provides only an additional 8% reduction over the single-grid case when numerical derivatives are used.

Since analytical derivatives cannot be used in the V-cycle and full multiscale derivatives method, only the efficient numerical derivatives method is used with those methods. The V-cycle derivatives method and the full multiscale approach took about 29% and 32% less time to converge than the single-grid numerical derivatives approach, respectively. The full multiscale method achieves a 78% computational savings over the previous single-grid approach with analytical derivatives method. Note that much greater savings would be achieved at Level 4 because the computational savings increase for finer grids.

To find the best configuration of the full multiscale approach, several runs were conducted using the schemas in Figure 7.5. The estimated running time for a Level 4 case (which has about 6,500 state variables) using the previous analytical derivatives single-grid model would be between 10 to 12 months, which is not practical to run the actual model. As shown in Figure 7.7, the best performance is achieved by Schema 2, which follows a "checkmark" stencil (see Figure 7.5) and found the optimal solution within 8.8 days. In fact, for Schema 2, the optimal control model was able to converge with only 3 additional iterations at the finest level (Level 4). The full multiscale approach starting

from Level 1 (i.e., Schema 1) is the second fastest with a total CPU time of 10.8 days. These results are estimated to be more than 30 times faster than the previous optimal control model using a single grid and analytical derivatives. Schema 3 finished with a total CPU time of 11.9 days, which is slightly higher than Schema 2. Both Schemas 2 and 3 were able to converge with only 4 additional iterations at the finest level. It is possible that Schema 2 follows a slightly different search path and thus converges faster.

Schemas 1, 2 and 3 are all significantly faster than Schemas 4 and 5, indicating the advantages of incorporating the V-cycle derivatives approach in the full multiscale method. Both Schemas 4 and 5 use only the one-way spatial multiscale method with efficient numerical derivatives and converge with only 5 additional iterations at the finest level. Since both schema 4 and 5 do not use the V-cycle derivatives calculation, they exhibit a loss of performance.

These results show that inexact derivatives at the early stage of the optimization (as in the V-cycle derivatives method) can play a significant role in reducing computing time, especially for large-scale cases. In addition, all of the schemas show the importance of considering the interaction of PDE discretization and the optimization procedure. Due to the nature of PDE-constrained optimization problems, where solving PDEs is only the subproblem of the optimization problem, refining optimization solutions must be carried out simultaneously with the mesh refinement for the PDE. As can be seen from Figure 7.7, multiple spatial scales and mesh refinement can provide significant computational savings while still maintaining satisfactory convergence of the optimization algorithm in

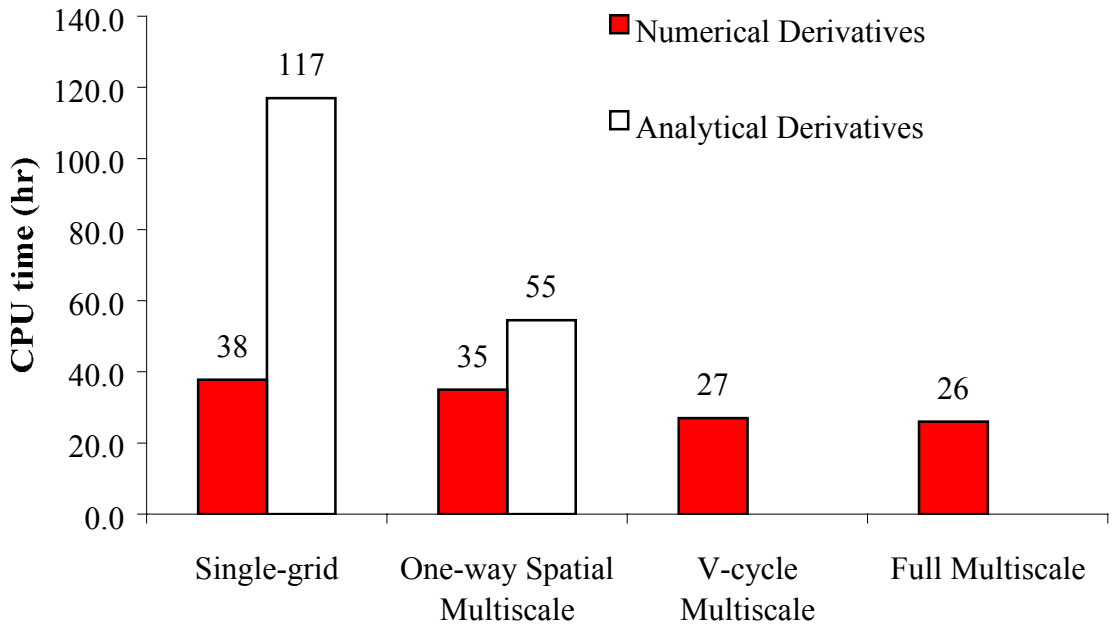

Figure 7.6: Performance comparison of different methods

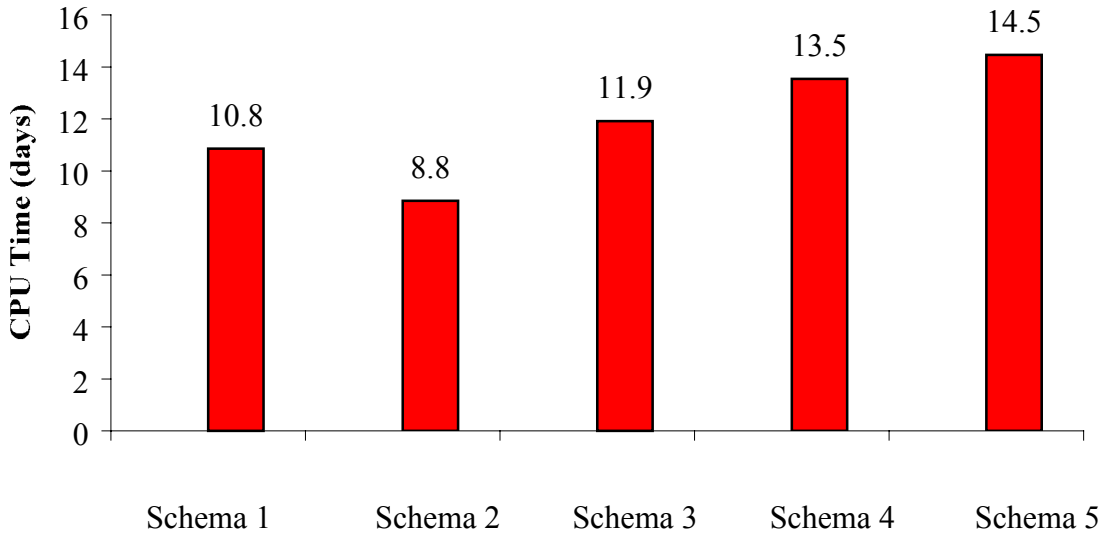

Figure 7.7: Performance comparison of among different configurations of full multiscale approach

the early stages of the search. However, once the model reaches the finest level, it is near the optimal solution and accurate derivatives are necessary. This is a general principle for solving any PDE-constrained optimization problem regardless of the optimization algorithm used.

Finally, the results indicate that three spatial levels are usually sufficient to provide good results and computational savings. For example, Schemas 1 and 3 only differ in the starting level and the total number of levels, but the difference in terms of computing time is only about 10%. Similarly, Schemas 4 provides only 7% computational savings over schema 5, which has one less level. Moreover, with four levels it is more difficult to ensure that pumping well locations remain in the coarsest mesh. While methods exist to interpolate wells between mesh points (e.g., Huang and Mayer 1997), it is not clear that the computational savings would be worth the added complexity.

7.4 Summary

We presented a full multiscale method for an optimal control model of groundwater in-situ bioremediation in this chapter. This method integrates the one-way spatial multiscale method, the efficient numerical derivatives method, and the V-cycle multiscale numerical derivatives method developed in previous chapters. Application of the method starts from the coarsest mesh and solves for the optimal solution at that level, then uses the optimal solution obtained as the initial guess for the finer mesh. While at the finer mesh, the method switches back to the coarser mesh to solve for the derivatives

and uses those derivatives to interpolate back to the finer mesh. This procedure continues until convergence is achieved at the finest level.

Application of the full multiscale method to a case with about 6,500 state variables shows substantial performance gains over previous approaches. The CPU time for the full multiscale approach ranges between 8.8 days and 11.9 days, depending on the configuration of the approach. These are significant computational savings compared to the previous single-grid model using analytical derivatives, which is estimated to require nearly one year to converge. Combinations of the one-way spatial multiscale method, efficient numerical derivatives and V-cycle multiscale derivatives method always outperform methods with only one individual component.

The interaction of PDE discretization and optimization is discovered in this study. Since solving PDEs is only a subproblem with PDE-constrained optimization, it is critical that refining optimization solutions be performed simultaneously with the mesh refinement for the PDE. At the early stage of the optimization, a coarse mesh for the PDE can be used to facilitate broad search of the decision space. Once the search is close to the optimal, a finer mesh is needed for the PDEs to provide more accurate information on state variables and expedite fine-tuning of the optimal solution. This is a general principle for solving any PDE-constrained optimization problem regardless of the optimization algorithm used. For the derivative-based optimization algorithms, such as the SALQR method used in this research, V-cycle derivatives calculation is very beneficial for the early stage of the optimization and should be used in conjunction with the one-way spatial multiscale method. We found that using the V-cycle multiscale derivatives method

at the finest level is not beneficial. Once the model reaches the finest level, it is already near the optimal solution, and inexact derivatives are not beneficial for fine tuning the optimal solution.

The number of levels used in the full multiscale approach can be traded off with the additional complexities of interpolating pumping rates at the coarsest level when well locations are between mesh nodes. As a rule of thumb, a three-level mesh hierarchy appears to be sufficient for obtaining the greatest performance gains. In the case study shown, there is no significant difference between the four-level and three-level full multiscale method, as indicated by Schemas 1 and 3, as well as Schemas 4 and 5 because most of the computing time is still spent on the finest level.

Chapter 8

Concluding Remarks

8.1 Conclusions

Applying formal optimization algorithms such as the SALQR method to assist in optimal design of large-scale in-situ bioremediation of groundwater is expected to be highly rewarding because substantial cost savings could be achieved if optimal designs can be used. However, solving an optimal control model for in-situ bioremediation design poses a computational challenge even for the most advanced supercomputing power available today. The results and insights obtained in this research can substantially reduce the computational burden associated with solving the SALQR optimal control model for in-situ bioremediation. Furthermore, the multiscale methods developed in this research are also expected to be applicable for other large-scale PDE-constrained optimization problems, which are commonly encountered in various engineering and science disciplines.

The SALQR optimal control model of in-situ bioremediation of groundwater uses a management period formulation, where the pumping rates change only every management period instead of every simulation period. Due to the dynamics and nonlinearity of bioremediation systems, the simulation model usually requires small

simulation time steps. Thus, it is necessary to use a management period formulation to avoid changing pumping rates too frequently and unrealistically. However, this causes a significant computational burden in calculating the first derivatives of the transition equation with respect to the state and control variables, which are needed for the SALQR method. Our analysis found that the two-step analytical derivatives method is the computational bottleneck of the SALQR optimal control model of in-situ bioremediation with a management period formulation, requiring over 90% of the total computing time. The first step requires a matrix inversion and the second step requires dense matrix multiplication, both of which are on the order of N^3, where N is the number of state variables. Since bioremediation models usually need a fine numerical mesh, which means large numbers of state variables, the cubic growth rate of the computing time with respect to the number of state variables prohibits the application of this model to large-scale design. To improve the computational performance of the model and overcome the "scale" issue, new approaches to reduce both the total number of iterations and the CPU time per iteration must be developed. The multiscale methods developed in this work meet such objectives.

Since the bioremediation optimal control model is governed by a set of nonlinear PDEs, which describe the system response under given pumping rates, an accurate solution of the simulation model is necessary. However, the discretization of PDEs introduces a large number of unknown state variables if only a single fine-grid model is used. Because solving PDEs is only a subproblem of optimization in our study, we must search for the optimal pumping rates and obtain accurate simulation results

simultaneously. The full multiscale method developed in this work achieves this goal by using approximate solutions early in the run when a broad search of the decision space is being performed. As the solution becomes more refined later in the run, more accurate estimates are needed to finetune the solution and finer spatial discretizations are used.

The full multiscale approach integrates a one-way spatial multiscale method, an efficient numerical derivatives method, and a V-cycle multiscale derivatives method. The one-way spatial multiscale method proceeds "one-way" from the coarsest the finest mesh, with the solution successively interpolated from coarse to fine level. This method is applicable to any PDE-constrained optimization problems, as long as the governing PDEs can be discretized into different spatial levels. For derivative-based optimization algorithms, the one-way spatial multiscale method is independent of the approach used to calculate derivatives (i.e., analytical or numerical derivatives). Application of the method to a case study showed over 50% reduction of computing time relative to the previous single-grid model.

The efficient numerical derivatives method exploits the procedure for calculating the first derivatives of the transition equations with respect to the state variables and reduces computational effort by an order of magnitude compared to the previous analytical derivative method. The numerical derivatives method also decouples the calculation of the derivatives at different nodes in the spatial discretization mesh so that V-cycle multiscale derivatives method can be applied.

The V-cycle multiscale derivatives method approximates the fine-grid derivatives by first switching back to the coarser level to obtain the coarser-grid derivatives and then

interpolating back to the fine level. These inexact derivatives values are beneficial only for the early stage of the optimization when large changes in the pumping rates are made and approximate response estimates are sufficient. About 25% reduction of computing time can be achieved by using the V-cycle multiscale derivatives method in theory and about 29% reduction in our case study.

Integrating the power of the one-way spatial multiscale method, the efficient numerical derivatives method and the V-cycle multiscale derivatives method enables solution of a case with about 6,500 state variables within 8.8 to 11.9 days, compared to one year needed by the original single-grid model with analytical derivatives.

Various modeling issues associated with using multiscale methods for optimal bioremediation design were identified in this research. Since multiple spatial scales are used in this model, there is no need to require the Peclet number to be within 2 for the finite element mesh at all levels except the finest level. The dispersivity values can also be changed to higher values at the coarser levels to overcome any numerical difficulties since the Peclet number may be too high at the coarser levels. The penalty weight used at different levels is also critical to the search for optimal pumping rates when the model moves up to a higher level. Our study shows that good results can be obtained when the penalty weight is decreased after interpolation to a finer mesh and when a terminal penalty weight is used that gives a maximum violation of the substrate concentration constraints of less than 1% of the standard. Finally, when designing the full multiscale approach, the number of levels can be traded off with the ease of setting up the pre-selected candidate pumping wells to avoid discontinuity. A three-level mesh hierarchy

was found to be sufficient for satisfactory performance in the case study examined in this work.

8.2 Future Work

There are a number of possible future directions that could be pursed for improving the multiscale methods developed in this work. Since the efficient numerical derivatives method developed in this work decouples the calculation of derivatives at different nodes, parallelization of the independent calculations of each derivative can be implemented readily. This will further reduce the cost of computing time per iteration and thus enable very large-scale design.

Another possible research direction is to use adaptive mesh refinement to effectively control the problem size even for highly heterogeneous sites. This would require much more sophisticated and advanced simulation models to be coupled with the optimal control algorithm. The full multiscale approach developed in this work can still be used in this context. However, the number of state variables will grow less dramatically than with the uniform mesh refinement method used in this research. Changing the governing PDE equations will likely change the way the derivatives are calculated if the SALQR method is used as the optimization algorithm, so more research would be needed on how to efficiently calculate the derivatives in such a context. The one-way spatial multiscale method and V-cycle derivatives calculation can be adapted to other 2-D or 3-D simulation models without major difficulties.

Since the current SALQR algorithm is relatively slow when it is near the optimal solution, it is possible to explore some new ideas on how to consider the augmented objective function as a level-dependent function and how to use multiscale methods to expedite the search in the objective function space. Since the penalty function incorporates the state variables into the objective function, the augmented objective function can be considered as level dependent. Thus it might be possible to design a multiscale method where the coarse grid problem is to find the descent gradient direction for the fine grid optimization problem.

It is also possible to extend the application of the multiscale methods developed in this work into other PDE-constrained optimization problems, such as groundwater inverse problems. Combining multiscale methods with other optimization algorithms (both derivative-based methods such as SQP and non-derivative-based methods such as evolutionary algorithms) is also possible.

Appendix

A. Simulation Model Bio2D

Transition equation (equation (1.2) in Chapter 1) describes the change in state vector X from one management period to the next under the current control policy U_k. The transition equation is a two-dimensional finite-element contaminant fate and transport simulation model called Bio2D. It can be described as a set of PDEs (equations (A.1), (A.2), (A.3) and (A.4)) before discretization, but in the numerical model it's a set of discrete equations (equations (A.6), (A.7), (A.8) and (A.9)).

$$\nabla \bullet (bK_h \nabla h) + \sum_{i \in U} u_{i,k} \delta(x_{i,} y_i) = 0 \qquad (A.1)$$

$$R_s b\theta \frac{\partial C_s}{\partial t} - \nabla \bullet (bD \bullet \nabla C_s) + bv \bullet \nabla C_s + b\theta C_b R_b r_s + \sum_{i \in U} u_{i,k} (C_s - C_s^{'}) \delta(x_{i,} y_i) = 0 \qquad (A.2)$$

$$b\theta \frac{\partial C_o}{\partial t} - \nabla \bullet (bD \bullet \nabla C_o) + bv \bullet \nabla C_o + b\theta C_b R_b F_{os} r_s + \sum_{i \in U} u_{i,k} (C_o - C_o^{'}) \delta(x_{i,} y_i) = 0 \qquad (A.3)$$

$$R_b b\theta \frac{\partial C_b}{\partial t} - \nabla \bullet (bD \bullet \nabla C_b) + bv \bullet \nabla C_b - b\theta R_b (Y_c r_s - r_b) c + \sum_{i \in U} u_{i,k} (C_b - C_b^{'}) \delta(x_{i,} y_i) = 0 \qquad (A.4)$$

where, equation (A.1) is the groundwater flow equation, solving for *h(hydraulic head)* in each management period for the pumping rates selected in that period; Equation(A.2), (A.3) and (A.4) describe changes in substrate(contaminant, C_s), oxygen(C_o), and biomass concentrations (C_b), respectively; Other variables are defined as follows:

$\delta(x_i, y_i)$ = Dirac delta function evaluated at location (x_i, y_i);

$\boldsymbol{D}$ = dispersivity tensor (m^2/d);

v = Darcy's velocity (m/d);

θ = Porosity;

b = Aquifer thickness (m);

C_o' = Oxygen concentration in injection water (mg/L);

C_s' = substrate concentration in injection water (mg/L);

C_b' = biomass concentration in injection water (mg/L);

Rs = Substrate Retardation factor;

F_{os} = Ratio of oxygen to substrate used;

Y_c = Yield coefficient (mg/mg);

r_b = Endogenous respiration rate for bacteria (1/day);

c = Background organic carbon concentration (mg/L);

r_s = rate of substrate degradation.

Note that the nonlinearity of the simulation model comes from the representation of variable r_s, as shown in equation (A.5).

$$r_s = \frac{\mu_{\max}}{Y_c}\left(\frac{C_s}{K_s + C_s + \frac{(C_s)^2}{K_i}}\right)\left(\frac{C_o}{K_o + C_o}\right) \qquad (A.5)$$

where,

μ_{max} = Maximum specific growth rate for biomass(1/day);

K_s = Substrate half-saturation coefficient (mg/L);

K_i = Substrate inhibition coefficient (mg/L);

K_o = Oxygen half-saturation coefficient (mg/L).

The discretized version of the Bio2D is described as follows, where [ ] denotes matrix and { } denotes vector. The definitions of matrices and vectors in equations (A.6), (A.7), (A.8) and (A.9) can be found in Minsker and Shoemaker (1996).

Hydraulic head equation:

$$[A]\{h_{t+1}\} = [P_h]\{u_t\} + \{F_h\} \tag{A.6}$$

Substrate (contaminant) concentration equation:

$$\left([N] + \frac{[M_s]}{\Delta t} + \sum_{i=1}^{m} u_{t,i}[P_c]^i\right)\{C_{s,t+1}\} = \frac{[M_s]}{\Delta t}\{C_{s,t}\} + \sum_{i=1}^{m} u_{t,i}[P_c]^i C_s^{'} + \{F_s\} \tag{A.7}$$

Oxygen concentration equation:

$$\left([N] + \frac{[M_o]}{\Delta t} + \sum_{i=1}^{m} u_{t,i}[P_c]^i\right)\{C_{o,t+1}\} = \frac{[M_o]}{\Delta t}\{C_{o,t}\} + \sum_{i=1}^{m} u_{t,i}[P_c]^i C_o^{'} + \{F_o\} \tag{A.8}$$

Biomass concentration equation:

$$\left([N] + \frac{[M_b]}{\Delta t} + \sum_{i=1}^{m} u_{t,i}[P_c]^i\right)\{C_{b,t+1}\} = \frac{[M_b]}{\Delta t}\{C_{b,t}\} + \sum_{i=1}^{m} u_{t,i}[P_c]^i C_b^{'} + \{F_b\} \tag{A.9}$$

B. Optimal Control Model of In-Situ Bioremediation of Groundwater

The optimal control model of groundwater in-situ bioremediation used in this research can be described as (Minsker and Shoemaker 1998b):

$$\underset{U_1..U_2}{Min} \quad J(U) = \sum_{k=1}^{K} G\ (X_k, U_k, k) \tag{B.1}$$

Subject to

$$X_{k+1} = Y(X_k, U_k, k), k = 1,..., K \tag{B.2}$$

$$c_{s,K}(j) - c_{\max}(j) \le 0, \forall j \in \Phi \tag{B.3}$$

$$c_{s,k}(j) - c_{\max}(j) \le 0, k = 1,..., K, \forall j \in \Psi \tag{B.4}$$

$$h_k(j) - h_{\max}(j) \le 0, k = 1,..., K, \forall j \in \Omega \tag{B.5}$$

$$-h_k(j) + h_{\min}(j) \le 0, k = 1,..., K, \forall j \in \Pi \tag{B.6}$$

$$-U\max_k^{ext} \le U_k^{ext} \le 0, k = 1,..., K \tag{B.7}$$

$$0 \le U_k^{inj} \le U\max_k^{inj}, k = 1,..., K \tag{B.8}$$

where the objective function *J(U)* in equation (B.1) is the sum of cost functions *G* in each management period *k; K* is the number of management periods; the control vector U_k is the pumping rates; the state vector X_k includes hydraulic heads and concentrations of contaminants, oxygen and biomass. The cost function is defined as (Minsker and Shoemaker 1998b):

$$G(X_k, U_k, k) = \sum_{i \in U} a_i \sqrt{1 + u_{i,k}^2} \tag{B.9}$$

where $u_{i,k}$ = pumping rate at location (x_i, y_i) in management period k (m^3/d); U = set of pumping sites; a_i = constant relative cost coefficient; and i = index for entries in the

control vector U_k. Note that in this cost function, X_k is only an implicit variable that affects U_k through equations (B.3) and (B.4).

The transition equation (B.2) describes the change in state vector X_k from one management period to the next under the current control policy U_k. The transition equation $Y(X_k, U_k, k)$ is a two-dimensional finite-element contaminant fate and transport simulation model called Bio2D.

Equations (B.3)-(B.8) are constraints, where $c_{max}(j)$ = water quality goal at node j (mg/L); $c_{s,k}(j)$ = substrate concentration in period k at node j (mg/L); Φ = set of nodes with monitoring wells where water-quality compliance must be attained by the end of the cleanup; Ψ = set of nodes with monitoring wells at the downgradient end of the solution domain where water quality compliance must be maintained in every management period; $h_{max}(j)$ = maximum hydraulic head allowed at node j in period k (m); Ω = set of nodes with injection wells; $h_{min}(j)$ = minimum hydraulic head allowed at node j in periods k (m); Π = set of nodes with extraction wells; $h_k(j)$ is the hydraulic head in period k at node j (m); $U\max_k^{ext}$ = maximum allowed extraction pumping rate vector in period k (m^3/d); U_k^{ext} = extraction rate vector in period k ((m^3/d); $U\max_k^{inj}$ = maximum allowed injection pumping rate vector in period k (m^3/d) and U_k^{inj} = extraction rate vector in period k (m^3/d).

The constraints in equation (B.3) ensure that the water-quality standard will be met at the specified monitoring wells by the end of the clean-up period. The constraints listed in (B.4) prevent the contaminant plume from migrating by requiring contaminant

concentrations at the downgradient edge of the solution domain to remain below the water-quality goal in every management period. The hydraulic head constraints in (B.5) are needed to prevent the model from selecting injection rates that cause unrealistically high hydraulic heads. Similarly, the constraints in (B.6) prevent excessively low hydraulic heads due to high rates of extraction pumping. Constraints (B.7) and (B.8) set lower and upper bounds on the pumping rates at extraction and injection wells, respectively. Usually only one constraint on either hydraulic head or pumping rates would be specified for each well. For the cases studied in this research, constraints (B.7) and (B.8) were not used.

Equations (B.3)-(B.8) are incorporated into the objective function when this model is solved using the following penalty function:

$$y = \sum_{k=1}^{K} \sum_{q=1}^{n_q} r[\max(0, f_{kq})]^{2.001} \qquad (B.10)$$

where y = the penalty that is added to the objective function in equation (B.1); f_{kq} = violation of the constraint q in period k, where q is any of the constraints given in equations (B.3)-(B.6); n_q = the number of constraints in equations (B.3)-(B.6); and r = a scalar penalty weight greater than zero. The penalty weight r is initially set to a small value (for the cases in this paper, the initial penalty weight is 50) and the optimal solution is found. Then the weight is increased successively by a factor of 10 and the problem is resolved until the constraint violations are sufficiently small.

C. First Derivatives of the Transition Equation with Respect to the State Variables and Control Variables

The first derivatives of the transition equation with respect to state variables and control variables over each simulation time period can be described as follows (also see Minsker and Shoemaker 1996).

In the following description, state variables are denoted as $\{x_t\} = \{h_t, c_{s,t}, c_{o,t}, c_{b,t}\}$ *and* control variables are denoted as $\{u_t\}$.

$$\left[\frac{\partial T}{\partial x_t}\right]_{4N\times 4N} = \left[\frac{\partial x_{t+1}}{\partial x_t}\right] = \begin{bmatrix} \frac{\partial h_{t+1}}{\partial h_t} & \frac{\partial h_{t+1}}{\partial c_{s,t}} & \frac{\partial h_{t+1}}{\partial c_{o,t}} & \frac{\partial h_{t+1}}{\partial c_{b,t}} \\ \frac{\partial c_{s,t+1}}{\partial h_t} & \frac{\partial c_{s,t+1}}{\partial c_{s,t}} & \frac{\partial c_{s,t+1}}{\partial c_{o,t}} & \frac{\partial c_{s,t+1}}{\partial c_{b,t}} \\ \frac{\partial c_{o,t+1}}{\partial h_t} & \frac{\partial c_{o,t+1}}{\partial c_{s,t}} & \frac{\partial c_{o,t+1}}{\partial c_{o,t}} & \frac{\partial c_{o,t+1}}{\partial c_{b,t}} \\ \frac{\partial c_{b,t+1}}{\partial h_t} & \frac{\partial c_{b,t+1}}{\partial c_{s,t}} & \frac{\partial c_{b,t+1}}{\partial c_{o,t}} & \frac{\partial c_{b,t+1}}{\partial c_{b,t}} \end{bmatrix} = \begin{bmatrix} 0 & 0 & 0 & 0 \\ 0 & \frac{\partial c_{s,t+1}}{\partial c_{s,t}} & \frac{\partial c_{s,t+1}}{\partial c_{o,t}} & \frac{\partial c_{s,t+1}}{\partial c_{b,t}} \\ 0 & \frac{\partial c_{o,t+1}}{\partial c_{s,t}} & \frac{\partial c_{o,t+1}}{\partial c_{o,t}} & \frac{\partial c_{o,t+1}}{\partial c_{b,t}} \\ 0 & \frac{\partial c_{b,t+1}}{\partial c_{s,t}} & \frac{\partial c_{b,t+1}}{\partial c_{o,t}} & \frac{\partial c_{b,t+1}}{\partial c_{b,t}} \end{bmatrix} \quad (C.1)$$

$$\left[\frac{\partial T}{\partial u_t}\right]_{4N\times m} = \left[\frac{\partial x_{t+1}}{\partial u_t}\right] = \begin{bmatrix} \frac{\partial h_{t+1}}{\partial u_t} \\ \frac{\partial c_{s,t+1}}{\partial u_t} \\ \frac{\partial c_{o,t+1}}{\partial u_t} \\ \frac{\partial c_{b,t+1}}{\partial u_t} \end{bmatrix} \quad (C.2)$$

The following sections list the individual non-zero components in equations (C.1) and (C.2). Note that the equation for $\left[\frac{\partial h_{t+1}}{\partial u_t}\right]$ is omitted here because it is only needed to calculate once per management period and is only $N \times m$, where N is the total number of unknowns in the finite element mesh and m is the dimension of control variables. Also note that the actual dimension of $\left[\frac{\partial T}{\partial x_t}\right]$ should be $(NH + NS + NO + NB) \times (NH + NS + NO + NB)$, where NH, NS, NO and NB stand for the number of unknowns of Heads, concentrations of substrate, oxygen and biomass, respectively. But for simplicity of notations and without losing generality, here these four state variables are assumed with the same size of N. Likewise, the actual dimension of $\left[\frac{\partial T}{\partial u_t}\right]$ is $(NH+NS+NO+NB) \times m$.

Define $[E_s]=\left[[N]+\frac{[M_s]}{\Delta t}+\sum_{i=1}^{m} u_{t,i}[P_c]^i\right]$, then we have

$$[E_S][\frac{\partial c_{s,t+1}}{\partial c_{s,t}}]=\frac{[M_S]}{\Delta t}+\left[\frac{\partial F_S}{\partial c_{s,t}}\right]$$

$$[E_S][\frac{\partial c_{s,t+1}}{\partial c_{o,t}}]=\left[\frac{\partial F_S}{\partial c_{o,t}}\right]$$

$$[E_S][\frac{\partial c_{s,t+1}}{\partial c_{b,t}}]=\left[\frac{\partial F_S}{\partial c_{b,t}}\right]$$

$$[E_S][\frac{\partial c_{s,t+1}}{\partial u_t}]_{N\times m}=[-[V_S]-\sum_{i=1}^{m} u_{t,i}[P_c]^i(c_{s,t+1}-c_s')e_{i,m}^T]$$

The above equations (except the last one, which is used to calculate the derivatives of state variables w.r.t. control variables) can be described using the following format:

$[\text{bandedMatrix1}]_{N\times N} * [\text{unknown}]_{N\times N} = [\text{bandedMatrix2}]_{N\times N}$

Minsker and Shoemaker's implementation uses the following computational stencil to solve the unknowns:

$[\text{unknown}]_{N\times N} = \text{Inverse}([\text{bandedMatrix1}]_{N\times N}) * [\text{bandedMatrix2}]_{N\times N}$

which leads to a matrix multiplication between a dense matrix and a banded matrix.

Similarly, we can define $[E_o] = \left[[N] + \frac{[M_o]}{\Delta t} + \sum_{i=1}^{m} u_{t,i} [P_c]^i \right]$, and we have the derivatives of transition equation w.r.t. oxygen:

$$[E_o][\frac{\partial c_{o,t+1}}{\partial c_{s,t}}] = \left[\frac{\partial F_o}{\partial c_{s,t}} \right]$$

$$[E_o][\frac{\partial c_{o,t+1}}{\partial c_{o,t}}] = \frac{[M_o]}{\Delta t} + \left[\frac{\partial F_o}{\partial c_{o,t}} \right]$$

$$[E_o][\frac{\partial c_{o,t+1}}{\partial c_{b,t}}] = \left[\frac{\partial F_o}{\partial c_{b,t}} \right]$$

$$[E_o][\frac{\partial c_{o,t+1}}{\partial u_t}]_{N\times m} = [-[V_o] - \sum_{i=1}^{m} u_{t,i} [P_c]^i (c_{o,t+1} - c_o')e_{i,m}^T]$$

and w.r.t. biomass (after defining $[E_b] = \left[[N] + \frac{[M_b]}{\Delta t} + \sum_{i=1}^{m} u_{t,i} [P_c]^i \right]$):

$$[E_b][\frac{\partial c_{b,t+1}}{\partial c_{s,t}}] = \left[\frac{\partial F_b}{\partial c_{s,t}}\right]$$

$$[E_b][\frac{\partial c_{b,t+1}}{\partial c_{o,t}}] = \left[\frac{\partial F_b}{\partial c_{o,t}}\right]$$

$$[E_b][\frac{\partial c_{b,t+1}}{\partial c_{b,t}}] = \frac{[M_b]}{\Delta t} + \left[\frac{\partial F_b}{\partial c_{b,t}}\right]$$

$$[E_b][\frac{\partial c_{b,t+1}}{\partial u_t}]_{N\times m} = [-[V_b] - \sum_{i=1}^{m} u_{t,i}[P_c]^i (c_{b,t+1} - c_b')e_{i,m}^T]$$

All the above derivative evaluations are $O(N^3)$. To get derivatives at the management time periods, an additional $O(N^3)$ operations are needed (see equations (C.3) and (C.4) below).

Derivatives of the transition equation over a management period can be described as follows (also see Culver and Shoemaker 1992).

$$\left[\frac{\partial Y}{\partial X_k}\right]_{4N\times 4N} = \prod_{t=p}^{p+d-1}\left[\frac{\partial T}{\partial x_t}\right] \qquad \text{(C.3)}$$

Equation (C.3) describes that the derivatives of transition equation over a management time period is the product of simulation time period derivatives over one management period. In Minsker and Shoemaker's implementation (1996), after each simulation time period, the newly obtained simulation time period derivatives will be multiplied by the previous obtained part of ∂Y/ ∂X.

$$\left[\frac{\partial Y}{\partial U_k}\right]=\left[\frac{\partial T}{\partial u}\right]_{p+d-1}+\left[\frac{\partial T}{\partial x}\right]_{p+d-1}\left[\frac{\partial T}{\partial u}\right]_{p+d-2}+\left[\frac{\partial T}{\partial x}\right]_{p+d-1}\left[\frac{\partial T}{\partial x}\right]_{p+d-2}\left[\frac{\partial T}{\partial u}\right]_{p+d-3}+\ldots\ldots$$
$$\ldots\ldots\ldots+\prod_{t=p+1}^{p+d-1}\left[\left(\frac{\partial T}{\partial x}\right)_t\right]\left(\frac{\partial T}{\partial u}\right)_p \qquad \text{(C.4)}$$

where $p = (k-1)d+1$, and d is the number of simulation time steps per one management period and k is the management period counter.

D. Constrained SALQR Method

Constrained SALQR(Successive Approximation Linear Quadratic Regulator) algorithm with management periods is described in this appendix. Note that the algorithm given here is only the basic version of SALQR. As the penalty weight increases, penalty term in C_k matrix (see the definition in the algorithm description) increases and C_k becomes more and more ill conditioned. To avoid inaccuracy and convergence difficulty, Liao and Shoemaker (1990) developed a method to partition the matrices *A, B, C* into A_1, A_2, B_1, B_2, C_1, C_2. C_1 and C_2 are inverted separately, which involves QR factorization, and then "reattached". This advanced version of SALQR is used in the code for this research but not presented here. See Liao and Shoemaker (1990) for details. Notation is adapted from Yakowitz and Rutherford (1984), Culver and Shoemaker (1992) and Liao and Shoemaker (1991). Subscript *k* indicates management period counters, subscripts *x* and *u* indicate derivatives with respect to *X* and *U*, and superscripts *T* and -1 denote matrix transpose and inverse, respectively. $\hat{G}$ indicates the cost function, which has been augmented by the penalty associated with violating constraints by equation (3) in Chapter 1. The following steps and the flow chart that follows can describe this algorithm.

Step 0: Select a nominal policy $\overline{U}_k$ for $k = 1, \ldots, K$.

Step 1: Initialize parameters and compute loss and trajectory associated with the given policy:

(1) set $P_{K+1} = 0_{NxN}$, $Q_{K+1}=0_{1xN}$, $\theta_{K+1}=0$;

(2) $\overline{X}_1$ given and fixed, $X_{k+1}=Y(\overline{X}_k, \overline{U}_k, k)$, $k=1,\ldots,K$;

(3) $J(U) = \sum_{k=1}^{K} \hat{G}_k(\overline{X}_k, \overline{U}_k, k)$.

Step 2: Backward sweep: perform the following four procedures recursively, for $k = K,\ldots,1$.

1. Compute A_k, B_k, C_k, D_k, E_k, as follows:

$$A_k = \frac{1}{2}(\hat{G}_{xx})_k + (\frac{\partial Y}{\partial X})_k^T P_{k+1} (\frac{\partial Y}{\partial X})_k$$

$$B_k = (\hat{G}_{xu})_k + 2(\frac{\partial Y}{\partial X})_k^T P_{k+1} (\frac{\partial Y}{\partial U})_k$$

$$C_k = \frac{1}{2}(\hat{G}_{uu})_k + (\frac{\partial Y}{\partial U})_k^T P_{k+1} (\frac{\partial Y}{\partial U})_k$$

$$D_k = (\frac{\partial \hat{G}}{\partial U})_k + Q_{k+1} (\frac{\partial Y}{\partial U})_k$$

$$E_k = (\frac{\partial \hat{G}}{\partial X})_k + Q_{k+1} (\frac{\partial Y}{\partial X})_k$$

2. Compute P_k and Q_k according to

$$P_k = A_k - \frac{1}{4} B_k^T C_k^{-1} B_k$$

$$Q_k = -\frac{1}{2} D_k^T C_k^{-1} B_k + E_k$$

Store P_k and Q_k in memory, replacing P_{k+1} and Q_{k+1}.

3. Compute α_k and β_k according to

$$\alpha_k = -\frac{1}{2} C_k^{-1} D_k$$

$$\beta_k = -\frac{1}{2} C_k^{-1} B_k$$

and store in memory.

4. Compute

$$\theta_k = -\frac{1}{2} D_k^T C_k^{-1} D_k + \theta_{k+1}$$

and store θ_k in place of θ_{k+1}.

Step 3: If $\theta_1 \leq \theta_{min}$ then

$\overline{U}_k$ is the optimal policy;

Otherwise,

Compute the updated control policy as follows:

(1) set $\varepsilon = 1.0$;

(2) compute U_k recursively for $k = 1,\ldots, K$ according to the control law:

$$U_k = \varepsilon\alpha_{k+} \beta_k(X_k - \overline{X}_k) + \overline{U}_k$$

$$X_{k+1} = Y(X_k, U_k, k)$$

(3) compute the loss,J:

$$J(U) = \sum_{k=1}^{K} \hat{G}_k(X_k, U_k, k).$$

(4) if $J(U)-J(\overline{U}) \leq \varepsilon(\theta_1/2)$,

set $\overline{U}_k = U_k$ *for k = 1,..,K and*

go to ***Step 1***.

Otherwise,

Perform a line search: set ε=ε/3 and

go to the second item (2) in ***Step 3***.

The following chart visually represents the steps involved when using SALQR method.

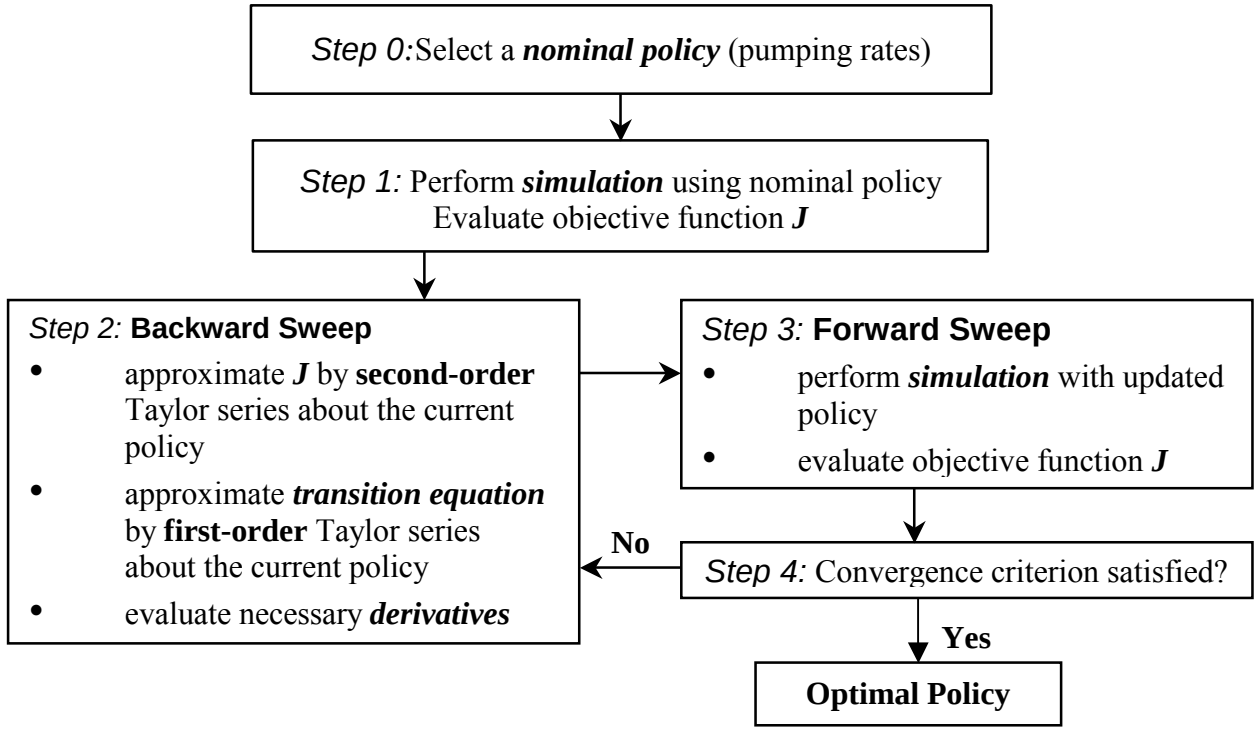

Figure D.1: Flow chart of SALQR method

References

Ahlfeld, D.P., Mulvey, J.M. and Pinder, G.F.(1986). Designing optimal strategies for contaminated groundwater remediation, *Advances in Water Resources,* 9, 77-84.

Ahlfeld, D.P., J.M. Mulvey, G.F. Pinder and E. F. Wood (1988). Contaminated groundwater remediation design using simulation, optimization, and sensitivity theory. 1. Model development, *Water Resour. Res.*, 24(3), 431-441.

Akian, M., Quadrat, J. P., and Chancelier, J.P. (1988). Dynamic programming complexity and application, in *Proceedings of the 27th IEEE Conference on Decision and Control*, Austin, TX, 1551-1558.

Arian, E., and Ta'asan, S. (1994a). Multigrid one shot methods for optimal control problems: infinite dimensional control, ICASE Report No.94-52, Institute for Computer Applications in Science and Engineering, NASA Langley Research Center, Hampton, Virginia.

Arian, E., and Ta'asan, S. (1994b). Shape optimization in one shot, in *Proceedings of the Workshop on Optimal Design and Control*, Blacksburg, VA, Apr. 8-9, 1994. (Borggaard, J. et al., eds.), Birkhäuser Boston, Cambridge, MA, 23-40.

Arnold, E. and Puta, H. (1994). An SQP-type solution method for constrained discrete-time optimal control problems. In "*Computational Optimal Control*" ed. By R. Bulirsch and D. Kraft., *International Series of Numerical Mathematics,* Vol.115. Birkhäuser Verlag, Switzerland.

Bartholomew-Biggs, M., Brown, S., Christianson, B., and Dixon, L. (2000). Automatic differentiation of algorithms, *Journal of Computational and Applied Mathematics*, 124(1-2), 171-190.

Bear, J., and Sun, Y.(1998). Optimization of Pump-Treat-Inject (PTI) design for the remediation of a contaminated aquifer: multi-stage design with chance-constraints, *J. of Contaminant Hydrology*, 29(3): 223-242.

Beckie, R., Wood, E. F., and Aldama, A. A. (1993). Mixed finite element simulation of saturated groundwater flow using a multigrid accelerated domain decomposition technique, *Water Resour. Res.*, 29(9), 3145-3157.

Biros, G., and Ghattas, O. (2000). A Lagrange-Newton-Krylov-Schur method for PDE-constrained optimization, *SIAG/OPT Views-and-News*, 11(2), August 2000.

Biros, G. and Ghatta, O. (1999). Parallel Newton-Krylov methods for PDE-constrained optimization, In *Proceedings of SC'99*, November 13-19, 1999, Portland, OR.

Boggs, P.T., and Tolle, J. W. (2000). Sequential quadratic programming for large-scale nonlinear optimization, *Journal of Computational and Applied Mathematics*, 124(1-2), 123-137.

Brandt, A. (1977). Multi-level adaptive solutions to boundary-value problems, *Math. Comp.*, 31, 333-390.

Brandt, A.(1997). The Gauss center research in multiscale scientific computation, *Electronic Transactions on Numerical Analysis*, 6, 1-34.

Brandt, A. (2001). Multiscale Scientific Computation: Review 2000. *Copper Mountain Conferences on Multigrid Methods*, Copper Mountain, CO., April 1-6, 2001, (http://www.mgnet.org/mgnet-cm2001.html).

Briggs, W.L.(1987). *A Multigrid Tutorial*, SIAM, Philadelphia.

Carriaga, C.C., and Mays, L.W.(1995). Optimal control approach for sedimentation control in alluvial rivers, *J. Water Resour. Plan. Manage.*, 121(6), 408-417.

Chang, L.-C., Shoemaker, C.A., and Liu, P. L.-F. (1992). Optimal time-varying pumping rates for groundwater remediation: application of a constrained optimal control algorithm, *Water Resour. Res.*, 28(12), 3157-3173.

Cheng, H.-P., Yeh, G.-T., Xu, J., Li, M.-H., and Carsel, R. (1998). A study of incorporating the multigrid method into the three-dimensional finite element discretization: a modular setting and application, *International Journal for Numerical Methods in Engineering*, 41(3), 499-526.

Chow, C.-S., and Tsitsiklis, J.N. (1991). An optimal one-way multigrid algorithm for discrete-time stochastic control, *IEEE Transactions on Automatic Control*, 36(8), 898-914.

Christianson, B., and Bartholomew-Biggs, M.(2000). Generalization of Pantoja's optimal control algorithm, *The 3rd International Conference/Workshop on Automatic Differentiation: From Simulation to Optimization*, June 19-23, 2000, Maison du Séminaire, Nice, France.

Culver, T.B., and Shoemaker, C.A. (1992). Dynamic optimal control for groundwater remediation with flexible management periods, *Water Resour. Res*., 28(3), 629-641.

Culver, T.B., and Shoemaker, C.A. (1993). Optimal control for groundwater remediation by differential dynamic programming with quasi-Newton, *Water Resour. Res*., 29(4), 823-831.

Douglas, C. C.(1984). Multi-Grid algorithms with applications to elliptic boundary-value problems, *SIAM J. Numer. Anal.*, 21(2), 236-254.

Douglas,C.C.(1996). Multigrid methods in science and engineering, *IEEE Computational Science & Engineering*, 3(4), pp.55-68.

Dunn, J.C., and Bertsekas, P.B.(1989). Efficient Dynamic Programming Implementations of Newton's Method for Unconstrained Optimal Control Problems. *Journal of Optimization Theory and Applications*, 63(1), 23-38.

Dreyer, T., Maar, B., and Schulz, V. (2000). Multigrid optimization in applications, *Journal of Computational and Applied Mathematics*, 120(1-2), 67-84.

EPA (Environmental Protection Agency). (1997). *Cleaning Up the Nation's Waste Sites: Markets and Technology Trends*. EPA 542-R-96-005. Washington, D.C.: EPA, Office of Solid Waste and Emergency Response.

Ferraresi, M., Todini, E., and Vignoli, R. (1996). A solution to the inverse problem in groundwater hydrology based on Kalman filtering, *Journal of Hydrology*. 175(1-4), 567-572.

Gelhar, L.W., Welty, C. and Rehfeldt, K. R. (1992). A critical review data on field-scale dispersion in aquifers, *Water Resour. Res.*, 28(7), 1955-1974.

Gorelick, S.M., Voss, C.I., Gill, P.E., Murray, W., Saunders, M.A. and Wright, M.H.(1984). Aquifer reclamation design: the use of contaminant transport simulation combined with nonlinear programming, *Water Resour. Res.*, 20(4), 415-427.

Graham, W.D., and McLaughlin, D.B. (1991). A stochastic model of solute transport in groundwater: application to the Borden, Ontario, tracer test, *Water Resour. Res.*, 27(6), 1345-1359.

Hackbusch, W.(1979). On the fast solving of parabolic boundary control problems, *SIAM J. Control and Optimization*, 17(2), 231-244.

Hackbusch, W.(1985). *Multi-grid Methods and Applications*, Springer-Verlag, Berlin.

Hoppe, R.H.W.(1986). Multi-grid methods for Hamilton-Jacobi-Bellman equations, *Numerische Mathematik*, 49, 239-254.

Hovland, P. D., Keyes, D. E., McInnes, L. C., and Samyono, W. (2000). Using automatic differentiation for second-order matrix-free methods in PDE-constrained optimization, Preprint ANL/MCS-P855-1100, Mathematics and Computer Science Division, Argonne National Laboratory.

Huang, C. and Mayer, A. S.(1997). Pump-and-treat optimization using well locations and pumping rates as decision variables. *Water Resour. Res*., 33(5), 1001-1012.

Iserles, A.(1996). *A First Course in the Numerical Analysis of Differential Equations*. Cambridge University Press, New York.

Jones, L., Willis, R., and Yeh, W. W-G (1987). Optimal control of nonlinear groundwater hydraulics using differential dynamic programming, *Water Resour. Res.,* 23(11), 2097-2106.

Jones, J.E., and Woodward C.S.(2001). Newton-Krylov-multigrid solvers for large-scale, highly heterogeneous, variably saturated flow problems, *Advances in Water Resources*, 24(7), 763-774.

Joppich, W., and Mijalković, S. (1993). *Multigrid Methods for Process Simulation*, Springer-Verlag /Wien, New York.

Kronsjö, L., and Dahlquist, G. (1971). On the design of nested iterations for elliptic difference equations, *BIT*, 11,63-71.

Lewis, R. M., and Nash, S.G.,(2000) A multigrid approach to the optimization of systems governed by differential equations. In *Proceedings of the 8th AIAA/USAF/NASA/ISSMO Symposium on Multidisciplinary Analysis and Optimization*, Sept.6-8, 2000, Long Beach, CA.

Li, G., and Mays, L.W. (1995). Differential dynamic programming for estuarine management, *J. Water Resour. Plan. Manage.*, 121(6), 455-462.

Li, M.-H., Cheng, H.-P., and Yeh, G.-T. (2000). Solving 3D subsurface flow and transport with adaptive multigrid, *Journal of Hydrologic Engineering*, 5(1), 74-81.

Liao, L.-Z., and Shoemaker, C.A (1990). Constrained differential partitioning and QR factorization to avoid numerical ill-conditioning of penalty function for constrained nonlinear programming and control, *Proc. IEEE Conf. on Decision and Control*, Honolulu, Hawaii.

Liao, L.-Z., and Shoemaker, C.A. (1991). Convergence in unconstrained discrete-time differential dynamic programming, *IEEE Trans. Autom. Control*, 36, 692-706.

Liu,Y., Minsker, B.S., and Saied, F.(2001). A one-way spatial multiscale method for optimal bioremediation design, *J. Water Resour. Plan. Manage.*,127 (2), 130-139.

Liu, Y. and Minsker, B.S. (2001, in press). Efficient multiscale methods for optimal in-situ bioremediation design, *J. Water Resour. Plan. Manage.* , in press.

Mackay, D.M., Freyberg, D.L., and Roberts, P.V. (1986). A natural gradient experiment on solute transport in a sand aquifer 1. approach and overview of plume movement, *Water Resour. Res.*, 22(13), 2017-2029.

Mansfield, C. M. and Shoemaker, C. A.(1999). Optimal remediation of unconfined aquifers: Numerical applications and derivative calculations, *Water Resour. Res.,* 35(5), 1455-1470.

Mansfield, C. M., Shoemaker, C. A., and Liao, L-Z. (1998). Utilizing sparsity in time-varying optimal control of aquifer cleanup, *J. Water Resour. Plan. Manage.,* 124(1), 39-46.

Maar, B., and Schulz, V. (2000). Interior point multigrid methods for topology optimization, *Struct. Multidisc. Optim*., 19(3), 214-224.

Mavriplis, D.J., and Jameson, A. (1990). Multigrid solution of the navier-stokes equations on triangular meshes, *AIAA JOURNAL*, 28(8), 1415-1425.

Mckeon, T. J., and Chu, W. (1987). A multigrid model for steady flow in partially saturated porous media, *Water Resour. Res.*, 23(4), 542-550.

McLaughlin, D., and Townley, L. R. (1996). A reassessment of the groundwater inverse problem, *Water Resour. Res.*, 32(5), 1131-1162.

Merckx, C. (1991). Optimal pumping strategy for groundwater decontamination, *Int. J. Control*, 53(4), 889-905.

Migdalas, A., Pardalos, P. M., and Värbrand, P. (1998). *Multilevel Optimization: Algorithms and Applications*, Kluwer Academic Publishers, Netherlands.

Minsker, B. S., and Shoemaker, C. A. (1996). Differential a finite element biodegradation simulation model for optimal control. *Water Resour. Res*., 32(1),187-192.

Minsker, B. S., and Shoemaker, C.A. (1998a). Computational issues for optimal *in-situ* bioremediation design, *J. Water Resour. Plan. Manage.*, 124(1), 39-46.

Minsker, B. S., and Shoemaker, C.A. (1998b). Dynamic optimal control of *in-situ* bioremediation of groundwater, *J. Water Resour. Plan. Manage.*, 124(3), 149-161.

Mjolsness, E., Garrett, C.D., and Miranker, W.L. (1991). Multiscale optimization in neural nets, *IEEE Transactions on Neural Networks*, 2(2), 263-274.

Murray, D.M., and Yakowitz, S.J. (1979). Constrained differential dynamic programming and its application to multireservoir control, *Water Resour. Res.*, 15(5),1017-1027.

Murray, D.M., and Yakowitz, S.J. (1984). Differential Dynamic Programming and Newton's Method for Discrete Optimal Control Problems. *Journal of Optimization Theory and Applications*, 43(3), 395-414.

Nash, S.G. (2000). A multigrid approach to discretized optimization problems, *Optimization Methods & Software*, 1(8), 1-18.

National Research Council (1994). *Alternatives for Ground Water Cleanup*, National Academy Press, Washington, D.C..

Pantoja, J.F.A. De O. (1988). Differential Dynamic Programming and Newton's Method. *Int. J. Control*, 47(5), 1539-1553.

Russell, M., Colglazier, E. W., and English, M.R. (1991). *Hazardous Waste Remediation: The Task Ahead.* Knoxville: University of Tennessee, Waste Management Research and Education Institute.

Saied, F. S., and Mahinthakumar, G. (1998). Efficient parallel multigrid based solvers for large-scale groundwater flow simulations, *Computers Math. Applic*., 35(7), 45-54.

Schulz, V., Bardossy, A., and Helmig, R.(1999). Conditional statistical inverse modeling in groundwater flow by multigrid methods, *Computational Geosciences*, 3(1), 49-68.

Stüben, K., and Trottenberg, U. (1982). Fundamental algorithms, model problem analysis and applications, *Multigrid Methods*, edited by W. Hackbusch and U. Trottenberg, *Lecture Notes in Mathematics*, Vol. 960, 1-176.

Ta'asan, S.(1991). "One Shot" methods for optimal control of distributed parameter systems I: finite dimensional control, ICASE Report No.91-2, Institute for Computer Applications in Science and Engineering, NASA Langley Research Center, Hampton, Virginia.

Whiffen, G.J., and Shoemaker, C.A. (1993). Nonlinear weighted feedback control of groundwater remediation under uncertainty, *Water Resour. Res.*, 29, 3277-3289.

Whiffen, G.J.(1995). Optimal control for deterministic and uncertain groundwater remediation, Ph.D. thesis, School of Civil and Environmental Engineering, Cornell Univ., Ithaca, New York.

Woodbury, A. D., and Ulrych, T. J. (2000). A full-Bayesian approach to the groundwater inverse problem for steady state flow, *Water Resour. Res.,* 36(8), 2081-2094.

Yakowitz, S., and Rutherford, B. (1984). Computational aspects of discrete-time optimal control, *Applied Mathematics and Computation*, 15, 29-45.

Yoon, J.-H., and Shoemaker, C.A. (1999). Comparison of optimization methods for ground-water bioremediation, *J. Water Resour. Plan. Manage.*, 125(1), 54-63.

Zio, E. (1997). Approaching the inverse problem of parameter estimation in groundwater models by means of artificial neural networks. *Progress in Nuclear Energy*. 31(3), 303-315.

Vita

Yong Liu received his Bachelor of Engineering and Master of Engineering degrees, both in Environmental Engineering, from Tsinghua University, Beijing, China, in 1994 and 1997, receptively. During his graduate study from 1994 to 1997 in Tsinghua University, he developed a regional environmental resources and information system using technologies from geographic information system, remote sensing and management information systems. He was also a member of the research and development team for China's provincial level environmental information systems from 1994 to 1996, where he was responsible for the database schema design and system analysis. In August 1997, he was admitted to the Ph.D. program in Civil and Environmental Engineering at the University of Illinois at Urbana-Champaign. He held one-year Computational Science and Engineering fellowship from 1997 to 1998. He received his Master of Computer Science degree from the University of Illinois at Urbana-Champaign in May 2001. His interests include groundwater remediation design, PDE-constrained optimization, environmental information technology, and computational informatics.